14153
22141842

904

FAR INFRARED STUDIES OF DIATOMIC CUBIC CRYSTALS BY DISPERSIVE FOURIER TRANSFORM SPECTROSCOPY

AMANULLAH MEMON

A Thesis submitted for the internal Degree of Doctor of Philosophy (Ph D) in the Faculty of Science, University of London

August 1981

Withdrawn from
WESTFIELD UNIV. LONDON COLLEGE

ProQuest Number: 10107332

All rights reserved

INFORMATION TO ALL USERS
The quality of this reproduction is dependent upon the quality of the copy submitted.

In the unlikely event that the author did not send a complete manuscript
and there are missing pages, these will be noted. Also, if material had to be removed
a note will indicate the deletion.

ProQuest 10107332

Published by ProQuest LLC(2016). Copyright of the Dissertation is held by the Author.

All rights reserved.
This work is protected against unauthorized copying under Title 17, United States Code
Microform Edition © ProQuest LLC.

ProQuest LLC
789 East Eisenhower Parkway
P.O. Box 1346
Ann Arbor, MI 48106-1346

ABSTRACT

The far infrared optical properties and complex dielectric response functions of two alkali halide crystals (CsI and KI) and two III-V compound semiconductor crystals (InAs and InP) have been studied using the technique of dispersive Fourier transform spectroscopy. The values of the transverse optic and longitudinal optic phonon frequencies at wave vector q=0 determined from these results agree quite well with published values, and the dielectric functions were used to calculate the imaginary parts of the anharmonic self-energies $\Gamma(oj,\nu)$ of the q=0 transverse optic modes.

These are the first reported measurements on CsI by dispersive Fourier transform spectroscopy, and reasonable agreement is obtained between the frequencies of measured features in $\Gamma(oj,\nu)$ and published two-phonon frequencies. In the case of KI the present measurements have been made at a higher resolution than any reported previously, and they provide a sensitive test of the validity of various theoretical calculations available in publications. Also, in the case of KI some two-phonon difference bands have been observed and assigned in the spectrum of $\Gamma(oj,\nu)$ for the first time.

No measurements of the optical constants of InP in the far infrared region using this technique have been reported before, and, for both InAs and InP, these are the first reported experimental determinations of the imaginary part of the frequency dependent damping function. A number of features in

the spectra of $\Gamma'(\omega,\nu)$ for InAs and InP are revealed and attributed to two-phonon decay processes with the aid of a critical point analysis based on published data for these materials.

Since the performance of the dispersive reflection interferometer was limited by the specimen size a prototype focused beam interferometer was constructed, and its performance has been demonstrated by recording a water vapour absorption spectrum at a resolution of 2 cm^{-1} using end mirrors 5mm in diameter.

ACKNOWLEDGEMENTS

My deepest heartfelt thanks go to Dr. T. J. Parker for suggesting and supervising this research project and for his constant invaluable help advice, and encouragement. He has enlightened me through many thoughtful discussions and helped me on problems that I put before him.

I am greatly indebted to Dr. W. G. Chambers for his enthusiastic help in all aspects of computational work. Thanks are also due to Dr. G. A. Gledhill for knowledgeable discussions from which I have greatly benefited and to Dr. C. L. Mok and Mr. G. Zhang for their constant help during the course of this project.

I acknowledge also the help of the technical staff of the Phyics Department. Many thanks are due to Mr. P. Heaver, the Chief Technician, Messrs J. Oliver, W. Howard, F. Hermann of the Physics Workshop, M. Curati and T. Brooks of the Electronic Workshop, and Mr R. Collins for the delicate task of crystal polishing.

I am grateful for the tremendous support given by my family during the course of my studies.

I would finally like to gratefully acknowledge financial assistance from the Government of Pakistan which has enabled me to carry out this postgraduate research.

CONTENTS

CHAPTER 1

INTRODUCTION

The exploration and application of the far infrared region of the electromagnetic spectrum have progressed steadily over the last twenty years. The method of studying electromagnetic spectra by Fourier transform spectroscopy was pioneered by Michelson [1902].

The main obstruction to the progress of Fourier spectroscopy during the period of Michelson and up to the late 1950's was the absence of adequate computing facilities to perform the Fourier transformation of the interferograms.

The major breakthrough came in the late 1950's and the early 1960's following the experimental realisation of the multiplex and throughput advantages by Fellgett (1957) and Jacquinot (1954), respectively, and their application by Gebbie and Vanasse (1956), and Strong (1957). This, together with the exploitation of digital computers and the development of infrared sources and detectors like the pneumatic Golay cell, and highly sensitive bolometers led to the present state.

In conventional spectroscopy the most common method for obtaining the optical constants is to measure the power reflectivity over as wide a spectral range as possible and to analyse the results using a Kramers-Kronig (K-K)analysis. On the other hand, the main aim of measurements by infrared power transmission spectroscopy is usually to obtain only limited information about the specimen under investigation such as the frequencies of particular spectral features, rather than to make a complete

analysis of the spectra including an absolute determination of the optical constants.

The application of K-K analysis to spectroscopy was first discussed by Robinson and Price (1953), and has been used in calculating the optical constants in the electromagnetic region from the far infrared to the ultraviolet. The values of the optical constants so obtained are in error because of the truncation of the infinite integral. Another difficulty in using a Kramers-Kronig analysis, especially in the case of alkali halides is that these crystals have very low reflectivity in part of the spectral region of interest, which leads to an inaccurately calculated phase. Thus it is not practically possible to determine very accurate values of the optical constants from infrared power spectroscopy.

Following the initial development of dispersive Fourier transform spectroscopy some two decades ago [Chamberlain et al (1963), Bell (1966), Russell and Bell (1966)] it has been established that suitable amplitude and phase spectra for solids, liquids, and gases can always be determined by using a variety of experimental techniques. In all these techniques the specimen is placed in an appropriate configuration in one arm of a two-beam interferometer rather than in front of the detector as for conventional power spectroscopy.

The optical constants can then be calculated directly from the measured values of the complex amplitude reflection coefficient or amplitude transmission coefficient and phase by using Fresnel's relations.

In this work the technique of dispersive Fourier reflection

spectroscopy has been used to determine the optical constants of diatomic cubic crystals in the far infrared in the immediate vicinity of the reststrahlen band where the crystals are very highly absorbing. The results obtained by using this technique are satisfactory, but elsewhere the phase change produced on reflection is very small [Johnson and Bell (1969) Parker and Chambers (1976), Pai et al (1978)], and therefore the absorption index, $k(\nu)$, cannot be measured satisfactorily by using this technique. In such circumstances, however, the measurements for the determination of the optical constants with reasonable accuracy can be made satisfactorily by using the technique of dispersive transmission spectroscopy [Johnson and Bell (1969)].

The technique of dispersive reflection spectroscopy has been previously used below ambient temperature, but no dispersive transmission measurements on solids below room temperature have been reported outside this laboratory. To perform low temperature measurements on solids a single pass transmission interferometer was built in this laboratory which permits measurements at normal incidence in the temperature range 77 to 300K.

Also at low temperature, reflection measurements have been performed successfully down to 7K by Parker at el (1979). Details of the transmission and reflection interferometers together with the associated problems are given in chapter 4.

In the case of the reflection interferometer, since the measurements are restricted by the size of the specimens, we designed a prototype of a focused beam interferometer using very few optical components as compared to other interferometers [Gast

and Genzel (1973)]. The design of the instrument permits measurements on specimens as small as 5mm in diameter. A description of this interferometer, together with a demonstration of its feasibility is given in chapter 4.

The main subject of this thesis was the investigation of the far infrared optical properties of diatomic cubic crystals like the alkali halides and some group III - V compound semiconductors. The optical constants of these crystals were measured in the vicinity of their transverse optic phonons of wave vector q=0 at room temperature and low temperatures using two Michelson interferometers operated in the asymmetric mode, as described in chapter 4.

In the case of KI crystals good agreement was obtained with the previous room temperature measurements of Berg and Bell (1971), whereas for CsI there appear to have been no similar measurements by dispersive Fourier transform spectroscopy reported before.

The results obtained for KI and CsI were used to calculate the frequency dependence of the imaginary part of the anharmonic self-energy of the q=0 transverse optic mode of both materials at room temperature and at low temperature. Structure associated with anharmonicity was revealed that had not previously been observed by K-K analysis of the power reflectivity. The frequencies of the transverse optic modes determined from the positions of the peak values of the conductivity are in good agreement with values reported by Lowndes and Martin (1969), and a detailed discussion of this is presented in chapter 6. The overall agreement for KI is in good agreement quantitatively and qualita-

tively with the calculation of Berg and Bell (1971) and Eldridge and Kembry (1973), and that of CsI with the calculation of Beairsto and Eldridge (1973) which includes the contribution from cubic anharmonicity. A detailed discussion of these results and their comparison with other theoretical calculations is given in chapter 6.

The measurements on III - V compound semiconductors like InAs and InP within the reststrahlen frequency band and below the transverse optic phonon frequency were performed only by the dispersive reflection technique since the pure crystals used for these measurements were completely opaque in this region so that it was not possible to perform dispersive transmission measurements. Nevertheless the dielectric constant results obtained at room temperature are satisfactory, particularly in the case of InP, for which no measurements of the optical constants in the far infrared have been reported before using the dispersive technique.

The frequency dependence of the imaginary part of the anharmonic self-energy of the transverse optic phonon of wave vector q=0 is calculated for these compound semiconductors using the measured values of the dielectric constants as described in chapter 6. Many features are revealed in the spectra of these crystals for the first time and attributed to two-phonon decay processes with the aid of a critical point analysis based on published data for the dispersion curves. The complete lists of observed two-phonon summation and difference processes for these semiconductors are presented in chapter 6.

CHAPTER II

GENERAL THEORY OF FOURIER TRANSFORM SPECTROSCOPY

2.1) Introduction

The main concern of this chapter is to provide a brief description of the mathematical methods involved in Fourier transform spectroscopy. Many theoretical details are omitted since the publications by Bell (1972), Chamberlain (1979), and Martin (1980) provide detailed descriptions of Fourier transform spectroscopy, hereafter called FTS.

In late 1950 the work of Fellgett led to the modern interferometric technique. Fellgett not only realised the advantage of the multiplex principle, but he also realised that the necessary Fourier transformation could be easily handled by the use of advanced techniques developed in computer programming and the computer itself. Nowadays with the fast Fourier transform algorithm of Cooley and Tukey (1965) one can perform the analysis of a large number of data points in a matter of seconds.

In a Michelson interferometer one common procedure in the far infrared region is to record the signal as a stepping motor moves the mirror, and hence an interferogram is recorded in terms of intensity as a function of optical path difference, and by means of Fourier transformation it is then converted into intensity versus frequency. In practice this tedious calculation is performed by a computer, which is why FTS was not a practical proposition until computers became readily available.

The discussion in this chapter starts by deriving a

fundamental relation used in FTS, and then two major advantages of FTS are discussed. These are the superior light gathering power and the multiplex advantage. It is shown that for a given resolving power the light grasping power of a Michelson interferometer can be of the order of one hundred times better than that of a grating spectrometer. This advantage can either be used to reduce the scanning time by a factor of 100 or improve the signal to noise ratio by a factor of 10. Besides these advantages the response of the instrument to monochromatic and polychromatic radiation,viz, the instrumental line shape due to the limitation on maximum optical path difference of a Michelson interferometer, is described. Also, the effects of apodization on the resolution of the spectrum are discussed. The chapter is concluded by describing sampling of an interferogram and the phenomenon of aliasing.

2.2) Fundamental relation of FTS

In order to derive the fundamental relation of FTS, we consider a Michelson two beam interferometer, as illustrated in fig(2.1).

The radiation from the source is divided by the beam divider into two beams of equal amplitude which are reflected from mirrors and return to the beam splitter for a second splitting. We are interested in only those two partial beams which reach the detector and interfere.

If we assume that the incident monochromatic radiation has a frequency ν_o (in wave numbers) and amplitude A , then, by displacing one of the mirrors of the interferometer, a phase

delay of $\delta = 2\pi\nu_o x$ is introduced, where x is the optical path difference between the two beams. Now by applying the law of linear superposition the complex amplitude so obtained is given as

$$A = A_o \ (1 + e^{i\delta}) \qquad (2.1a)$$

Then the intensity of monochromatic radiation at the detector is obtained by multiplying Eq(2.1a) by its complex conjugate, i.e,

$$I = A \cdot A^* = 2A_o^2 [1 + \cos(2\pi\nu_o x)] \qquad (2.1b)$$

Hence the signal registered at the detector as a function of optical path difference is given as

$$I(x) = 2B[1 + \cos(2\pi\nu_o x)], \qquad (2.1c)$$

where $B=A_o^2$ now represents the intensity of the superimposed beams. The function I(x) goes through maxima and minima as the optical path difference x is varied, and this is achieved by displacing the moving mirror along the optical axis. If now we consider that the source is polychromatic instead of monochromatic, then the spectrum can be obtained by integrating (2.1c) between the limits 0 and infinity, i.e

$$I_R(x) = 2\int_0^\infty B(\nu)[1 + \cos(2\pi\nu\ x)]\ d\nu \qquad (2.2)$$

$$= 2\int_0^\infty B(\nu)\ d\nu + 2\int_0^\infty \cos(2\pi\nu x)\ B(\nu)\ d\nu \qquad (2.3)$$

For equal mirror displacements from the beam splitter (i.e,x=0) we calculate

$$I_R(0) = 2\int_0^\infty 2B(\nu)\ d\nu \qquad (2.4)$$

and for infinite mirror displacement i.e, $x=\infty$ we have

$$I(\infty) = (1/2)\ I_R(0) + \lim_{x\to\infty} \int_0^\infty 2B(\nu)\ \cos(2\pi\nu x)\ d\nu \qquad (2.5)$$

In (2.5), as x tends to infinity the $\cos(2\pi\nu x)$ term oscillates very rapidly and averages to zero. Therefore, only at x=0 does constructive interference of all frequencies take place. This means that $I_R(x)$ has its maximum with this mirror displacement, and by (2.4) the maximum intensity is then observed at the detector. For large optical path differences it follows from (2.5) that only half of the maximum intensity is then observed at the detector, and the other half returns to the source. Inserting (2.4) in (2.5) we then obtain

$$I_R(x) - (1/2)\ I_R(0) = \int_0^\infty 2B(\nu)\ \cos(2\pi\nu x)\ d\nu \qquad (2.6)$$

The expression on the left hand side of (2.6) is called the interferogram, which is the sum of the fluxes of the patterns produced by each wave number present in the broad bandwidth, and the method of Fourier transformation interprets the interferogram to provide the pattern for each frequency and hence determines the magnitude of the fluxes at that frequency.

As the interferogram and spectrum form a Fourier transform pair, we can therefore obtain the spectrum, $B(\nu)$, by Fourier transformation of the interferogram :

$$B(\nu) = (1/2)\int_0^\infty [I_R(x) - (1/2)I_R(0)]\ \cos(2\pi\nu x)\ dx \qquad (2.7)$$

Eq(2.7) states that at a given wave number, if the flux versus optical path difference is known as a function of x, the cosine Fourier transform of the interferogram will produce the spectrum. In order to obtain the complete spectrum (2.7) must be integrated

for the whole frequency spectrum under observation.

Since the spectrum $B(\nu)$ is an even function in the whole frequency range we can write the following pair of Fourier transform integrals as given by Chamberlain (1979) :

$$I_c(X) = \int_{-\infty}^{+\infty} B(\nu)\cos(2\pi\nu X)d\nu \qquad (2.8)$$

where $$I_c(x) = [I_R(x) - (1/2)I_R(0)] \qquad (2.9)$$

and $$B(\nu) = \int_{-\infty}^{+\infty} I_c(x)\cos(2\pi\nu x)dx \qquad (2.10a)$$

In the equations above we observe that we have used physically very large values of the optical path difference for the calculation of the spectral distribution $B(\nu)$. We will discuss the limits on this optical path difference later in this chapter. Furthermore, since the optical system in the interferometer is not always perfectly balanced, it is useful (Bell 1972) to use complex Fourier transforms instead of cosine Fourier transforms. Therefore we have

$$I_c(x) = \int_{-\infty}^{+\infty} B(\nu)\, e^{+i2\pi\nu x}\, d\nu \qquad (2.10)$$

and the spectrum

$$B(\nu) = \int_{-\infty}^{+\infty} I_c(x)\, e^{-i2\pi\nu x}\, dx \qquad (2.11)$$

Thus relation (2.7) represents the fundamental relation of FTS and the rest of the derivation relied on the Fourier transform integral theorem and mathematical manipulation.

2.3) Multiplex and throughput advantages

The two main features which distinguish FTS from conventional spectrometry, i.e, prism or grating spectrometry, are the multiplex and light gathering advantages. We will first consider the multiplex advantage. In an interferometer a black body source emits radiation of broad bandwidth and the intensities of all spectral elements which are present in the broad bandwidth are simultaneously observed by the detector during the entire period of measurement. Suppose that we are to observe a spectrum made of N spectral elements in time T, each spectral increment being equal to the resolution. Then with a conventional spectrometer each element will be observed for a time T/N, and the signal to noise ratio in the observed spectrum will be proportional to the square root of the observing time

i.e $$(S/N)_G \propto (T/N)^{\frac{1}{2}} \qquad (2.12a)$$

In the case of an interferometer the situation is different because, here, each spectral element is observed all the time so that the signal to noise ratio will be proportional to the square root of T, i.e,

$$(S/N)_I \propto (T)^{\frac{1}{2}} \qquad (2.12b)$$

Comparing the $(S/N)_I$ with $(S/N)_G$, we see that

$$\frac{(S/N)_I}{(S/N)_G} = (N)^{\frac{1}{2}} \qquad (2.12c)$$

for the same constant of proportionality. It therefore follows that the interferometric system is superior to the conventional system by the factor of $(N)^{\frac{1}{2}}$. This improvement is termed the

Fellgett, or multiplex advantage. In order to fully achieve this advantage, the system must be detector noise limited. This advantage is not applicable in the visible and ultraviolet regions where the principle source of noise is photon noise due to fluctuation in the size of the signal.

Another significant advantage of interferometers was pointed out by Jacquinot. According to him an interferometer possessing circular symmetry has an angular admission advantage over a grating spectrometer which employs a slit and consequently has no such symmetry. Jacquinot showed that the radiant throughput of an interferometr is much higher than that of a grating spectrometer. The throughput of a Michelson interferometer is calculated below and is compared with that of a grating spectrometer.

The amount of radiation flowing out from a point source P within a small solid angle subtended by an element (mirror) of area dA' at a distance r [fig(2.2a)] is proportional to the solid angle. Then we can obtain the flux (dF) by dividing the area of dA' projected normal to the rays by r^2. Hence the flux dF is given as

$$dF = \text{constant } (dA'/r^2) \cos\phi \qquad (2.13)$$

In practice the source can never be a point. We therefore consider it as an element of area ds which is inclined at an angle θ between the source normal and the optical axis, as shown in fig(2.2b). If we assume that the given source radiates according to Lamberts law, i.e, the flux is proportional to

$\cos\theta$ ds, the flux will now be proportional to the projected area of ds as well, therefore

$$dF = B\,[ds\cos\theta\, dA'\cos\phi]\, r^{-2} \qquad (2.14)$$

where B, the proportionality constant, is the source brightness, with units of $w\ m^{-2}ster^{-1}$. We can define in (2.14) the solid angle subtended by the source as

$$d\Omega = (\cos\theta\ ds)\ r^{-2} \qquad (2.15a)$$

and the projected area of the collimator as

$$dA = \cos\phi\ dA' \ . \qquad (2.15b)$$

Substituting these values of $d\Omega$ and dA in (2.14) we have

$$dF = B\ dA\ d\Omega$$

or

$$E = (dF/B) = dA\ d\Omega \qquad (2.16)$$

Let us assume that losses due to absorption in the optical system are negligible. It then follows that for an interferometer the quantity $dA\ d\Omega$ is a constant, and one can therefore use large values of $dA\ d\Omega$ in the interferometer and have high resolution which is independent of the quantity $dA\ d\Omega$, which is called etendue. From above it follows that one may consider the flux throughput at any point in a lossless optical system for, in such a system, the brightness of an object is equal to the brightness of an image.

In order to compare the throughput of the two systems, i.e, a Michelson interferometer and a grating spectrometer, we will first consider the throughput of a Michelson interferometer E_M as

$$E_M = A_M \Omega_M \qquad (2.17)$$

[Bell (1972)]. Here $\Omega_M = (\pi D^2/F^2)$ is the solid angle subtended by the source of circular diameter D at the collimator of focal length F. The resolving power of a Michelson interferometer is defined as

$$R_M = \frac{\nu_o}{\Delta\nu} \tag{2.18}$$

In a collimated interferometer off axis rays are present because of the finite size of the limiting aperture and this introduces a spread in wave number which is written as

$$\nu = \nu_o \left[1 - \frac{\Omega}{2\pi}\right] \tag{2.19a}$$

[Fleming (1974), Bell (1972), Connes (1958)] and the total wave number spread is written

$$\Delta\nu = \nu_o \frac{\Omega_M}{2\pi} \tag{2.19b}$$

From (2.18) and (2.19) we have the resolving power R_M as

$$R_M = \frac{2\pi}{\Omega_M} \tag{2.20}$$

Putting the value of solid angle from (2.20) in (2.17) we have

$$E_M = (2\pi)\ (A_M / R_M) \tag{2.21}$$

This relation represents the throughput of a Michelson interferometer.

In a grating spectrometer the resolving power and throughput power are limited by the slit width. The solid angle of a grating spectrometer in terms of its slit width 'b' and length 'l' and the focal length F of the collimator is given as

$$\Omega_G = bl / F^2 \tag{2.22}$$

Also

$$R_G = (2F \tan\theta)/ b \tag{2.23}$$

[Bell (1972)]. Here R_G is the resolving power of a grating spectrometer , and θ is the angle of rotation of the grating. Now substituting the value of 'b' from (2.23) in (2.22), and using the definition of etendue as given in (2.16), the throughput of a grating spectrometer is written as

$$E_G = A_G \cdot \Omega_G = (1/F)\ (A_G / R_G)\ 2 \tan\theta \qquad (2.24)$$

Thus the maximum efficiency of a grating instrument can be obtained as follows. For maximum efficiency, θ is chosen to be ~ 30 . Then we have $2 \tan\theta \sim 1$

hence $$E_G = (1/F)\ (A_G / R_G) \qquad (2.25)$$

If we assume that $A_G \sim A_M$, and that the focal lengths for the collimators, and the resolving powers of both the instruments are almost the same, then the ratio of interferometer and grating throughputs can be expressed as

$$E_M / E_G = 2\pi\ (F/1) \qquad (2.26)$$

For the best grating spectrometers the ratio of the focal length of the collimator to the slit length is never less than 30. Thus the etendue of a Michelson interferometer is nearly 200 times better than that of a grating spectrometer.

2.4) Finite path difference and instrumental line shape

So far we have been considering the limits of optical path difference (x) to be infinite, i.e, x varies form $-\infty$ to $+\infty$, but in practice this is not possible since the optical path of an interferometer is restricted by the length of its moving mirror arm. Therefore we are forced to truncate the integral within

the limits of $-L \leqslant x \leqslant +L$, say.

To obtain an expression for the instrumental line shape produced by a finite optical path difference we have to study, within the finite maximum optical path limits, the form of the spectrum produced by the Fourier transform of the interferogram when a monochromatic source is used. Considering the complex Fourier transform relation given by (2.10), the interferogram function is given as

$$I_c(x) = \int_{-\infty}^{+\infty} B(\nu)\, e^{+i2\pi\nu x}\, d\nu \qquad (2.27)$$

If we assume that the source is emitting monochromatic radiation (ν_o), and that the spectrum $B(\nu)$ obtained is in the form of a Dirac delta function, i.e,

$$B(\nu) = (1/2)\,[\delta(\nu - \nu_o) + \delta(\nu + \nu_o)] \qquad (2.27a)$$

then we have, from (2.27), the interferogram function as

$$I_c(x) = (1/2)\int_{-\infty}^{+\infty} [\delta(\nu - \nu_o) + \delta(\nu + \nu_o)]\, e^{+i2\pi\nu x}\, d\nu \qquad (2.28)$$

By using the definition of the Dirac delta function the above expression for the interferogram function reduces to

$$I_c(x) = 2\cos(2\pi\nu_o x) \qquad (2.29)$$

Hence the interferogram obtained from a monochromatic line of wave number ν_o is of the cosine form. Inserting the value of $I_c(x)$ from (2.29) in (2.11) we get

$$B(\nu) = \int_{-\infty}^{+\infty} 2\cos(2\pi\nu_o x)\, e^{-i2\pi\nu x}\, dx \qquad (2.29a)$$

Since the integral of the odd function is zero, after applying

finite path limits (2.29a) reduces to

$$B(\nu) = \int_{-L}^{+L} \{[\cos(2\pi(\nu - \nu_o)x] + [\cos(2\pi(\nu + \nu_o)x]\} dx \quad (2.30)$$

Thus on integrating the above relation we have

$$B(\nu) = \frac{2L \sin 2\pi(\nu - \nu_o)L}{2\pi(\nu - \nu_o)L} + \frac{2L \sin 2\pi(\nu + \nu_o)L}{2\pi(\nu + \nu_o)L} \quad (2.31)$$

In (2.31) we observe that the second term is negligible compared to the first term if $\nu_o L \gg 1$ i.e, $L \gg \lambda$, which is always the case. Therefore we ignore the second term, and now the instrumental line shape can be expressed as

$$B(\nu) \approx \frac{2L \sin 2\pi(\nu - \nu_o)L}{2\pi(\nu - \nu_o)L} \quad (2.32)$$

$$\approx 2L (\sin y)/y \approx 2L \operatorname{sinc} y \quad (2.33)$$

where $$y = 2\pi(\nu - \nu_o)L \quad (2.34)$$

The quantity 2L sinc y is usually called the instrumental lineshape (ILS). A relation of this type exists for every spectrometer and ultimately limits its resolving power. The spectrum of a monochromatic source under finite maximum optical path limits (ILS) is presented in fig(2.3a)

2.5) Apodization and Resolution

Apodization

If we refer to fig(2.3) we observe that there are positive and negative side lobes besides the central peak of finite width which one can tolerate as an approximation to the monochromatic line within the resolution limit imposed by the truncation.

When an interferogram fails to decay to zero at maximum optical path difference the apparatus function tends to introduce spurious features in the computed spectrum, and they could be mistaken for real spectral features. It is therefore necessary to make the interferogram decay to zero smoothly at maximum optical path difference. We can achieve this by multiplying the interferogram function $I_c(x)$ in (2.10) by a triangular function $A(x)$ which is defined as

$$A(x) = 1 - |x/L| \quad \text{for} \quad -L \leqslant x \leqslant +L \tag{2.35}$$

The function $A(x)$ is called an apodizing function. Thus we obtain the computed apodized spectrum as

$$B(\nu) = \int_{-\infty}^{+\infty} I_c(x)\, A(x)\, e^{-i2\pi\nu x}\, dx \tag{2.36}$$

Now applying the condition established for the apodizing function in (2.35), and also since the interferogram function from a monochromatic line is the cosine distribution as given in (2.29), then using (2.29) and (2.35), relation (2.36) reduces to

$$B(\nu) = 2 \int_{-L}^{+L} (1 - |x/L|)\, \cos(2\pi\nu_o x)\, e^{-i2\pi\nu x}\, dx \tag{2.37}$$

Using Euler's formula we have

$$B(\nu) = 2 \int_{-L}^{+L} (1-|x/L|)\, \cos 2\pi\nu_o x (\cos 2\pi\nu x - i \sin 2\pi\nu x)\, dx \tag{2.38}$$

and then using a trigonometric identity, and dropping the $\cos[2\pi(\nu + \nu_o)x]$ term since its contribution is very small, equation (2.38) reduces to

$$B(\nu) = \int_{-L}^{+L} (1 - |x/L|) \cos[2\pi(\nu - \nu_o)x]\, dx \tag{2.39}$$

$$= \frac{2\{1 - \cos[2\pi(\nu - \nu_o)]L\}}{[2\pi(\nu - \nu_o)]^2 L} \tag{2.40}$$

Again using a trigonometric relation, we have

$$B(\nu) = L \operatorname{sinc}^2 [\pi (\nu - \nu_o) L] \qquad (2.41)$$

Besides triangular apodization there are several other functions commonly used for apodization, of which two are

$$A(x) = [1 - (x/L)^2] \qquad (2.42)$$

and

$$A(x) = \cos (\pi x/2L) \quad . \qquad (2.43)$$

The Fourier transform of the triangular apodization function itself can be given as $L\operatorname{sinc}^2[\pi\nu L]$, which has positive side lobes and theoretically represents the same apparatus function as that of a grating spectrometer. For a monochromatic input we obtain the output as given by (2.41).

The apodization process is of course not limited to a monochromatic input only, but can equally be applied to the case of a polychromatic input which can be considered as a linear superposition of Dirac delta functions. From fig(2.3) we see the effects of triangular apodization. The line width is broadened and consequently the resolution obtainable will be decreased. But on the other hand we notice that the undesirable side lobes are all positive and are considerably smaller than in the case of the unapodized spectrum produced by the apparatus function. As a result an improved spectral profile is obtained. The process of removing the unwanted feet is termed apodization, and is widely used in Fourier transform spectroscopy.

Resolution

The spectral resolution obtained in Fourier spectroscopy is primarily determined by the maximum path difference attained during the interferogram recording. When no apodization is applied to the spectrum the instrumental line shape is given by "sinc y", where $y = 2\pi(\nu - \nu_0)L$. This type of relation exists for all spectrometers and provides the basis for estimates of the resolving power.

One possible definition of the resolution can be obtained from the width of the sinc function at half its peak value, normally called the half width. From fig(2.3b) we observe that the intensity drops to half its peak value when $y = \pm 0.607\pi$. Hence the full half-width is of the order of 1.21π. Therefore when $y = 1.21\pi = 2\pi(\nu - \nu_0)L$ we obtain the resolution of the interferometer in terms of wavenumber as

$$\Delta\nu = \frac{1.21}{2L} \qquad (2.44)$$

Thus we arrive at a simple definition of the resolution available with a Michelson interferometer, namely that it is approximately the reciprocal of twice the maximum mirror movement from the zero optical path difference position.

Resolution can also be defined in terms of the Rayleigh criterion, which considers two neighbouring lines in a spectrum. Thus for any two spectral elements to be resolved, their respective contributions to the interferogram must be out of phase by at least 2π [Martin (1967)], i.e they are separated

such that the peak of one resonance falls at the first zero of the other resonance. If we assume that the two resonances have instrumental line shapes given by $\text{sinc}^2 (y/2)$, then for a monochromatic input the intrumental line shape for a triangularly apodized interferogram is given in the form of (2.41) i.e,

$$B_A(\nu) \propto \text{sinc}^2 (y/2) \qquad (2.45)$$

For the same input the unapodized instrumental line shape can be written as

$$B_U(\nu) \propto \text{sinc} (y) \qquad (2.46)$$

According to the Rayleigh criterion the separation between the peaks of the two resonances in terms of 'y' is given for (2.45) as

$$2\pi = (y_o - y') \qquad (2.47)$$

where $$y_o = [2\pi(\nu - \nu_o)L] \qquad (2.48)$$

and $$y' = [2\pi(\nu - \nu')L] \qquad (2.49)$$

where L is the maximum optical path difference and the two resonant frequencies are ν_o and ν'. Substituting the values of y and y' in (2.47) we arrive at the definition of resolution for a triangularly apodized interferogram, i.e,

$$(\nu' - \nu_o) = \Delta\nu = 1/L \qquad (2.50)$$

We may consider (2.50) as a measure of the resolution of an interferometer, but we cannot give a fixed definition of the resolution for a Michelson interferometer because of the effects of apodization. However, in every case we reach the same general conclusion that the resolution of an interferometer varies

inversely as the maximum optical path difference.

2.6) Sampling and the phenomenon of aliasing

As we have seen earlier, the interferogram function $I_c(x)$ and the spectral distribution $B(\nu)$ are the Fourier transforms of each other. The spectrum can therefore be obtained by determining the integral of the relation given in (2.11), and the interferogram by its Fourier transform. In order to solve (2.11) using a digital computer it is necessary for the interferogram to be digitised into a number of discrete values which are the input data of the computer. Hence we record the interferogram at equal intervals of optical path differnce to make use of the fast Fourier algorithm of Cooley and Tukey (1965).

Since the interferogram is to be recorded in equal steps, we have to refer to our Eq(2.11), and have to replace the integration by a summation. Hence the sample interferogram, $I_s(x)$, so obtained is not the continuous interferogram $I_c(x)$. The two interferograms however, can be related with the help of the Shah function :

$$I_s(x) = \text{Ш}\left(\frac{x}{\Delta x}\right) I_c(x) \qquad (2.51)$$

where $\text{Ш}\left(x/\Delta x\right)$ is the Shah function, which allows only those values for the sampled interferogram for which

$x = 0, \pm\Delta x, \pm 2\Delta x, \pm 3\Delta x, + - - - - -$

The distance Δx between the successive sampling points is the sampling distance. Mathematically the Shah function is defined as an infinite sum of Dirac delta functions i.e,

$$\text{Ш}(x) = \sum_{N=-\infty}^{N=+\infty} \delta(x - N) \qquad (2.52)$$

where N is an integer. Using the property of the Shah function which states that the inverse Fourier transform of a Shah function is a Shah function, we can deduce the effects of the sampling procedure on the final computed spectrum, and also using the definition of the delta function and change of variable relation from Bell (1972) we have

$$\mathcal{F}^{-1}\{\text{Ш}(\Delta x)\} = (1/\Delta)\ \text{Ш}(\nu/\Delta) \qquad (2.53)$$

Here the symbol $\mathcal{F}$ represents the Fourier transform, recalling that the sampled spectrum $B_s(\nu)$ can be defined from Eq(2.11) as

$$B_s(\nu) = \mathcal{F}^{-1}\{I_s(x)\} \qquad (2.54)$$

and the complete spectrum

$$B_c(\nu) = \mathcal{F}^{-1}\{I_c(x)\} \qquad (2.55)$$

After taking the inverse Fourier transform of (2.51) we get

$$\mathcal{F}^{-1}\{I_s(x)\} = \mathcal{F}^{-1}\{\text{Ш}(x/\Delta x)\ I_c(x)\} \qquad (2.56)$$

Now substituting the values from (2.51) and (2.55) and using the convolution theorem we have

$$B_s(\nu) = \mathcal{F}^{-1}\{\text{Ш}(x/\Delta x)\} * B_c(\nu) \qquad (2.57)$$

Now applying the property of the Shah function stated in (2.53) we get

$$B_s(\nu) = \Delta x\ \text{Ш}(\nu\Delta x) * B_c(\nu) \qquad (2.57a)$$

which leads to

$$\mathcal{F}^{-1}\{I_s(x)\} = B_s(\nu) = \sum_{N=-\infty}^{N=+\infty} B_c(\nu - N\Delta\nu) \qquad (2.58)$$

where $$\Delta\nu = 1/\Delta x \qquad (2.59)$$

Hence the complete spectrum is obtained for $\nu = N\Delta\nu$ for all values of N when we compute the inverse Fourier transform of the sampled interferogram.

We can easily identify the region of frequency from zero to maximum if the repeated spectra do not overlap. Overlapping i.e, aliasing of these spectra may occur depending on the magnitude of $\Delta\nu$. If we choose the value of Δx to be very small, then by (2.59) the value of $\Delta\nu$ will be very large and therefore the spectra will be separated, but, on the other hand, if Δx is very large then there will be bad overlapping and then it will be rather difficult to determine the true spectrum from the sampled interferogram. Fig(2.4) shows clearly the aliasing phenomenon. A continuous interferogram $I_c(x)$ recorded on both sides of zero optical path position gives both positive and negative frequency values for a continuous spectrum $B_c(\nu)$, that is, from $-\nu_{max}$ to $+\nu_{max}$. Fig(2.4a) shows a solid curve and dashed curve representing positive and negative spectra, respectively, as computed from a sampled interferogram. Fig(2.4b) shows the total spectrum as would be computed from the sampled interferogram.

The separation of spectra can be achieved by making $\Delta\nu$ big enough such that the contribution from the maximum positive frequency spectrum does not overlap with the negative one. This can be achieved by setting

$$\Delta x \leq 1/2\nu_{max} \qquad (2.60)$$

which shows that the largest frequency now permitted is directly related to the sampling interval.

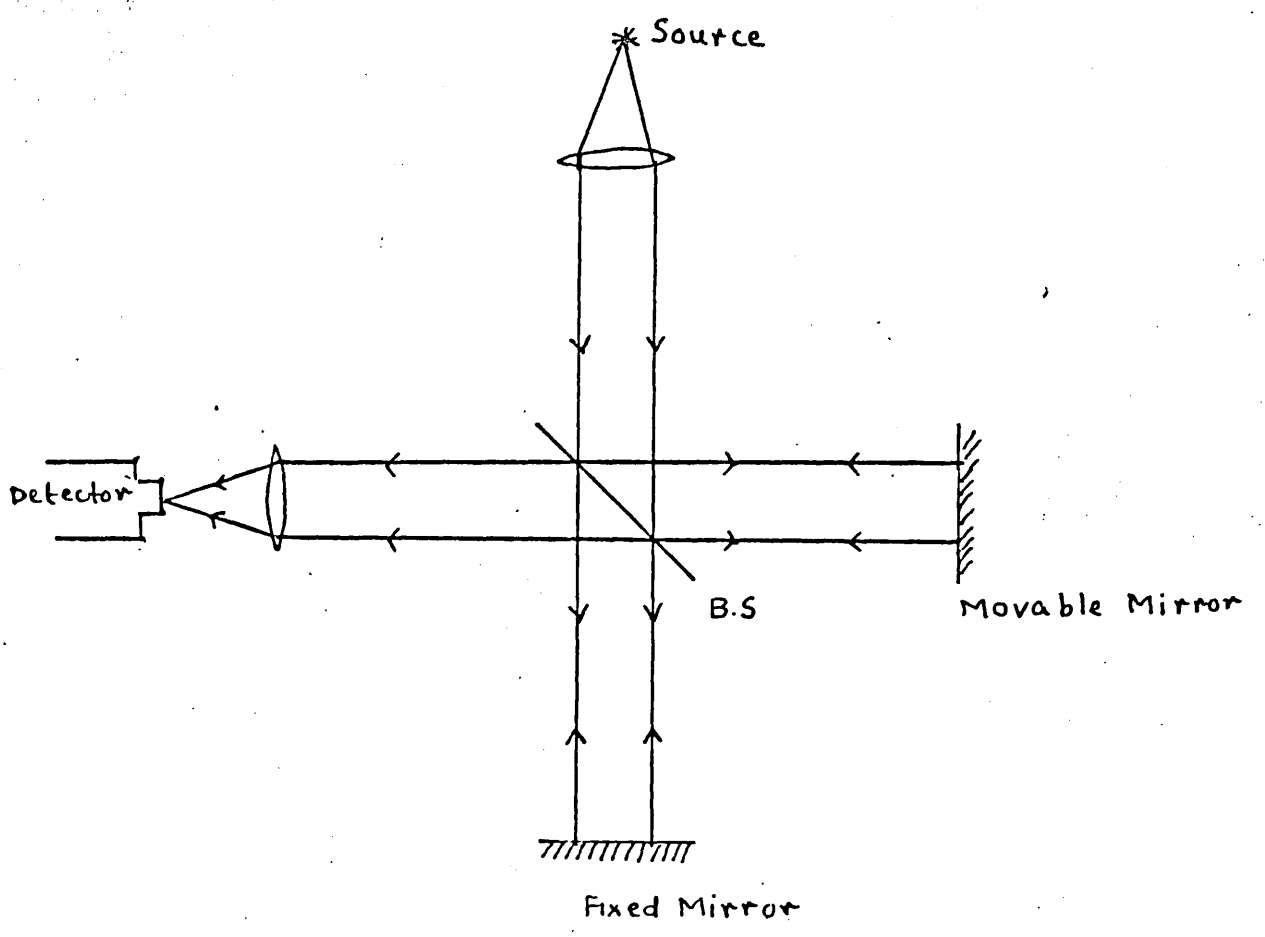

Fig(2.1) Michelson two beam interferometer

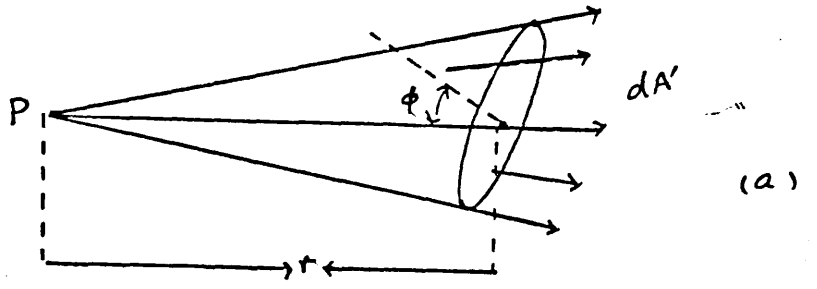

Fig(2,2) Optical diagram of point source together with collecting optics.

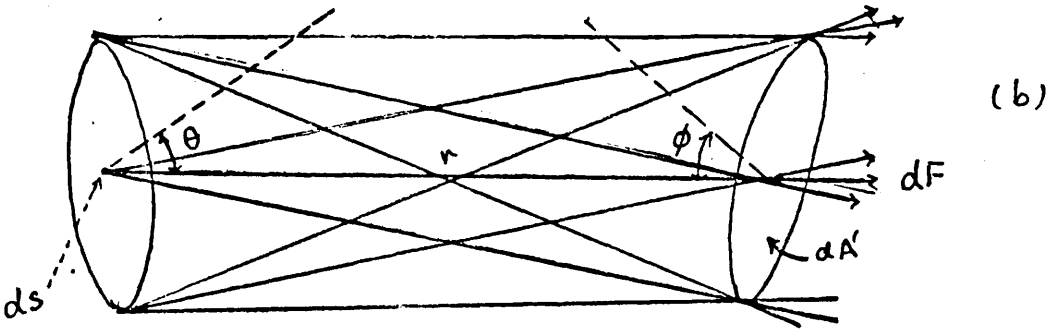

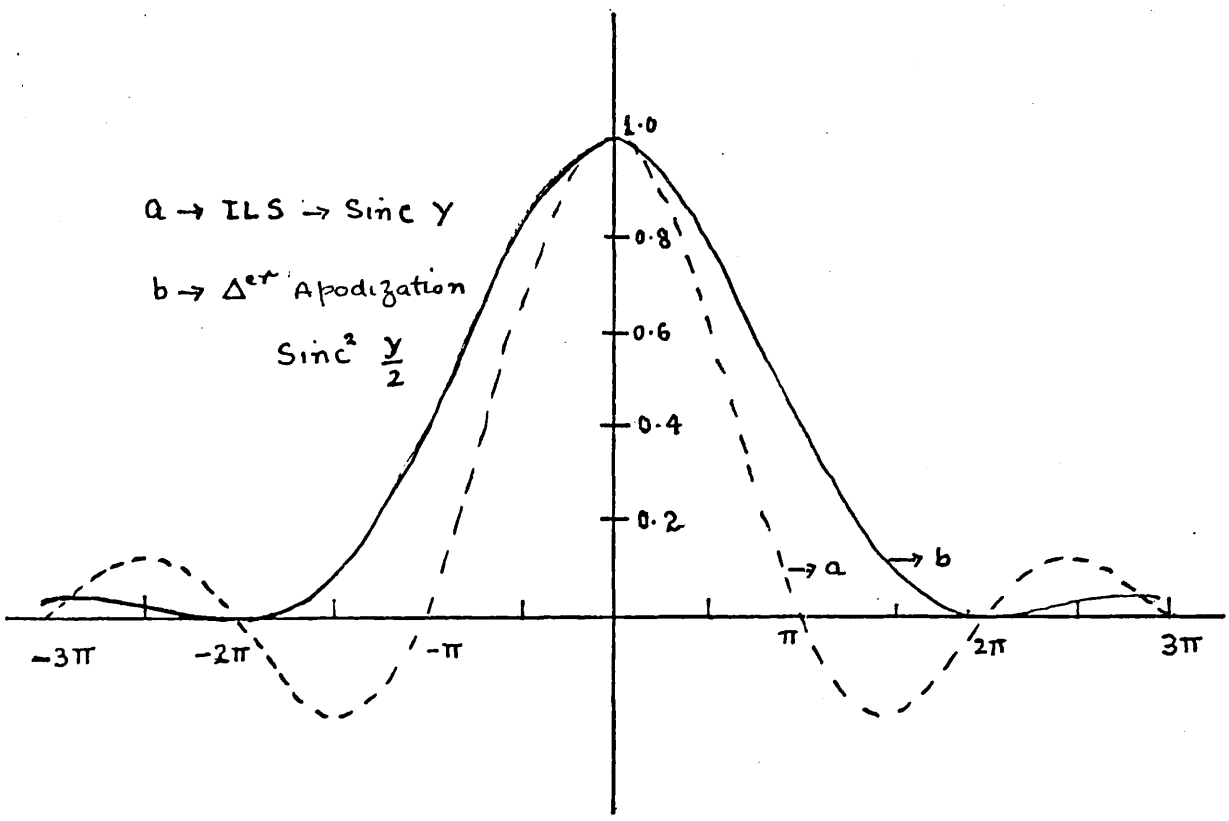

Fig(2.3) Effects of triangular apodization on ILS

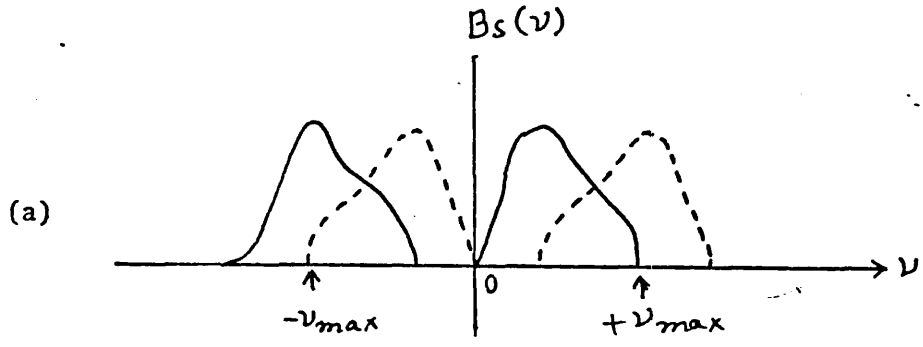

Computed spectral components of a sampled interferogram

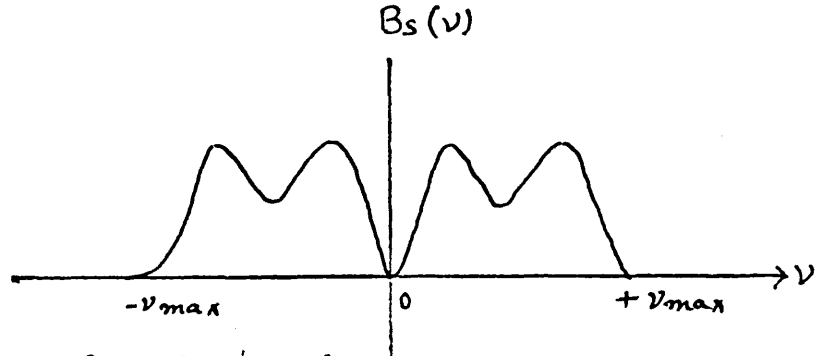

Total spectrum for all spectral components

Fig(2.4) Represents the phenomenon of aliasing

CHAPTER III

GENERAL ASPECTS OF DISPERSIVE FOURIER TRANSFORM SPECTROSCOPY

3.1) Introduction

In conventional FTS in the millimetre and submillimetre region the optical constants of a medium have usually been determined from the measured power reflection or power transmission spectrum of a specimen by the use of an indirect analysis like the Kramers-Kronig method [Robinson and Price (1953)].

The recent development of dispersive FTS, in which the amplitude attenuation and phase shift produced by a specimen are directly measured, provides a precise method for obtaining the optical constants without the use of the Kramers-Kronig relations [Russell and Bell (1966), Bell (1966), Chamberlain (1969), Chantry (1971), Birch and Parker (1979)].

The main difference between the two techniques is the positioning of the specimen in the interferometer. In FTS the specimen is usually placed in the combined beam in front of the detector, and because of the symmetry of the measurement the phase shift caused by the specimen is present in both the partial beams, and hence it cannot be recovered from the intensity pattern at the detector. Therefore only one quantity, the power attenuation of the specimen, is measured. Thus it is not possible to calculate both optical constants directly.

In dispersive FTS, on the other hand, the specimen is placed in one of the arms of the interferometer and either the complex spectral transmittance or reflectance can be measured,

depending on the optical configuration of the interferometer. Therefore, when the specimen is introduced in one of the interferometer arms, the interferogram becomes asymmetric. Each spectral component is now reduced in amplitude and its phase is shifted. The ratio of the complex Fourier transforms of the interferograms recorded with and without the specimen yields the complex spectrum which contains both the amplitude attenuation and phase shift caused by the specimen. Hence a single measurement can determine two quantities which are directly related to the extinction coefficient and refractive index.

For the determination of the optical constants from the technique of dispersive FTS the measurement of the phase spectrum requires high stability of the optical path lengths in the arms of the interferometer, and the way in which this stability is achieved is described in chapter 4. Now comes the choice of interferometer configuration, which is dictated by the nature and behaviour of the specimen under study. Three basic interferometric configurations are illustrated in fig (3.1). For transmitting specimens the optical arrangement is shown in fig (3.1a). In this arrangement the specimen is placed in the fixed mirror arm of the interferometer and the radiation passes through it twice, and this is called a double pass measurement. For those specimens which are highly absorbing but still marginally transparent the optical arrangement is modified. Here the optics is so arranged that the radiation only passes through the specimen once, and this is termed a single pass measurement, and is shown in fig (3.1b). For very highly absor-

bing substances, the reflection instrument is illustrated in fig (3.1c), and here the specimen replaces the fixed mirror of the interferometer. The detailed mechanism for achieving this is dealt with in chapter 4.

3.2) Complex index of refraction

The transmission of infra red radiation through a medium and its behaviour at the interface between two media is explained by Maxwell's field equations. These equations are

$$\text{Curl } \underline{E} = -\frac{\partial \underline{B}}{\partial t} \tag{3.1}$$

$$\text{Curl } \underline{H} = J + \frac{\partial \underline{D}}{\partial t} \tag{3.2}$$

$$\text{div } \underline{B} = 0 \tag{3.3}$$

$$\text{div } \underline{D} = \rho \tag{3.4}$$

where $\underline{E}$ is the electric field, $\underline{B}$ the magnetic induction, $\underline{H}$ the magnetic field and $\underline{D}$ the electric displacement. J and ρ represent the current and charge densities, respectively. The response of the conduction electrons to the electric field is given by Ohm's law

$$J = \sigma \underline{E} \tag{3.5}$$

where σ is the electrical conductivity. The constitutive relation between the electric displacement $\underline{D}$ in terms of the dielectric permittivity of vacuum ε_o and polarization $\underline{P}$ which represents the electric dipole moment per unit volume is given as

$$\underline{D} = \varepsilon_o E + \underline{P} \tag{3.6}$$

Now the dielectric susceptibility or the polarizability, χ can be

defined by

$$\underline{P} = (\varepsilon - \varepsilon_0)\ \underline{E} \tag{3.7}$$

$$= \chi \varepsilon_0 \underline{E} \tag{3.8}$$

where

$$\chi = \frac{\varepsilon}{\varepsilon_0} - 1 \tag{3.9}$$

In the case of an isotropic medium the quantity χ is a scalar, having the same value for any direction of the applied electric field, but for an anisotropic medium the magnitude of the polarization varies with the direction of the applied field.

If we now consider a homogeneous electrically neutral medium, then the charge density $\rho = 0$, and therefore we can rewrite (3.1-3.4) as

$$\text{Curl } \underline{E} = -\mu\mu_0 \frac{\partial \underline{H}}{\partial t} \tag{3.10}$$

$$\text{Curl } \underline{H} = \sigma \underline{E} + \varepsilon\varepsilon_0 \frac{\partial \underline{E}}{\partial t} \tag{3.11}$$

$$\text{div } \underline{H} = 0 \tag{3.12}$$

$$\text{div } \underline{D} = 0 \tag{3.13}$$

taking the curl of (3.10) and applying (3.11) we get

$$\text{Curl Curl } \underline{E} = -\mu\mu_0 \varepsilon\varepsilon_0 \frac{\partial^2 \underline{E}}{\partial t^2} + \mu\mu_0 \sigma \frac{\partial \underline{E}}{\partial t} \tag{3.14}$$

therefore $$\nabla^2 \underline{E} = \mu\mu_0 \varepsilon\varepsilon_0 \frac{\partial^2 \underline{E}}{\partial t^2} + \mu\mu_0 \sigma \frac{\partial \underline{E}}{\partial t} \tag{3.15}$$

Thus by eliminating the magnetic field vector from Maxwell's equations we have deduced the wave equation of the electric field vector $\underline{E}$. A solution of (3.15) can be written as

$$\underline{E} = \underline{E}_0 \exp i(K \cdot r - wt) \tag{3.16}$$

where w is the angular frequency of the radiation and K is the

wave vector, of magnitude $|K| = 2\pi/\lambda$, where λ is the wave length of the radiation, and r is a vector. If we consider a simple example of a wave travelling in the positive z direction, then we have a plane wave

$$\underline{E} = E_o \exp i(Kz - wt) \qquad (3.17)$$

which is the solution of a second order differential equation, i.e,

$$\frac{\partial^2 \underline{E}}{\partial z^2} = \mu\mu_o \varepsilon\varepsilon_o \frac{\partial^2 \underline{E}}{\partial t^2} + \mu\mu_o \sigma \frac{\partial \underline{E}}{\partial t} \qquad (3.18)$$

Thus, substituting (3.17) in (3.18) then yields the square of K as

$$\hat{K}^2 = w^2\mu\mu_o \left(\varepsilon\varepsilon_o + i\frac{\sigma}{w} \right) \qquad (3.19)$$

$$\hat{K} = w\left\{\mu\mu_o\varepsilon\varepsilon_o + \mu\mu_o i\frac{\sigma}{w}\right\}^{\frac{1}{2}} \qquad (3.20)$$

For free space the wave vector is a real quantity, hence we see that in a medium the phase velocity of a plane wave propagating is given as K/w. Also, since we are concerned here with non-magnetic materials, $\mu = 1$. Hence (3.20) reduces to

$$\hat{K} = w\left\{\mu_o\varepsilon\varepsilon_o + i\mu_o\frac{\sigma}{w}\right\}^{\frac{1}{2}} \qquad (3.21)$$

We see that in a crystal the phase velocity is modified by the factor n which is given as

$$\hat{n} = (c/w)\,\hat{K} \qquad (3.22)$$

Here $\hat{n}$ represents the complex refractive index. Substituting the value of the phase velocity K/w from (3.21) in (3.22) we have

$$\hat{n} = c\left[\mu_o\left(\varepsilon\varepsilon_o + i\frac{\sigma}{w}\right)\right]^{\frac{1}{2}} \qquad (3.23)$$

but since

$$c = (1/\mu_0 \varepsilon)^{\frac{1}{2}} \qquad (3.24)$$

therefore (3.23) reduces to

$$\hat{n} = \left(\varepsilon + \frac{i\sigma}{\omega \varepsilon_0}\right)^{\frac{1}{2}} = n + ik \qquad (3.25)$$

and also

$$\hat{n} = (\hat{\varepsilon})^{\frac{1}{2}} \qquad (3.26)$$

where n is the real refractive index, k is the extinction coefficient, and $(\hat{\varepsilon})$ stands for the complex dielectric constant. By a variety of measurements like reflection and transmission these quantities are measured in dispersive FTS. By squaring and equating real and imaginary parts in (3.26) we get

$$n^2 - k^2 = \varepsilon' \qquad (3.26a)$$

$$2nk = \frac{\sigma}{\varepsilon_0 \omega} = \varepsilon'' \qquad (3.27)$$

Thus the real and imaginary parts of the complex dielectric constant are presented as

$$\hat{\varepsilon} = \varepsilon' + i\varepsilon'' \qquad (3.28)$$

and from (3.22) we have

$$n + ik = (c/w)\hat{K} \qquad \hat{K} = nw/c + ikw/c \qquad (3.28a)$$

The effects of absorption due to a medium through which the wave propagates can be determined by putting (3.28a) into the equation for a plane wave (3.16).

Hence

$$\underline{E} = \underline{E}_0 \exp\left[iw\,(nz/c - t)\right] \exp\,(-kwz/c) \qquad (3.29)$$

The above equation represents a wave progressing in the direction of the wave vector, i.e the z direction, and the term n/c in the first exponential gives the reciprocal phase velocity in the z direction. Hence the relative decrease in the amplitude

of the wave vector per unit length is exp (-kw/c). The damping, of course, is due to absorption of electromagnetic radiation in the medium.

Since the energy in the wave at a given point is proportional to $|E|^2$, then the energy varies with distance as exp(-2kw/c). Hence 2kw/c is the power absorption coefficient per unit length within the medium and is normally written as

$$\alpha = 2kw/c = 4\pi k/\lambda = 4\pi k\nu \qquad (3.30)$$

where λ is the wavelength and ν is given in wave numbers.

3.3) Fresnel's relations

When electromagnetic radiation passes from a medium of complex refractive index $\hat{n}_1$ (in our case vacuum) to one of complex refractive index $\hat{n}_2$ the change in the electric and magnetic fields is continuous and takes place within a thin transmission layer at the boundary. Hence to satisfy the law of conservation of energy we have to apply the above mentioned boundary conditions.

Thus the most general form of Fresnel's relations using these boundary conditions can be given for the components of the reflected and transmitted waves in terms of the complex index of refraction of the two media as [Born and Wolf 1970]

$$\hat{r}_{\parallel} = \frac{\hat{n}_1\cos\theta_t - \hat{n}_2\cos\theta_i}{\hat{n}_1\cos\theta_t + \hat{n}_2\cos\theta_i} \qquad (3.31)$$

$$\hat{r}_{\perp} = \frac{\hat{n}_1\cos\theta_i - \hat{n}_2\cos\theta_t}{\hat{n}_1\cos\theta_i + \hat{n}_2\cos\theta_t} \qquad (3.32)$$

$$\hat{t}_{\parallel} = \frac{2n_1 \cos\theta_i}{n_1 \cos\theta_t + n_2 \cos\theta_i} \tag{3.33}$$

$$\hat{t}_{\perp} = \frac{2n_1 \cos\theta_i}{n_1 \cos\theta_i + n_2 \cos\theta_t} \tag{3.34}$$

In Eqs (3.31-3.34), each wave is resolved into components parallel (denoted by $\parallel$) and perpendicular (subscript $\perp$) to the plane of incidence, and $\hat{t}$ and $\hat{r}$ are the amplitude transmission and amplitude reflection coefficients, respectively. Here θ_i and θ_t refer to the angles of incidence and of refraction or transmission, respectively.

For normal incidence we have $\theta_i = 0$, and consequently $\theta_t = 0$. Also, if we consider medium 1 to be vacuum then $n_1 = 1$, and therefore the above set of relations reduces to

$$\hat{r} = r_{\parallel} = \hat{r}_{\perp} = \hat{r}_{12} = (1 - \hat{n}_2)/(1 + \hat{n}_2) \tag{3.35}$$

and $$\hat{t} = \hat{t}_{\parallel} = \hat{t}_{\perp} = \hat{t}_{12} = 2/(1 + \hat{n}_2) \tag{3.36}$$

Hence for normal incidence the distinction between parallel and perpendicular components disappears. The subscript order in the above relations indicates incidence from medium 1 on to medium 2. If the order is reversed i.e, now the incidence is from medium 2 onto medium 1, then we have

$$\hat{r}_{21} = -\hat{r}_{12} \tag{3.37}$$

and $$\hat{t}_{21} = \hat{n}_2 \hat{t}_{12} \tag{3.38}$$

A more suitable form of (3.35-36) which provides the attenuation and phase terms, can be given in the exponential form i.e

$$\hat{r}_{12} = r_{12} \exp i\phi_{12} \tag{3.39}$$

The equation above represents the complex attenuation of an

electric field vector on suffering reflection at the interface, and the amplitude attenuation and phase shift are given by quantities like γ_{12} and ϕ_{12}^{r} respectively.

If we now consider normal incidence then the power reflection coefficient can be obtained from (3.35) by using the relation $\hat{n} = n + ik$, and dropping the subscript on $\hat{n}$ we have

$$\hat{r}_{12} = r_{12} \exp i\hat{\phi}_{12} = [1 - (n + ik)]\,[1 + (n + ik)]^{-1} \qquad (3.40)$$

Now equating real and imaginary parts in (3.40) then yields

$$r_{12} \cos\phi = [(1 - n^2 - k^2)]\,[(n + 1)^2 + k^2)]^{-1}$$

$$r_{12} \sin\phi = (2k)\,[(n + 1)^2 + k^2)]^{-1} \qquad (3.41)$$

Hence from (3.41) we have

$$\tan\phi = (2k)\,[(n^2 + k^2 - 1)]^{-1} \qquad (3.42)$$

$$\text{also} \qquad r^2 = \{[(1 - n)^2 + k^2)] \cdot [(1 + n)^2 + k^2)]^{-1}\} \qquad (3.43)$$

Considering now the limiting behaviour of the absorption index, we can derive the relation for the change in phase which takes place due to reflection from transparent and opaque media for normal incidence from vacuum

$$\text{Thus} \qquad \lim_{K \to 0} \hat{\phi}_{12} = \lim_{K \to 0} \tan^{-1} [(2k)/(n^2 - 1)] \qquad (3.44)$$

$$\text{and} \qquad \lim_{K \to \infty} \phi_{12}^{r} = \lim_{K \to \infty} \tan^{-1} [2/k] \qquad (3.45)$$

Since the refractive index is chosen to be greater than unity for the medium, therefore ϕ_{12}^{r} is of the order of π radians. For an opaque medium the result is very useful in dispersive

reflection measurements, where we compare the complex reflectivity of the unknown substance (in this case a solid) under study with that of a reference silvered surface, since for the silvered surface the phase ϕ_{12} is normally π radians.

Before we derive the exact form of the power transmission coefficient it is to be borne in mind that while the power reflectivity of the interface is r_{12}^2, the quantity $\hat{t}_{12}^2$ is not the power transmission coefficient. The correct form of the power transmission coefficient is given by the expression

$$t_{12}^2 = 1 - r_{12}^2 \tag{3.46}$$

Thus following the process of deriving the amplitude reflection coefficient we can write the amplitude transmission coefficient in complex form as

$$\hat{t}_{12} = t_{12} \exp i\phi_{12}^t \tag{3.47}$$

Thus from (3.47) we have

$$\tan\phi = (-k)/(n+1)$$

$$\phi = \tan^{-1}[(-k)/(n+1)] \tag{3.48}$$

where $t_{12}^2 = \left[4[(1+n)^2 - (k)^2] / [(1+n)^2 + (k)^2] \right]$ (3.49)

represents the power transmission coefficient.

3.4) The interface effects of a plane parallel specimen

When a plane EM wave of wavenumber ν is propagated through a medium of refractive index $n(\nu)$, and absorption index k then its amplitude is attenuated according to $\exp[-\frac{\alpha(\nu)}{2} \cdot x]$, where $\alpha = 4\pi\nu k$, and its phase is shifted by a factor $[2\pi\nu n(\nu)\ x]$, where x is the distance through which the radiation travels in the medium. The combined efects of these two quantities can be

represented in terms of a complex quantity called the complex propagation factor of the medium represented as

$$\hat{a} = \exp\left[-\alpha x/2\right] \exp\left[2\pi i n \nu x\right] \qquad (3.50)$$

$$\hat{a} = \exp\left[2\pi i \nu \hat{n} x\right] \qquad (3.51)$$

Here $\hat{a}$ is the complex propagation factor within the medium and is given in terms of the complex refractive index $\hat{n}$.

If we assume that the medium is bounded between two parallel planes, as shown in fig (3.2), i.e, at x=0 and x=d, then part of the incident radiation is reflected from the surface at x=0, i.e, at the first boundary and the rest of it passes through the medium and suffers attenuation in amplitude and phase at the second boundary i.e, at x=d, as described above. Part of this penetrates the second boundary but a fraction is reflected back to the first where partial transmission and reflection again take place. This phenomenon repeats, leading to a multiply reflected beam within the medium. The direct beam suffers reflection losses at the boundaries in addition to attenuation within the medium, and similar losses are suffered by the multiply reflected beam, with the consequence that it becomes weaker as the number of reflections and transits of the layer increases. The emerging components become correspondingly weaker. Therefore the resultant transmitted amplitude is the sum of the direct transmitted beam and the multiply reflected beams.

Let us now consider a beam of radiation of unit amplitude incident on a plane parallel specimen of refractive index $\hat{n}_2$(i.e medium 2), surrounded by medium 1 of refractive index n_1 (generally vacuum). As we have described above, the incident

radiation suffers multiple internal reflection at the interfaces, and the resultant electric field amplitude which is the sum of the reflected and transmitted partial waves, as seen in fig (3.2), can be given as

$$\hat{T}_{12} = \hat{t}_{12}\,\hat{a}_2\,\hat{t}_{21} + \hat{t}_{12}\,\hat{a}_2^3\,\hat{r}_{21}^2\,\hat{t}_{21} + \hat{t}_{12}\,\hat{a}_2^5\,\hat{r}_{21}^4\,\hat{t}_{21} + \qquad (3.52$$

$$\hat{R}_{12} = \hat{r}_{12} + \hat{t}_{12}\,\hat{a}_2^2\,\hat{r}_{21}\,\hat{t}_{21} + \hat{t}_{12}\,\hat{a}_2^4\,\hat{r}_{21}^3\,\hat{t}_{21} + \qquad (3.53)$$

Equation (3.52) can also be written as

$$\hat{T}_{12} = \hat{t}_{12}\,\hat{t}_{21}\,\hat{a}_2 \sum_{m=0}^{m=\infty} (\hat{a}_2\,\hat{r}_{21})^{2m} \qquad (3.54)$$

Then, since from Fresnel's relations, i.e, (3.37-38) we have

$$\hat{r}_{21} = -\,\hat{r}_{12} \qquad (3.55)$$

equation (3.54) reduces to

$$\hat{T}_{12} = (1 - \hat{r}_{12}^2)\,a_2\,\hat{M}_{12} \qquad (3.56)$$

In this equation $\hat{t}_{12}\,\hat{t}_{21} = (1 - \hat{r}_{12}^2)$ (3.57)

gives the fraction of the complex amplitude remaining after boundary reflection losses from the direct beam and

$$\hat{M}_{12} = \sum_{m=0}^{m=\infty} (\hat{a}_2\,\hat{r}_{21})^{2m} \qquad (3.58)$$

gives the relation for multiple reflections for $(m \geq 1)$. In (3.52) and (3.53) quantities like $\hat{r}_{12}$ and $\hat{r}_{21}$ represent the complex amplitude reflection factor and $\hat{t}_{12}$ and $\hat{t}_{21}$ represent the complex transmisson factor, and $\hat{a}$ is the complex propagation factor for a distance equal to the thickness of the specimen. Relations (3.52-53) are the most useful form of the complex transmission and reflection coefficients of a plane parallel specimen, and are widely used in dispersive FTS and FTS.

In dispersive FTS the phase sensitivity of the interferome-

ter resolves the contribution of each partial wave given in Eqs(3.52-53). Thus the first term in relation (3.52) is the single pass transmission coefficient and the first term in (3.53) represents the front surface reflection coefficient of the specimen. For thick specimens, since the signatures in the recorded interferogram are well separated, therefore for the determination of the optical constants only the first term in (3.52) is needed. On the other hand, for the determination of the optical constants of thin specimens the contribution of all partial waves is to be taken into account. Therefore we can rewrite (3.52-53), after taking the sum of all the partial waves, as

$$\hat{T}_{12} = \frac{\hat{a}_2 (1 - \hat{r}_{12}^2)}{(1 - \hat{a}_2^2 \hat{r}_{12}^2)} \qquad (3.59)$$

$$\hat{R}_{12} = \frac{\hat{r}_{12} (1 - \hat{a}_2^2)}{(1 - \hat{a}_2^2 \hat{r}_{12}^2)} \qquad (3.60)$$

The full application of the above equations is discussed in the following section.

3.5) Relation between the interferogram and spectrum for dispersive FTS.

Before deriving the relation between the interferogram and the spectrum it is essential to introduce a complex quantity termed the complex insertion loss, because this is the factor which is measured in dispersive FTS. Chamberlain (1972) has investigated the role of the complex insertion loss in dispersive FTS using an elementary wave theory aproach. He defines the complex insertion loss,

$$\hat{L}(\nu) = L(\nu) \exp i\,\phi_L(\nu) \qquad (3.61)$$

as the ratio of the complex propagation of the specimen to the corresponding factor for a vacuum or reference surface. We will derive the relation between $\hat{L}(\nu)$ and the optical constants later in this chapter.

In order to determine the optical properties of a given crystal we will assume that our specimen is placed in the fixed mirror arm of the Michelson interferometer as shown in fig (3.1c) and that the law of linear superposition holds, and also that the electric fields are real functions.

The essential expression for the electric field propagating in a Michelson Fourier spectrometer in a vacuum can be given in terms of a Fourier integral as

$$\underset{\sim}{E} = \int_{-\infty}^{+\infty} E_o(\nu) \exp\,[2\pi i \nu(z-ct)]\, d\nu \qquad (3.62)$$

(Birch and Parker 1979), where $E_o(\nu)$ is the amplitude, z is a coordinate in the directon of propagation and t is time. Thus if this electric field is propagated in the moving mirror arm, and the mirror is displaced by a distance $x/2$ from its optical zero path position, then the output from that arm can be written as

$$\hat{E}_1 = \int_{-\infty}^{+\infty} \hat{E}_o(\nu) \exp\,[2\pi i \nu (z + x - ct)]\, d\nu \qquad (3.63)$$

If we now consider a specimen of complex insertion loss $\hat{L}(\nu)$ as defined by (3.61) placed in the fixed mirror arm, then the modified output beam can be given as

$$\hat{E}_2 = \int_{-\infty}^{+\infty} \hat{E}_o(\nu)\, L(\nu) \exp i[2\pi (z - ct) + \phi_L(\nu) + \phi_o(\nu)]\, d\nu \qquad (3.64)$$

Here $\phi_o(\nu)$ is a residual phase difference corresponding to a small error in the path difference

i.e $$\phi_o(\nu) = 2\pi\nu\xi_o(\nu) \qquad (3.65)$$

This phase difference can arise due to lack of symmetry in the interferometer caused by imperfect alignment, or it can be caused if we ignore the effects of compensating windows, which are employed in the interferometer.

Now invoking the law of linear superposition the resultant electric field amplitude, which is the sum of the amplitudes from the two arms of the interferometer propagating towards the detector, is

$$\hat{E}_R = \hat{E}_1 + \hat{E}_2 = \int_{-\infty}^{+\infty} g(\nu, x) \exp [i2\pi\nu (z - ct)] \, d\nu \qquad (3.66)$$

where $g(\nu, x) = \hat{E}_o(\nu) [L(\nu) \exp i\phi(\nu) + \exp (2\pi i\nu x) \qquad (3.67)$

and $$\phi(\nu) = \phi_L(\nu) + \phi_o(\nu) \qquad (3.68)$$

The intensity reaching the detector is proportional to $g(\nu, x)\, g(\nu, x)^*$, where * indicates the complex conjugate.

Therefore
$$I(x) = \int_{-\infty}^{+\infty} |g(\nu, x)|^2 \, d\nu \qquad (3.69)$$
$$= \int_{-\infty}^{+\infty} |E_o(\nu)|^2 [1 + L(\nu)^2] \, d\nu$$
$$+ 2\int_{-\infty}^{+\infty} |E_o(\nu)|^2 L(\nu) \cos [\phi(\nu) - 2\pi\nu x] \, d\nu$$

The first term in (3.69) is constant and is independent of the displacement, whereas the second term is the interference function. Therefore, the information on the spectrum is provided by

the varying part of the interference function, i.e, the cosine term and hence, using a trigonometric identity it can be written as the sum of two parts i.e, even and odd :

$$I_s(x) = \int_{-\infty}^{+\infty} \rho(\nu) \cos \phi(\nu) \cos (2\pi\nu x)\, d\nu + \int_{-\infty}^{+\infty} \rho(\nu) \sin \phi(\nu) \sin (2\pi\nu x)\, d\nu \qquad (3.70)$$

The factor $\rho(\nu)$ in the equation above stands for $2 |F_o(\nu)|^2 L(\nu)$ and it is the factor which represents the transmitted power spectrum. Taking the sine and cosine transform of $I_s(x)$ we have

$$p(\nu) = \int_{-\infty}^{+\infty} I_s(x) \cos (2\pi\nu x)\, dx = \rho(\nu) \cos \phi(\nu) \qquad (3.71)$$

$$q(\nu) = \int_{-\infty}^{+\infty} I_s(x) \sin (2\pi\nu x) dx = \rho(\nu) \sin \phi(\nu) \qquad (3.72)$$

Hence the spectrum is given as

$$S(\nu) = p(\nu) + i\, q(\nu) = \rho(\nu) \exp i\phi(\nu) \qquad (3.73)$$

with a modulus $\rho(\nu) = [\, p^2(\nu) + q^2(\nu)\,]^{\frac{1}{2}}$ (3.74)

Thus from (3.71) and (3.72) we obtain the phase as

$$\phi(\nu) = \tan^{-1} [\, q(\nu)/\, p(\nu)\,] \qquad (3.75)$$

Now using relation (3.61), and with (3.68) and (3.70-73), we can relate the complex insertion loss to the complex Fourier transform of the interferogam :

$$\text{i.e,} \quad 2 |E_o(\nu)|^2 \hat{L}(\nu) \exp i\phi_o(\nu) = \int_{-\infty}^{+\infty} I_s(x) \exp (i 2\pi\nu x)\, dx \qquad (3.76)$$

Now the special case of the background interferogram with the specimen absent is included in the above treatment by replacing $I_s(x)$ by

$$I_o(x) = \int_{-\infty}^{+\infty} \rho_o(\nu) \cos [\phi_o(\nu) - 2\pi\nu x] \, d\nu \qquad (3.77)$$

where $$\rho_o(\nu) = 2 \left| \hat{E}_o(\nu) \right|^2 \qquad (3.78)$$

The cosine and sine transforms of (3.77) then yield

$$p_o(\nu) = \int_{-\infty}^{+\infty} I_o(x) \cos (2\pi\nu x) \, dx = \rho_o(\nu) \cos \phi_o(\nu) \qquad (3.79)$$

$$q_o(\nu) = \int_{-\infty}^{+\infty} I_o(x) \sin (2\pi\nu x) \, dx = \rho_o(\nu) \sin \phi_o(\nu) \qquad (3.80)$$

Therefore the background spectrum is written as

$$S_o(\nu) = p_o(\nu) + i\, q_o(\nu) = \rho_o(\nu) \exp i\phi_o(\nu) \qquad (3.81)$$

Here $S_o(\nu)$ is a complex quantity having a modulus

$$\rho_o(\nu) = [p_o^2(\nu) + q_o^2(\nu)]^{\frac{1}{2}} \qquad (3.82)$$

and a phase $\phi_o(\nu) = \tan^{-1} [q_o(\nu)/p_o(\nu)] \qquad (3.83)$

Ideally, $q_o(\nu)$ is zero, so that the computed spectrum $S_o(\nu)$ is real and $I_o(x)$ is even, but there is generally a small non-zero sine transform. Hence we have the spectrum as

$$\hat{S}_o(\nu) = \int_{-\infty}^{+\infty} I_o(x) \exp (i2\pi\nu x) \, dx \qquad (3.84)$$

Thus from (3.79 - 82) we have

$$2 \left| \hat{E}_o(\nu) \right|^2 \exp i\phi_o(\nu) = \int_{-\infty}^{+\infty} I_o(x) \exp (i2\pi\nu x) dx \qquad (3.85)$$

Hence we can obtain the complex insertion loss from (3.76) and (3.85) as the ratio of two complex Fourier transforms, and it can be given as

$$\hat{L}(\nu) = \frac{\int_{-\infty}^{+\infty} I_s(x) \exp (i2\pi\nu x) \, dx}{\int_{-\infty}^{+\infty} I_o(x) \exp(2i\pi\nu x) \, dx} \qquad (3.86)$$

$$\hat{L}(\nu) = \frac{FT\{I_s(x)\}}{FT\{I_o(x)\}} \qquad (3.86a)$$

The simple approach for obtaining the real values of the quantity $L(\nu)$ and $\phi_L(\nu)$ is to use sine and cosine Fourier transforms of the sample and background interferograms. Hence using (3.71) and (3.72), and (3.81 - 82), respectively, we get

$$L(\nu) = [\, p^2(\nu) + q^2(\nu) \,]^{\frac{1}{2}} \cdot [\, p_o^2(\nu) + q_o^2(\nu) \,]^{-\frac{1}{2}} \qquad (3.86b)$$

and

$$\phi_L(\nu) = \tan^{-1}[q(\nu)/p(\nu)] - \tan^{-1}[q_o(\nu)/p_o(\nu)] \qquad (3.86c)$$

Thus using the above two quantities we can obtain the complex refractive index, as shown in the following section.

3.6) Determination of optical constants by reflection

A suitable method for the determination of the optical constants of highly absorbing solids is by measuring their front surface complex amplitude reflection coefficient (Bell 1966). We can obtain the simplest relation for reflection from a single surface of the crystal provided we consider normal incidence.

In a Michelson interferometer the measurement at normal incidence is possible since the radiation after reflection from the front surface of the sample may return to the beam divider along the same path as that of the incident radiation.

In practice it is necessary to record first the background interferogram $I_o(x)$ i.e, no sample in the beam, and then to obtain the interferogram $I_s(x)$ with the sample replacing the mirror in the fixed mirror of the spectrometer, as illustrated in fig (3.3). It is necessary, however, for the end mirror to be accurately replaced in position by the sample so that there will be no unknown shift in the position of zero optical path difference in the interferometer. Since the sample is highly absorbing only the first term in (3.53) describing amplitude reflectivity is taken into account. Hence the amplitude reflectivity of the mirror can be represented as

$$\hat{r}_m(\nu) = r_o(\nu) \exp i\, \phi_r(\nu) \qquad (3.87a)$$

where $r_o(\nu)$ is the modulus, and $\phi_r(\nu)$ is the phase for a plane mirror which is a very good conductor and therefore $\phi_r(\nu) = \pi$ and $r_o(\nu) = 1$. Hence

$$\hat{r}_m(\nu) = \exp i\pi \qquad (3.87b)$$

The amplitude reflectivity of the specimen can be written as

$$\hat{r}(\nu) = r_o(\nu) \exp i \phi_r(\nu) \qquad (3.87c)$$

The grand maxima i.e, the bright fringes of the two interferograms $I_o(x)$ and $I_s(x)$ will be at nearly the same position of the moving mirror because the phase delay $\phi_r(\nu)$ of the specimen lies between π and 2π. Thus one can record both interferograms from the same starting point. Hence, the phase spectrum is calculated by choosing the starting point as reference. Therefore the complex insertion loss of the specimen in reflection measurements is obtained from (3.87) as

$$\hat{L}(\nu) = r_o(\nu) \exp i[\phi_r(\nu) - \pi] \qquad (3.88)$$

Hence for normal incidence, the complex refractive index in terms of the complex amplitude reflection coefficient as described in (3.55) is obtained as

$$\hat{n}(\nu) = \frac{[1 - \hat{r}(\nu)]}{[1 + \hat{r}(\nu)]} \qquad (3.89)$$

Thus by substituting the values of complex $\hat{n}$ and $\hat{r}$ from (3.25) and (3.40), and equating real and imaginary parts we finally arrive at the values of n and k as

$$n(\nu) = [1 - r_o^2(\nu)]/[1 + 2r(\nu) \cos\phi_r(\nu) + r_o^2(\nu)] \qquad (3.89a)$$

$$k(\nu) = -[2r_o(\nu) \sin\phi_r(\nu)]/[1 + 2r_o(\nu) \cos\phi_r(\nu) + r_o^2(\nu)] \qquad (3.89b)$$

Thus we are able to compute the complex refractive index of a sample by measuring its front surface complex amplitude reflectivity.

3.7) Single pass transmission measurement on thick and thin specimens.

In order to study the relation between the complex insertion loss of a specimen and its complex transmission coefficient in terms of its complex refractive index it is beneficial to look into the procedure by which measurements are performed. The normal method is that at first the background interferogram $I_o(x)$, and then the specimen interferogram $I_S(x)$ is recorded. Suppose that the interferogram without the specimen, $I_o(x)$ is recorded with wings of equal optical path length (x), symmetrically about optical zero path position, so that the total optical path length is 2x. If we now put the sample in the beam of the fixed mirror arm and record the sample interferogram $I_S(x)$ of optical path length similar to that of the background i.e, 2x, then the bright fringe of the specimen interferogram is shifted by

$$2D = (n - 1)d, \qquad (3.90a)$$

as illustrated in fig (3.3), where d is the thickness of the sample and n is the average refractive index for material of nearly constant refractive index.

For computational advantages we define 2D as the optical path difference between the origin and the position of grand maximum, i.e, D is the shift on the moving micrometer scale of the starting point of $I_S(x)$ from that of $I_o(x)$, as shown in fig (3.3). In dispersive FTS it is useful to designate the sampling point nearest the zero crossing at the center of the interferogram as the origin for both background and specimen. These points are indicated as x_o and x_s in fig (3.3).

If the specimen on which we are performing measurements is thick enough, then the signatures associated with each partial beam will be well separated on the recorded sample interferogram. Hence the optical constants can be completely determined by recording the first signature.

Thus for single pass transmission measurements, since d is taken as the thickness of the specimen and $\hat{n}(\nu)$ is its complex refractive index, then the optical path in the sample is the product $\hat{n}(\nu)d$ and the phase in the sample is given as $2\pi\nu\hat{n}(\nu)d$. If the measurement is performed in such a way that only the main specimen interference signature $I_s(x)$ is recorded then we can obtain the complex transmission coefficient by employing only the first transmitted partial beam given by relation (3.52). Thus by using (3.36), (3.38), and (3.51) we can write (3.52) as follows :

$$\hat{t}(\nu) = t(\nu) \exp i\phi(\nu) \qquad (3.90)$$

$$\hat{t}(\nu) = \frac{4\hat{n}(\nu)}{[1 + \hat{n}(\nu)]^2} \exp [i2\pi\nu\hat{n}(\nu)d] \qquad (3.91)$$

Also the complex ratio in terms of the complex insertion loss is given as

$$\hat{L}'(\nu) = [FT\, I_s(x)]/[FTI_o(x)] \qquad (3.92)$$

where

$$\hat{L}'(\nu) = L'(\nu) \exp i\phi_L'(\nu) \qquad (3.93)$$

The complex ratio given above, determined from the complex transform of the two interferograms can be obtained by equating the complex insertion loss to the transmission coefficient of (3.90), by including the large phase shift $4\pi\nu D$ associated with the specimen, which causes a large displacement of the

starting point of the two interferograms. Hence after including this large phase factor, the complex insertion loss is written in terms of experimentally measured quantities as

$$\hat{L}(\nu) = L'(\nu) \exp i[\phi'_L(\nu) + 4\pi\nu D] \tag{3.94}$$

Hence the relation between the complex transmission coefficient and the complex insertion loss of the specimen can be given in terms of the complex refractive index as

$$\hat{L}(\nu) = \hat{t}(\nu) \exp(-i2\pi\nu d) \tag{3.95}$$

$$= \frac{4\hat{n}(\nu)}{[1 + \hat{n}(\nu)]^2} \exp i2\pi\nu[\hat{n}(\nu) - 1]d$$

For highly dispersive substances the principle value of the phase difference between two complex spectra i.e, ϕ_L must therefore be replaced by $\phi'_L \pm 2m\pi$, where m can take the values 0, 1, 2,..... Here the factor $2\pi m$ is used to ensure continuity in ϕ'_L when the computed values of ϕ'_L change branches. As an illustration, the phase and amplitude spectra for single pass transmission coefficients for CsI are shown in fig (6.1). It can be seen from fig (6.1) that $\phi'_L(\nu)$ approaches zero at low frequencies, so that m=0 on this branch, and hence the remaining branches have order m=1,2,3,..... Thus for a specimen where $n(\nu)$ is large compared to $K(\nu)$ the values of n & k can be obtained from (3.94 - 95), and therefore

$$n(\nu) = 1 + \frac{[\phi'_L(\nu) + 4\pi\nu D + 2m\pi]}{[2\pi\nu d]} \tag{3.96}$$

and

$$k(\nu) = [1/2\pi\nu d]\ \ln[\ 4\, n(\nu)/\ [1 + n(\nu)]^2 L(\nu)] \qquad (3.97)$$

After having calculated the absorption index it can be related to the absorption coefficient by the relation

$$\alpha = 4\pi\nu k \qquad (3.98)$$

From above we see that the transmission measurements are much simplified when a sample is taken which is many wavelengths thick and there is still measurable radiation passing through it.

However, when the specimen used in transmission measurements is very thin the signatures associated with all the transmitted partial waves given by (3.52) will overlap on the sample interferogram, and it is then necessary to use the full series given by (3.52). The geometric sum of this series is given as

$$\hat{T}_{12} = [(1 - \hat{r}_{12}^2)\,\hat{a}_2]\ [\ 1 - \hat{a}_2\,\hat{r}_{12}^2\ ]^{-1} \qquad (3.99)$$

Therefore using (3.35) and (3.38) one can give the complex insertion loss as

$$L(\nu) = [4\hat{n}/(1 + \hat{n})^2\ ]\ \frac{\exp\, i2\pi(\hat{n} - 1)\nu\ d}{1 - [\ (1 - \hat{n})/(1 + \hat{n})]^2 \exp\, i4\pi\nu nd} \qquad (3.100)$$

where the complex insertion loss is related to the complex transmission amplitude by (3.90 - 3.93). Since these measurements are usually done close to the reststrahlen band, where the dispersion in the refractive index is high, there are many branches in the phase spectrum which makes it difficult to trace

the phase continuously to zero frequency. Hence some other source of information like an amplitude reflection mesurement is needed to ensure the absolute value of the phase at low frequencies.

Since the equation for $L(\nu)$ cannot be solved analytically for the refractive index, it must be solved numerically at each frequency by using an iterative procedure such as the secant method described by Conte and de Boor (1972). This procedure needs an initial estimate of the refractive index at some point on the spectrum, and starting values for n at the first spectral point above and below the reststrahlen band can be obtained from (3.96), or from a supplementary amplitude reflection measurement. The final values of n at these points are used as the starting values at the adjacent spectral points, and the process continues until $n(\nu)$ and $k(\nu)$ have been determined within the experimental uncertainty throughout the spectrum.

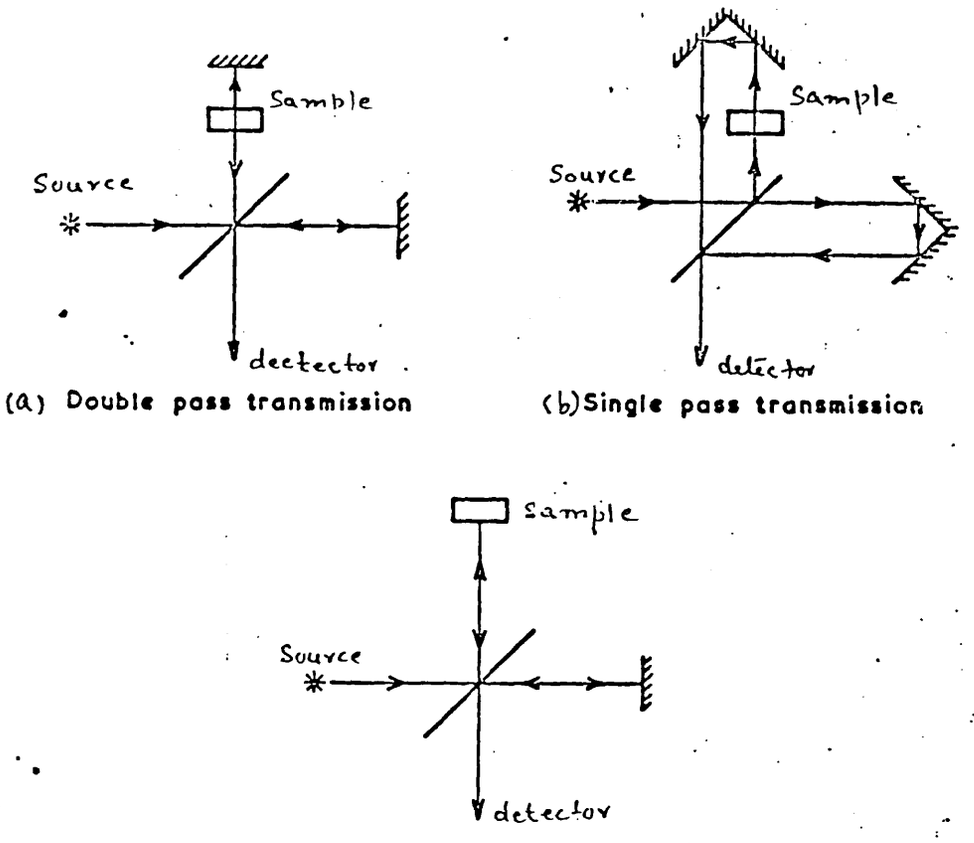

Fig(3.1) An illustration of three configurations in DFTS

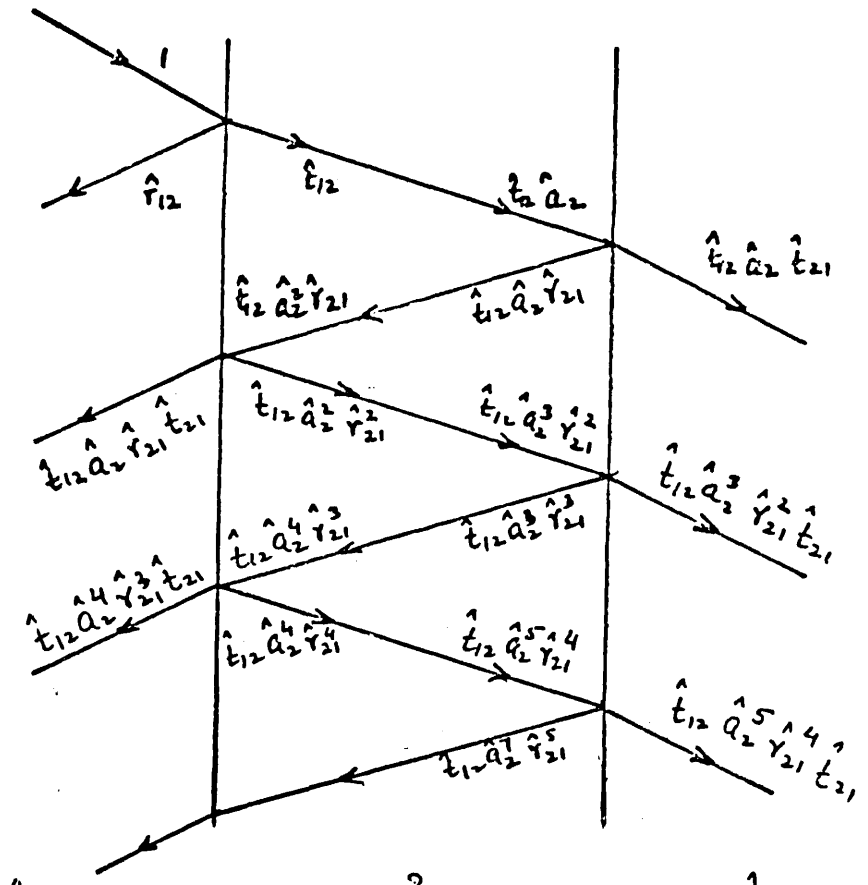

Fig(3.2)

Complex amplitudes of beams reflected and transmitted by a plane-parallel-specimen

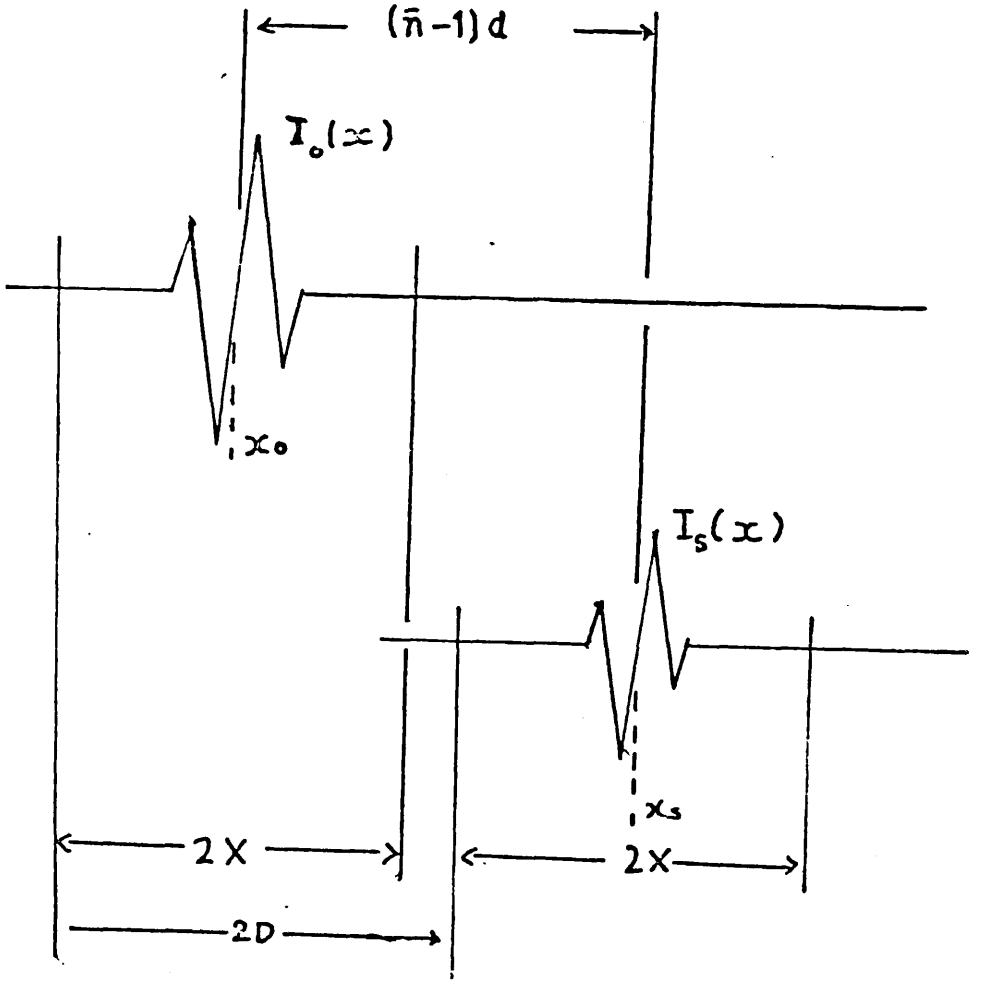

Fig(3.3) A diagram to show the relative starting points of background $I_o(x)$ and sample interferogram $I_s(x)$

CHAPTER 4

INTERFEROMETERS

4.1) Introduction

In this chapter we describe Michelson interferometers used for obtaining data by dispersive single pass transmission and amplitude reflection measurements on solids.

For performing measurements within the reststrahlen region a dispersive reflection interferometer was used and this is described in detail, and for performing low temperature measurements a cryostat built in this laboratory was used. The method exploited for exposing the aluminized and uraluminized specimen surface and for recording the background and specimen interferograms, respectively, is also discussed in detail here.

For dispersive single pass transmission measurements on solids a Martin-Puplett type interferometer has been designed by Parker et al (1978) to permit measurements at normal incidence in the temperature range of 77 - 300K. This interferometer is modified to work as a polarizing interferometer by replacing the mylar beam divider with a free-standing wire grid beam splitter, and by introducing a polariser and analyser in appropriate positions in the interferometer.

The essential accessories to the interferometer like beam dividers and detectors, etc, and problems related with the interferometers are dealt with here.

At the end of this chapter a new focused beam interferometer designed in this laboratory is described. This instrument allows measurements to be performed on specimens as

small as 5mm in diameter. The performance of this interferometer is assessed by recording a water vapour spectrum.

4.2) Dispersive single pass transmission spectrometer

The basic design of the single pass transmission spectrometer used for our measurements is illustrated in fig (4.1). The heart of the interferometer is the central cube, having a slot at 45 degrees at its center and capable of holding a Mylar beam divider stretched on a metallic frame. The ports in the four vertical faces of the cube allow four extensions to be bolted on to the cube. These four extensions contain the source, the sample or the fixed mirror, the moving mirror, and the detector housing.

The radiation source is a high pressure Mercury arc lamp (Philips 125-HPK), having a fused quartz envelope. The lamp is surrounded by a copper cylinder having a hole of 7mm diameter centered on the optical axis of the spectrometer in order to limit the aperture. The whole unit is mounted in a water cooled jacket which helps to keep the instrument near ambient temperature by removing the excess heat developed during the operation of the lamp. The radiation from the source is made incident on the beam divider by the use of a collimator unit which consists of a parabolic mirror and a plane mirror.

So far the set up of our instrument is similar to that of an NPL/Grubb Parsons modular interferometer. Beyond this, however, a large number of modifications have been carried out at Westfield College. For single pass dispersive transmission measurements the instrument was designed to permit a plane

parallel specimen to be inserted near the fixed mirror via a vacuum feedthrough system. The crystal can be easily taken out of the beam without disturbing the vacuum of the instrument for recording the background interferogram.

In order to achieve single pass transmission through the specimen, we have connected additional units which displace the collimator and detector optics laterally by 12.7mm in opposite directions with respect to the optic axis through the central cube. For restoring the continuity of the optical path between the source and the detector we installed roof-top mirrors in both the arms of the interferometer. In order to perform low temperature measurements a cold finger (dewar) was installed in the fixed mirror arm. The specimen could be inserted using a movable copper mount, as illustrated in fig (4.2). This copper mount holding the specimen is connected to the base of the liquid nitrogen cold finger with the help of a copper braid to provide good thermal contact. By using this method the specimen can be cooled down close to the nitrogen temperature, and the specimen can easily be taken in and out of the beam as desired.

In the movable mirror arm the roof-top mirror is provided with a special micrometer alignment system which is capable of sliding the mirror up and down perpendicular to the optic axis. The whole assembly is mounted on a stepping micrometer which is driven by an electric motor. The stepping motor and its related electronics system allows the roof-top mirror assembly to move in either direction i.e, reverse or forward, in steps of 2500, 5000, 7500, or 10000nm, respectively. The step size is chosen in accordance with the spectral limit allowed by the beam divider

response to avoid over lapping of the spectra, as discussed in chapter 2. The maximum displacement from the white light position for two-sided operation is 25mm in optical path. This corresponds to a theoretical resolution of $0.4cm^{-1}$ when triangular apodization and the Rayleigh criterion are applied.

The radiation, after being divided at the beam splitter, reaches the moving mirror via a plane mirror mounted on a vibrator held at 45 degrees to the optic axis. This vibrator unit provides phase modulation, i.e, the path difference is modulated by small periodic displacements of the mirror mounted on the vibrator. This vibrator unit is powered by an oscillator, and the frequency of oscillation of the vibrator can be varied in accordance with the detector response time. In the case of a Golay cell the maximum efficiency can be obtained by modulating the signal at 11 Hertz, which is the manufacturer's recommended frequency. The subject of modulation is discussed in detail later in this chapter.

After reflection of the radiation from the moving mirror and transmission through the specimen and reflection from the fixed mirror, the two beams are incident back on to the beam divider where they recombine and interfere according to the difference in the optical path in the two mirror arms, and the phase delay introduced by the specimen. The recombined beam is then finally focused either by using reflecting optics, using a design which is very close to a Pfund system, or by using a high density polyethylene lens doublet. We have used both these systems for different frequency regions. Using the above optical

setup the beam is finally focused on to the detector.

Besides the above setup, in order to improve the performance of the interferometer, we made provision for the optical stability of the instrument to be closely controlled. The temperature of the whole instrument was stabilised to better than ± 0.1K. This was achieved by circulating water from a commercial temperature controller through copper coils attached to the outside of each module of the system and then passing it through a radiator. The water is kept at a temperature a few degrees above room temperature by a thermostatic heater incorporated in the circulator. Also an extra booster circulator was coupled to the circulating system to achieve better temperature stability of the instrument. The circulating system was necessary to ensure mechanical stability in the lengths of the two arms of the interferometer, since slight instability will produce phase errors in the computed spectra. Hence it is necessary to stabilise the temperature of the system for accurate phase measurements.

As we know, in the far infrared region, if the instrument is not evacuated to a pressure of 10^{-1} torr, the sample spectra will be degraded due to high absorption by water vapour present in the system. This pressure was obtained by connecting the instrument to a rotary vacuum pump. At low temperature i.e, liquid nitrogen, the small amount of moisture present in the system may cause icing up on the specimen, and this may have serious effects on the phase spectrum. In order to prevent this, the system was mounted on a diffusion pump attached to the central cube i.e, the base of the beam divider module and the interfero-

meter can be evacuated to a pressure of 10^{-6} torr.

4.3) Polarizing interferometer

The main problem with a conventional interferometer is the performance of its beam divider. Because of the array of minima associated with dielectric beam dividers the performance of the interferometer may be effected. Also, if amplitude modulation is used there is a strong mean level of the interferogram, and any variation in this, which may be due to instability in the instrument will produce spurious features in the computed spectra. Hence in order to improve the throughput energy in the desired spectral range, one has to use an appropriate thickness of the dielectric beam divider. As the response of these beam dividers varies with thickness, by using a thick beam divider the low frequency response of the interferometer can be improved, but on the other hand the high frequency response will be very poor, and for a thin beam divider the process is reversed. Hence in order to cover a large spectral range, a number of beam dividers of different thicknesses are needed.

In order to improve the performance of the interferometer, a method of interferometric spectrometry depending on free standing wire grid beam dividers was developed by Martin and Puplett [1970] which allows operation over a wide range of spectral frequency without strong variations in efficiency. The high frequency cut off wavenumber of wire grid beam dividers is approximately equal to $1/2d$ cm^{-1}, where d is the spacing between two adjacent wires. The efficiency of a polarizing interferometer

is far better than that of a conventional interferometer in the sense that a polarizing interferometer equipped with a wire grid beam splitter eliminates the internal reflection problems associated with dielectric beam dividers.

The polarizing action of the interferometer is briefly given as follows. The radiation from the source is first polarized by the polarizer P1, as illustrated in fig(4.3a), such that the electric vector is inclined at 45 degrees to the vertical direction. The polarized beam is then incident on the free standing wire grid beam divider where it is partially transmitted with horizontal polarization towards the moving mirror arm and partially reflected with vertical polarization towards the fixed mirror arm. The roof-top mirror at the end of each arm behaves as a rotator for the polarisation vector of the incoming radiation. Hence the electric vector of the radiation moving towards the fixed-arm roof-top mirror will be flipped by 90 degrees, and on encountering the beam divider the second time will be completely transmitted, whereas the radiation from the moving mirror arm will now be reflected on returning to the beam divider. The beam then passes through the analyser P2. The resultant intensities with the analyser P1 parallel and perpendicular to the polarizer P2 can be given as

$$I_{\parallel} = (I_0/2)[1+\cos\Delta] \qquad (4.1)$$

$$I_{\perp} = (I_0/2)[1-\cos\Delta], \qquad (4.2)$$

respectively, (Martin and Puplett 1970),

where $\Delta = 2\pi\nu_0 x$. Here x is the path difference, ν_0 is the frequen-cy of a monochromatic source in wavenumbers, and I_0 is the

intensity of the plane polarized radiation incident on the beam divider. Both the outputs are modulated as the moving mirror scans and the resulting interferogram can be used to obtain spectra. We can obtain the difference signal by alternating the orientation of analyser or polarizer, and this is given as

$$I_{\parallel} - I_{\perp} = I_o \cos 2\pi \nu_o x \qquad (4.3)$$

Hence by modulating the polarization of the radiation the output will oscillate about a true zero, as in the case of phase modulation. This modulation is in some ways similar to amplitude modulation, but the large d.c background which is present in amplitude modulation is eliminated.

The design of our single pass transmission interferometer as shown in fig (4.3a) is similar to that of a Martin and Puplett polarizing interferometer. Therefore our instrument can be easily adapted to the polarizing mode. In order to do this we replace the Mylar beam divider with a free standing wire grid beam split-ter made out of 10 micron thick tungsten wire, with spacing 'd' of 25 microns between consecutive wires, which gives a high frequency limit of 200 cm^{-1}. The winding technique for making these wire grids and their spectral response is given in detail by Costley et al (1977) and Beunen et al (1981). Together with the beam divider, two more wire grids were introduced i.e, a polarizer and an analyser. The polarizer was placed in the beam inlet port, whereas the analyser was fixed between the beam divider and condensing optics at the detector end.

In order to modulate the radiation, instead of having fixed polarizer we mounted the polarizer on a rotating cylinder which

was driven by an electric motor, as shown in fig(4.3b). The frequency of modulation was varied in accordance with the detector requirements by simply changing the size of the rotating pulley which is connected to the motor. The polarizer is mounted on the rotating cylinder and is coupled to the pulley with the help of a rubber belt. Thus using this technique we have done measurements as low as 10 cm^{-1}, using a quartz Golay, and with a liquid helium cooled bolometer down to 3 cm^{-1}, but due to improper function of the bolometer the low frequency spectrum was loaded with fringes.

4.4) Dispersive reflection interferometer

A wide range of techniques have been developed at Westfield College for measuring the optical constants of solids by dispersive reflection spectroscopy. The common feature of the instruments developed for amplitude reflection spectroscopy has been the elimination of the need for the precise mechanical replacement of the reference mirror by the specimen. In the method developed in this laboratory by Parker at al [1976] the need for the precise replacement of the reflecting surface is avoided by aluminizing part of the sample surface. The fundamental design of our reflection spectrometer is similar to that of a phase modulated NPL/Grubb Parsons modular interferometer, and the design of our instrument is illustrated schematically in fig (4.4), and the instrument consists of two sections i.e, the interferometer and the cryostat.

The radiation from a high pressure mercury source MS passes

through the collimator C and then through a 1.3mm thick black polyethylene filter F. The reason for using the filter in the inlet port is that, being a good mid-infrared absorber, it will attenuate frequencies above 500 cm^{-1}, i.e, it will absorb a fair amount of undesired radiation which would otherwise increase the boiling rate of liquid helium held in the cryostat. In other words it helps to increase the hold time of the cryostat. The radiation after passing through the filter F is incident on a 6.25 micron beam splitter BS where it is partially transmitted and partially reflected into the two arms as usual.

The reflected beam then propagates through a 1.5mm thick white polyethylene vacuum window VW which isolates the vacuum system of the fixed mirror arm from the rest of the instrument. The radiation then falls on to the mirror IM which is inclined at 45 degrees to it. This mirror was made by aluminising the front surface of a 12.5 micron thick sheet of Mylar stretched on a metallic frame. Radiation, after being reflected from the front surface of the mirror IM travels vertically upward and encounters the specimen S in the fixed mirror arm of the instrument. The specimen S is attached to the base of the liquid helium can of the cryostat, details of which are shown in fig (4.5). The radiation is then reflected back at normal incidence from the sample towards the beam divider.

The radiation in the moving mirror arm, after first being transmitted through the beam divider, passes through a white polyethylene compensating window CW similar in thickness to VW on to a plane vibrating mirror VM mounted on a vibrator which is held at 45 degrees to the incoming beam. Finally the beam encou-

nters the moving mirror MM which is of 6cm diameter and is coupled to the non rotating shaft of a micrometer. The spindle passes through a vacuum seal, and the micrometer is driven by the stepping motor.

The beams returning from the two arms of the interferometer recombine at the beam divider. The combined beam is then focused by two low density polyethylene lenses PD, on to the detector D.

The cube assembly on the right, with IM held across its diagonal, has its upper port bolted to the base of the cryostat through a high vacuum coupling, and the lower end of the cube is similarly attached to a diffusion pump. Thus the fixed mirror assembly together with the cryostat can be evacuated to a pressure of 10^{-7} torr, which allows the specimen to be cooled down to liquid helium temperatures without any icing up problems. The rest of the instrument on the left of the window VW could be evacuated to a pressure of 10^{-2} torr with the help of a rotary pump, which is good enough to remove any water vapour traces present in the instrument.

For sensing the temperature of the specimen two carbon resistors of the order of 12K Ohms were calibrated at 300, 77, and 4K. The variation of resistance, R, with temperature, T, is given by the Clement and Quinell (Thor Cryogenics Ltd) three term relation i.e,

$$\log R + (K/\log R) = A + (B/T) \qquad (4.4)$$

where A, B and K are constants.

After calibration, one of the resistors was connected to the base

of the liquid helium can and the other to the specimen mount. In order to stabilise the temperature of the instrument the same technique was used as described in the dispersive transmission instrument.

The cryostat used here was designed by Parker and Lowndes (1979), and their publication describes all the engineering details. The principle features of the cryostat are shown in fig (4.5). The sample was fixed to the base plate of the liquid helium can as a complete unit as shown in fig (4.5). The sample mount is shown in vertical cross-section in fig (4.5a).

The major problem facing dispersive reflection spectroscopy (Johnson et al 1969, Berg et al 1971 , Zwick et al 1977) has always been the accuracy with which the phase can be measured, due to an apparent need for the physical replacement of a reference mirror with the sample. Parker and Chambers (1974), (1975), (1976), recognised that the solution to this problem was to metallise part of the sample surface.

To use this technique the crystal was first worked to an optical flatness of the order of 0.1 micron on its reflecting surface. Then the crystal was attached with the unpolished surface to the copper base with the help of a small spot of low temperature adhesive (G.E varnish cc-155). The polished surface of the specimen was then aluminised in four sections as shown in fig (4.6a). This aluminised surface then provides a reference surface which eliminates phase and amplitude errors obtained with sample-reference mirror interchanging. The copper plate holding this aluminised specimen was then bolted on to the base of the

liquid helium can with three equally spaced aligning screws and stainless steel springs. These screws were specially made of copper to provide good thermal contact.

We have used a switching mask similar to that described by Staal and Eldridge (1977). The mask was placed in front of the specimen and the crystal was accurately aligned parallel to a mirror fixed on the base of the cryostat. This mirror was used only for the purpose of alignment which was carried out with the aid of a laser by adjusting the aligning screws.

The switching mask was made out of a thin sheet of aluminium and was operated by two solenoids, and the screen geometry and solenoid mount are illustrated in figs (4.6b) and (4.6c) respectively. This mechanism works at all temperatures in the range 4-300k. In its extreme positions the screen exposes either the aluminised part of the specimen or the uncoated specimen to the incoming radiation. The operating power needed for switching the screen at 300, 77, and 4 K, is 200, 10, and 1 mW respectively.

When the screen is operated in the switching mode the mask alternately exposes the aluminised surface and the sample surface at each step of the moving mirror. The screen can also be operated in the conventional mode, in which the complete interferogram is recorded initially from the aluminised surface of the specimen and then from the exposed surface during independent scans of the moving mirror.

The major disadvantage of this technique is the restriction on the specimen size, since one has to aluminise part of the front surface of the specimen. Consequently it requires speci-

mens of large diameter. We have proposed a new type of interferometer design which allows the performance of dispersive reflection measurements on specimens as small as 5mm in diameter, which is 10 times smaller than that used in the above technique. The details of the new instrument are given at the end of this chapter.

4.5) Accessories for the interferometers

A) Beam dividers

One of the major factors which impose a restriction on the spectral range in Michelson interferometers is the performance of Mylar beam dividers. At low frequencies the output from a black body source like a mercury arc lamp is very low and in addition to this the throughput of the instrument drops rapidly due to a rapid fall in the beam splitter efficiency to less than 1/5 of its maximum value. Because of this we used wire grid beam dividers. Thus the operational frequency of the interferometer depends upon the choice of beam divider.

As we have extensively used Mylar for beam dividers to cover the frequency range from 30 to 500 cm^{-1} it is desirable to discuss its behaviour in the interferometer.

Let us consider an interferometer in which a beam of unit amplitude is incident upon a beam splitter held at 45° to the incoming beam, and let the proportion of the incident beam transmitted by the beam divider be T and that reflected be R. Then the incident radiation at the beam divider splits into four parts

having relative intensities TR, RT, R^2, T^2, where TR and RT interfere to give the interferogram whereas R^2 and T^2 return to the source. If we assume that there is no absorption, i.e,

$$R^2 + 2RT + T^2 = (R + T)^2 = 1 \qquad (4.5)$$

then the amount of usable radiation is $2RT=2R(1-R)$, and the maximum of 2RT occurs for R = T = 0.5. Thus the maximum efficiency of a perfect Michelson interferometer is 50%. In practice, however, transmittance and reflectance are not usually equal to 0.5 and there is also absorption in the beam divider. Furthermore, multiple reflections take place within the beam divider itself (Chamberlain and Chantry 1966), and its behaviour is strongly dependent on its thickness.

As a result of multiple reflections the efficiency varies with frequency from zero to (2RT). However only the primary transmitted and primary and secondary reflected beams are important, because the primary transmitted beam contains 83% of the incident flux, whereas the primary and secondary reflected beams contain 8.9 and 7.4% of the incident intensity, respectively (Bell 1972). The mylar film loses reflectivity when the optical path difference is an integral multiple of wave lengths. Therefore one can write the condition for interference as

$$m\lambda = 2d\,[n^2 - 1/2]^{\frac{1}{2}} \qquad (4.6)$$

(Bell 1972), where d is the thickness of the dielectric film and n its index of refraction. The condition for interference depends on the values of m. For constructive interference m=1/2, 3/2, 5/2, ... and for destructive interference the values of m are m= 0, 1, 2, 3, ... For all dielectric beam

splitters the efficiency is dictated by relation (4.6), and is zero if $\nu = 1/\lambda = 0$, since one of the reflected beams has a phase shift of π with respect to the other. Hence they interfere destructively. One can obtain other minima by choosing integral multiple values of λ in eq(4.6). In fig(4.7) the first order interference fringes are shown for varying thicknesses of mylar beam divider. It is clear from fig(4.7) that to obtain a good signal over a considerable spectral range a number of beam dividers are needed.

The polarizing effects of an interferometer due to the mylar beam divider can also be given. If we consider a beam of unpolarized radiation incident upon a dielectric beam splitter, the reflected and transmitted beams are partially polarized and their polarization depends upon the angle of incidence. The value of the Brewster angle for mylar of refractive index 1.75, at which the beam is 100% polarized is obtained by the relation $\tan \theta_B = n$. Therefore the Brewster angle is $\sim 60^\circ$. Since beam dividers are commonly used at an angle of incidence of 45°, principly for ease of construction, it follows that the emergent beam is partially polarised.

B) Infrared detectors

The detector which was most used in our measurements was the well known Golay cell, except for low frequency measurements for which we utilized a liquid helium cooled germanium bolometer.

For thermal detectors like a Golay cell the intrinsic response time i.e, the speed with which they respond to changes

in the incoming signal is about 50 ms. The Golay cell is sensitive throughout the whole infrared region, and works by the expansion of an inert gas heated by the incoming radiation. The inert gas is contained in a small cell, one wall of which is a flexible membrane which distorts under pressure, and the signal is obtained from the deflection of a light beam reflected off it.

The spectral response of a thermal detector is determined mainly by its window. Thus for frequencies below 250 cm^{-1} a Golay cell with a quartz window is used, whereas a diamond window Golay has no upper frequency cut off in the infrared, being transparent up to and beyond 10,000 cm^{-1}. The major advantage of a Golay cell is that it operates at ambient temperature.

In all detectors the useful sensitivity is limited by the noise, which is normally expressed by setting the minimum detectable signal power equal to the noise equivalent. This means that a signal is just detectable when the signal to noise ratio is unity. Basically there are three main sources of noise which effect the performance of a detector: fluctuation in the background radiation and in the light source itself, thermal and electrical fluctuations in the detector and finally the fluctuation in the amplifying circuit. Since the noise in the recording electronics varies inversely with the frequency of modulation, to minimize the noise one would like to chop the signal at as high a frequency as possible, but the chopping frequency is limited by the detector response time. In the case of a Golay cell the chopping frequency is of the order of 15Hz. Thus the disadvantage of a Golay detector is that it has a slow response time. But on the other hand the response time of a

liquid helium cooled detector is much faster i.e, of the order of 1μs. Therefore one can use a high frequency of modulation, and as a consequence noise in the cooled detector is considerably reduced.

At low spectral frequencies the output from a black body source like a mercury arc lamp is very low. In such a low energy region, the liquid helium cooled detector has proved to be very efficient on account of its high sensitivity. Furthermore, since the detector response time is now much faster one can use frequencies as high as 800 Hz. Typically the noise equivalent power of a helium cooled detector is 1000 times better than that of a Golay cell.

To obtain reliable results at low frequencies we have used a liquid helium cooled Antimony doped germanium thermal bolometer manufactured by QMC Industrial Research Limited, with a spectral range of 2 to 250cm^{-1}. The performance of this detector below 5cm^{-1} is doubtful because in that frequency range it produces spurious fringes in the computed spectra. Neverthless, its performance between 10 to 250 cm^{-1} is excellent. In recent years mercury cadmium telluride detectors have come into use. These operate at 77k and have a fast response time and their spectral limits are 400 to 5000 cm^{-1}.

C) Signal modulation

Modulation of the signal from the source is essential in the far infrared region because the power radiated by the source is proportional to the first power of the temperature

(Rayleigh Jeans law, Sears and Salinger 1975). Due to the large acceptance angle of a Golay nose (60 degrees) it receives a significant amount of radiation from the walls of the interferometer and other points in the field of view besides radiation from the lamp source. If the temperature of the surroundings were the same as that of the detector, then there would be no net flow of radiation from one to another which would be an ideal case, which one cannot achieve in practice. Therefore the signal in the interferometer is always modulated.

Thus it is common practice to modulate the signal emitted by the source. Different methods of modulating radiation can be used. The common form of modulation is a rotating chopper disc, which chops the signal radiated by the source. Chopping of this type is usually called amplitude modulation. All surfaces in the interferometer radiate energy according to their temperature, and so it is therefore preferable to carry out this type of modulation just before the collimator to discriminate against ambient temperature radiation.

The disadvantage of amplitude modulation (AM) is that a d.c level is carried at the detector together with the signal, the variation of which due to instrumental instabilities will produce spurious features in the resulting spectrum. Another disadvantage of AM is that one half of the total incident power is rejected by the chopper blades. Thus with AM, in order to achieve a.c amplification, some signal has to be sacrificed.

An alternate method for modulating radiaton is known as phase modulation. Here the path difference is modulated by making

one of the interferometer mirrors execute small oscillations along a line perpendicular to its surface. In an interferometer at time 't', if x is the path difference between the two mirror arms, then with the addition of jitter of one of the mirrors, i.e, oscillating with small amplitude 'a', and angular frequency 'w', we have the time dependent displacement caused by jittering as,

$$x' = x + a \sin(wt). \qquad (4.7a)$$

If we now consider that the interferometer is irradiated by monochromatic radiation of frequency ν_o then the phase difference between the two beams at time t is $2\pi\nu_o x'$ and their instantaneous resultant is proportional to

$$P[1 + \cos 2\pi\nu_o x'], \qquad (4.7b)$$

where P is a measure of the power. Since the constant term is blocked by the amplifying system the output signal is proportional to $[P\cos 2\pi\nu_o x']$

i,e
$$V(x,t) \sim P \cos 2\pi\nu_o(x + a \sin wt) \qquad (4.7c)$$

This function has time dependent parts which are not simple and the coefficients of their Fourier components are Bessel functions. Since, however, the only frequencies passed by the narrow band amplifier of the detecting system are close to f, the resulting output interferogram as given by Martin [1980], and Chantry [1971] has the form

$$I(x) \propto P(\nu)\, J_1(2\pi\nu_o a) \sin(2\pi\nu_o x)\, d\nu \qquad (4.8)$$

and for broad band radiation the interferogram function will be

$$I(x) \propto \int_o^\infty P(\nu)\, J_1(2\pi\nu_o a) \sin(2\pi\nu x)\, d\nu \qquad (4.9)$$

By using eq(4.9) the interferogram looks similar to the first derivative of that obtained by AM. The two situations are displayed in fig(4.8). The amplitude modulated interferogram is symmetrical about zero path difference, having a mean background level of ideally half the value of the grand maximum, whereas the phase modulated interferogram is antisymmetrical about zero path position. Since there is no d.c contribution to the signal the mean level is zero as is clear from the fig(4.8).

From eq(4.8) we observe that phase modulation imposes a Bessel function envelope on the throughput. The main advantages of using a phase modulation system are as follows. Firstly the whole of the radiation is utilized instead of approximately half when using AM. Secondly, the constant term is unmodulated, so drift problems are reduced and the noise due to fluctuations in the source is reduced. Also we get rid of mechanical vibrations associated with the chopper. Finally the Bessel function $J_1(2\pi\nu_o a)$ is frequency dependent and falls to zero at $(2\pi\nu_o a) = 3.8$. Thus, as a bonus one gets a non absorptive method of limiting the frequency range of the interferometer since the Bessel function maximises and minimises at frequencies dictated by the jitter amplitude ,a, of the vibrating mirror. Therefore by varying the current through the vibrator with the help of a power oscillator, the response in the desired spectral range can be optimised.

D) Focusing optics

In FTS in the far infrared region, reflecting and refracting optics are used to focus the radiation coming from the source and traversing the interferometer to the detector. The throughput of the interferometer is dependent on these focusing optics.

The two optical systems which we have used in our interferometers are shown in fig(4.9). For refracting optics a high density polyethylene doublet with a focal length of 50mm was used whereas the reflecting optics comprises a plane mirror and spherical mirror of 100mm focal length. The way in which the reflecting optics is arranged is similar to a Pfund system. The main features of the two systems are as follows.

The use of reflecting optics instead of refracting optics increases the throughput energy of the interferometer very considerably since the transmission losses in the polyethylene lens are removed. Also there is a local improvement of the signal at 73cm^{-1} because of the removal of the absorption due to a polyethlyene lattice band. But the advantage of using reflecting optics below 40cm^{-1} is very small because below this frequency the transmission losses in polyethlyene are negligible.

If we consider the behaviour of refracting optics in an interferometer equipped with a 12.5 micron beam divider and a quartz Golay then in a carefully aligned interferometer it is observed that the detector signal reaches one half the saturation value recommended by the manufacturers. Hence if one uses reflecting optics instead, it will overload the detector,

and then it becomes necessary to limit the signal with additional filters. In the case of refracting optics, the polye thylene being a mid infrared absorber, besides providing an adequate amount of signal, will also help in minimizing the phenomenon of aliasing associated with the interferometer.

E) Preparation of thin samples

In order to determine the optical constants of alkali halides like CsI and KI using a dispersive single pass transmission technique, fairly thin samples of the order of 120 micron in thickness were prepared in our laboratary using the following method.

The initial size of the alkali halide samples bought were of 2mm thickness and 25mm diameter. After lapping and polishing one of the surfaces of the sample the prepared surface was fastened with paraffin wax to a brass plate with a 20mm diameter hole at its center. This brass plate was then screwed to the inner end surface of a two part cylindrical sample holder for lapping and polishing the other side of the sample.

The exterior end surface of the specimen was then used as an adjustable reference plane, by which the thickness of the lapped sample was determined. During this preparation the hole was filled by a disk of brass of the same thickness as that of the brass plate in order to support the central region of the sample. When the operation had been completed the specimen was retained on the brass plate so that the danger of cracking the thin sample was minimized. Since the thickness of the sample should be uniform for dispersive transmission spectroscopy, care was taken

to keep the surfaces parallel, but a variation in the thickness of a few microns was impossible to avoid. The optically usable circular region of the prepared sample was of the order of 20mm diameter.

4.6) Electronics and data acquisition

The electronic setup for the transmission and reflection instruments is basically the same. The lay out of the electronics is shown in fig(4.10).

The signal from the detector first passes to a broad band amplifier. After amplification the signal is synchronously rectified by a phase sensitive detector (PSD) where the amplified signal is compared with a reference signal. In order to operate the PSD a reference voltage is derived from a power oscillator which drives the phase modulated mirror. The modified output is then passed through an RC filter of variable time constant. The a.c noise components which are associated with the resultant output are not coherent with the reference and the response of the electronics to noise depends on the time constant of the PSD. If a long RC time constant is employed we cannot run the spectrum too quickly, because by doing so the sharp features will be blurred out as the system has not enough time to respond to a sudden charge. The spectral scan time is chosen so that there is a minimum of dead time for each spectral point, and this is selected to provide an adequate signal to noise ratio.

The modified output after passing through the RC filter, can then be passed either to a chart recoder or a digital voltme-

ter (DVM) or to both in parallel, as desired. From the DVM the signal passes through a frequency counter to which is attached an external oscillator. The PSD can integrate the signal from a specific interferogram point for effectively 3sec, 1sec, 300msec, or 100msec. The DVM frequency counter is triggered by an external oscillator and counts the pulses for a time interval proportional to the input signal. The information is then collected on a paper tape.

The trigger electronics used in our system was designed and built at Westfield college. The complete cycle of stepping and sampling is derived from the trigger electronic unit. At first the moving mirror is stepped and then after a short time delay the signal to the PSD rises exponentially under the action of the RC filter. After this pre-fixed delay the frequency counter is triggered, the signal is then sampled for a finite reproducible time set by the external oscillator and the data is punched on the paper tape. The process is repeated after a short delay and is continued until the full interferogram is recorded on the paper tape. Manual control was also provided in the system to allow a quick check of the interferogram and to set the position of the starting point for recording the interferogram. Once the data is recorded on the paper tape it is submitted to the ULCC CDC M6000 or M6600 computer for Fourier transformation.

4.7) Focused beam interferometer

We have seen that in the dispersive reflection spectrometer

the minimum sample diameter needed to carry out measurements is of the order of 40 mm. Since most samples of this size are very costly we decided to modify the optical arrangement of the spectrometer to try to accommodate smaller specimens.

The novel features of this new Michelson type dispersive reflection interferometer are as follows. Firstly, now one can do measurements on samples as small as 5mm in diameter by using a focused beam in both arms of the interferometer. Secondly, very few optical components are employed to obtain the focused beam in each arm, as compared to that of Gast and Genzel(1973) who employed a much more complicated system.

The optical lay out of the interferometer is schematically illustrated in fig(4.11). Collimated radiation from a mercury source is incident on a mylar beam divider, which is held vertically along the diagonal of the central cube of the interferometer. The radiation after splitting at the beam splitter BS is then propagated into the two arms of the interferometer. The beam in the fixed mirror arm is first reflected from the plain mirror PM and is focused on to the sample or fixed mirror by a parabolic mirror P1, whereas the beam in the moving mirror arm of the interferometer is first reflected by a vibrating mirror VM and is focused on to the moving mirror MM by the parabolic mirror P2, and the interferometer is scanned by moving the mirror MM.

The two beams then pass from their respective arms to the beam divider once again, and the recombined beam is then focused on to the detector. In the moving miror arm a special mirror holder was made so that it could be mounted on the vibrator and

used as part of the focusing optics in that arm. The parabolic mirrors were of 200mm focal length, and were taken from commercially available collimator units made for the NPL/Grubb Parsons interferometer. It is better to use parabolic mirrors of short focal length in both arms, since the short focal length will reduce the optical path length of both the arms, and hence reduce the noise factor in the recorded signal.

The alignment system used with this instrument is the same as that of the original reflection spectrometer, and needs to be improved for this system, and so is the technique of sample replacement. Because of the smaller size of the specimen the technique of aluminizing part of the specimen cannot be used here. The temperature of the interferometer was stabilized to better than ± 0.1K using the same technique as described earlier, and the instrument was connected to a rotary pump to evacuate it to better than 10^{-1} torr.

Results of prototype interferometer

As a performance test and as a demonstration of the range of applicability, due a to lack of time, only a water vapour absorption spectrum together with a background spectrum are presented here. In order to record the background interferogram with mirrors in two arms of the interferometer, the system was evacuated to 10^{-1} torr to remove all water vapour present in the system. Also, to reduce the size of the mirrors in each arm an

aperture of 5mm diameter was introduced.

The interferometer was equipped with a quartz Golay and a 12.5 micron beam divider. After recording the background spectrum , as shown in fig(4.12), to record a water vapour absorption spectrum air was let into the system and the interferogram was then recorded. Thus the ratio of the Fourier transforms of the two interferograms gives the water vapour absorption spectrum which is illustrated in fig(4.13). The lines indicated are listed in a table of wave length standards by Narahari et al (1966). The spectrum was computed from a double sided interferogram of 1000 steps of 2500nm each on each side of the position of zero path difference. This is equivalent to 2 cm^{-1} theoretical resolution. The water vapour interferogram recorded from the unevacuated interferometer is presented in fig(4.14).

From the results presented above it is clear that with this design, the interferometer works satisfactorily, but that it needs further attention to obtain better quality measurements, and to provide low temperature facilities.

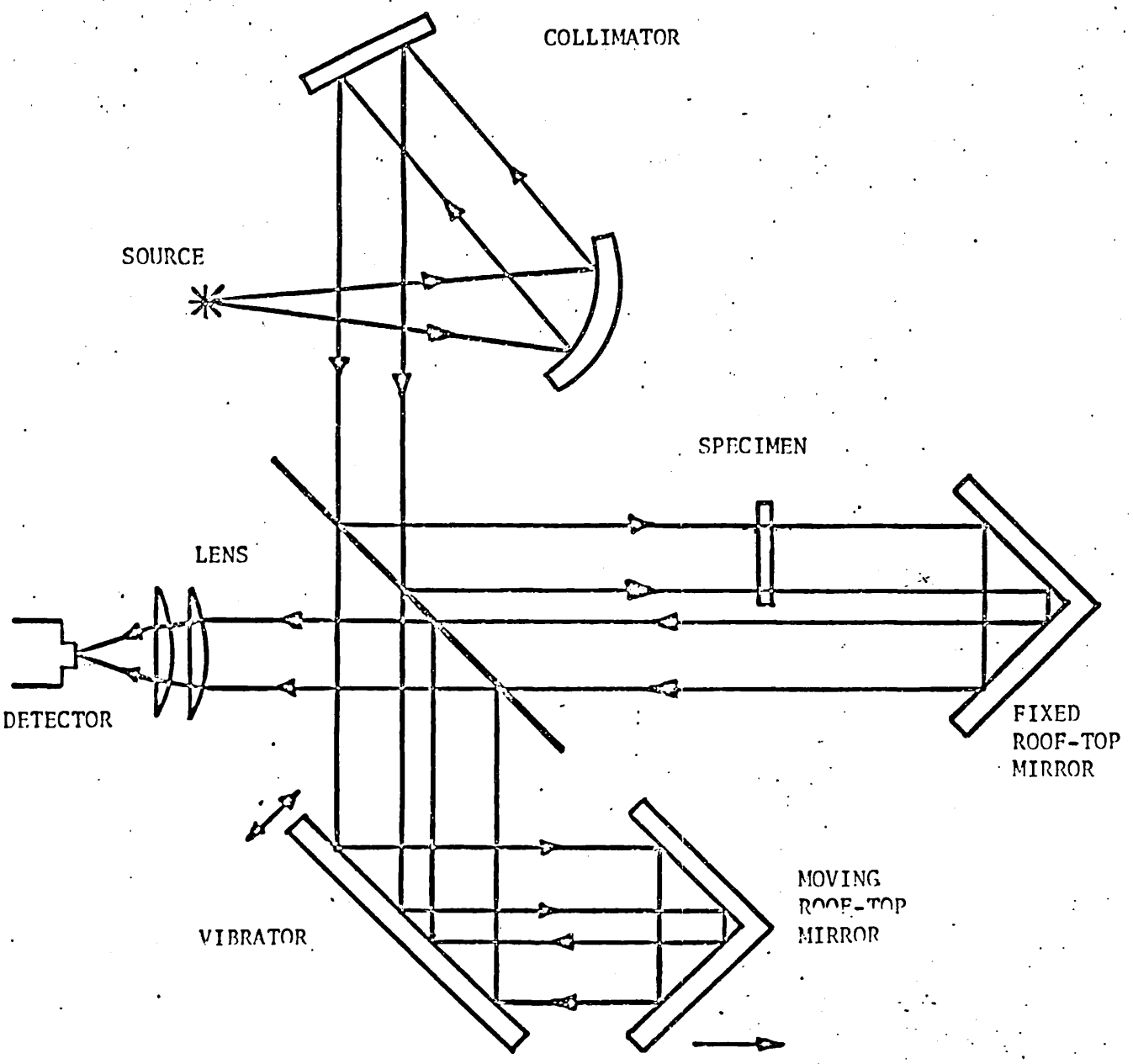

Fig(4.1) Represents the single pass dispersive transmission interferometer

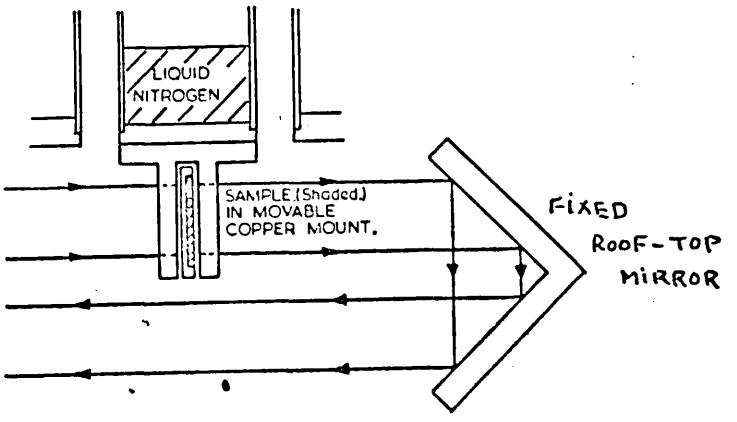

Fig(4.2) Sample holder for single pass transmission instrument

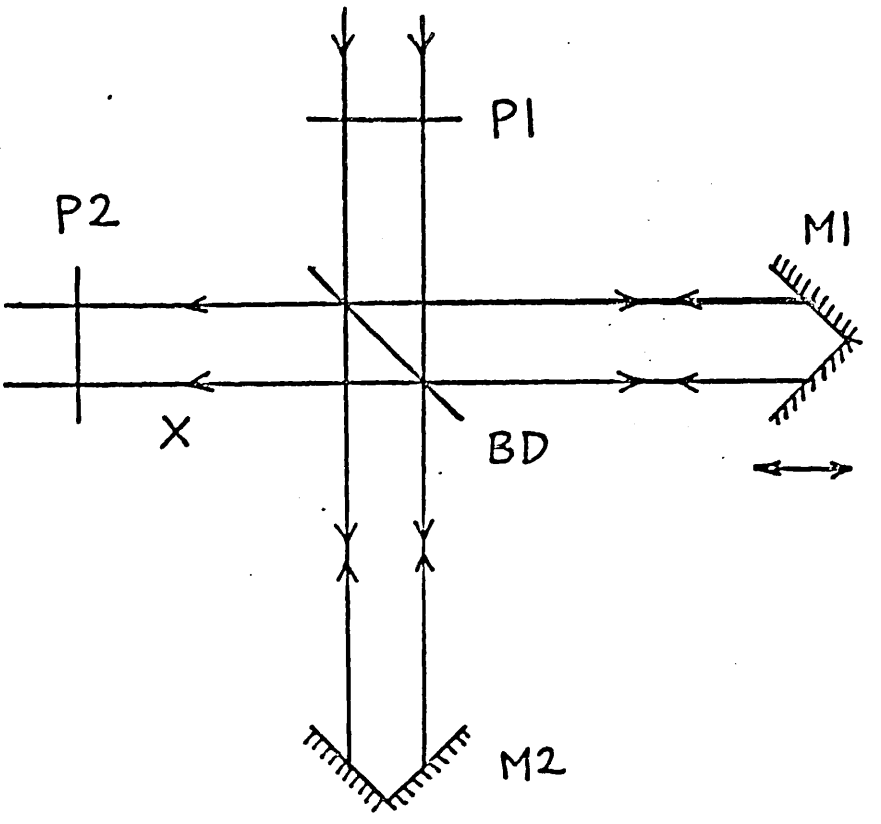

(a) Polarising interferometer

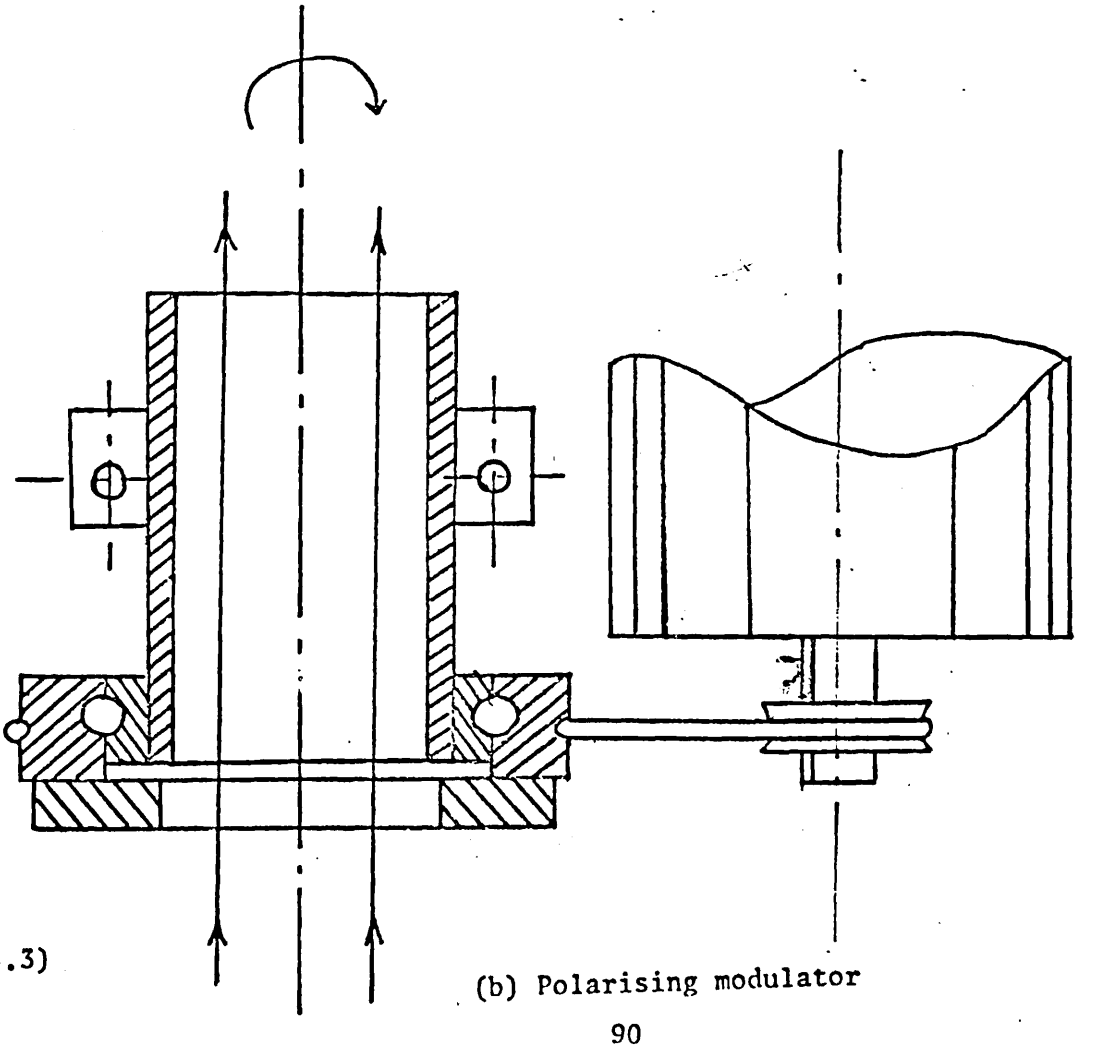

Fig(4.3)

(b) Polarising modulator

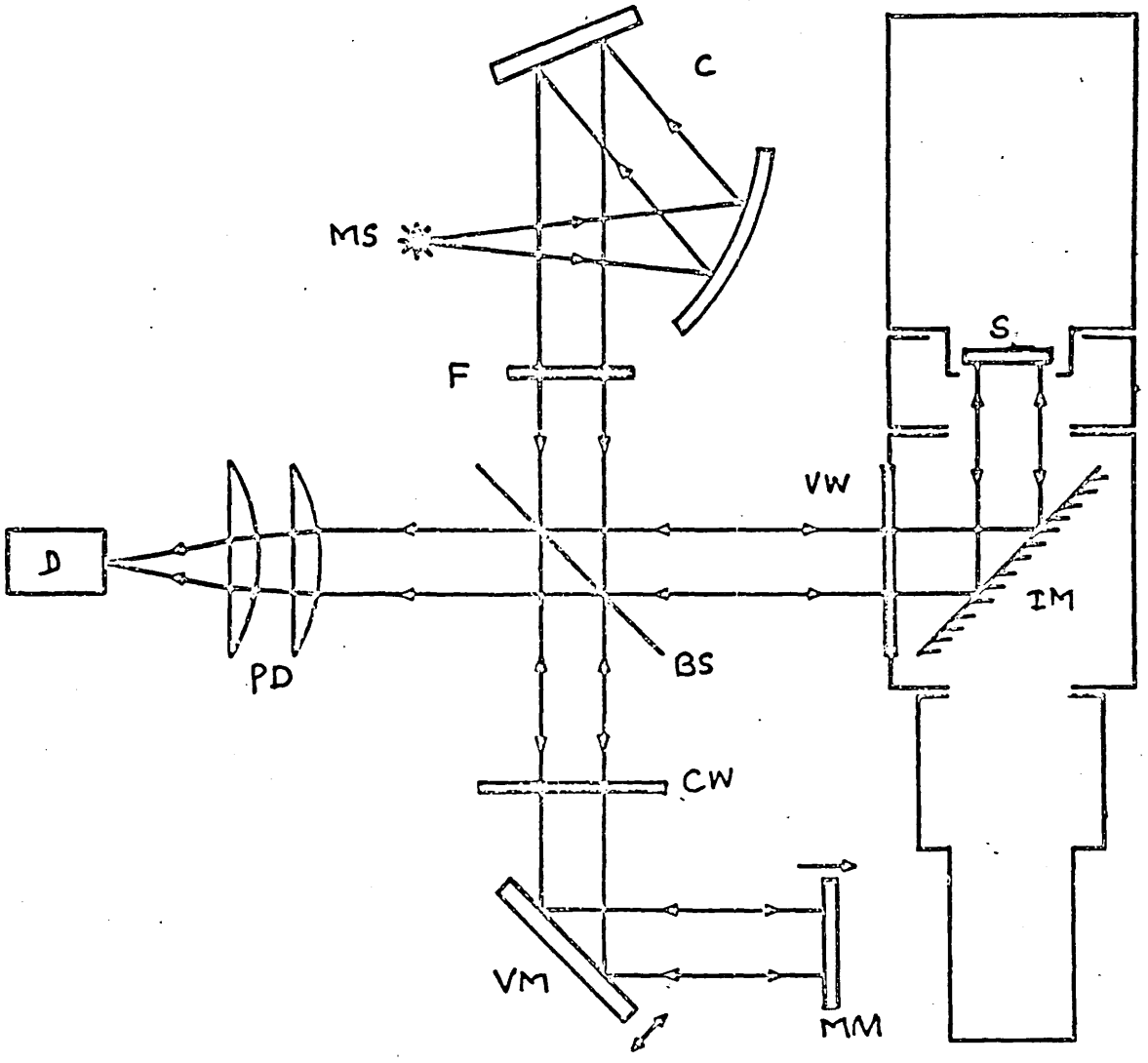

Fig(4.4) A schematic representation of the reflection interferometer

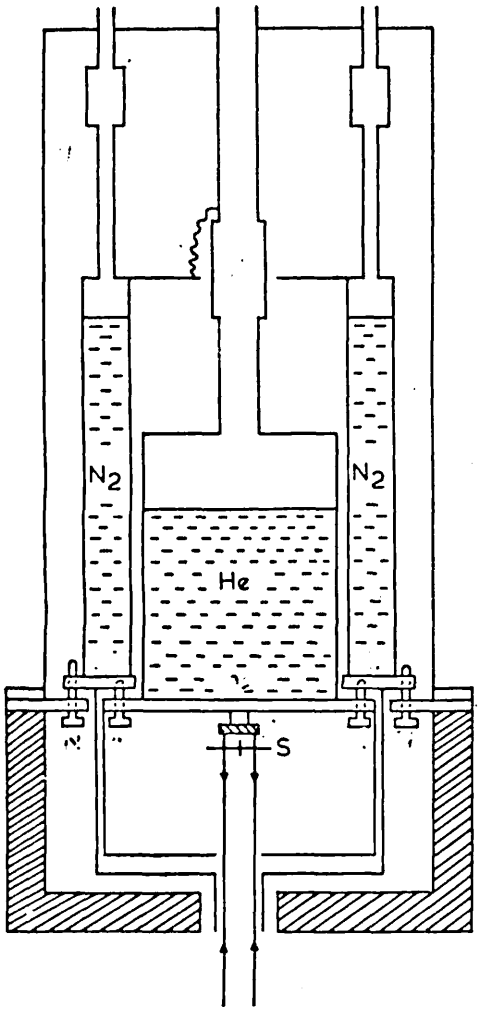

Liquid helium cryostat

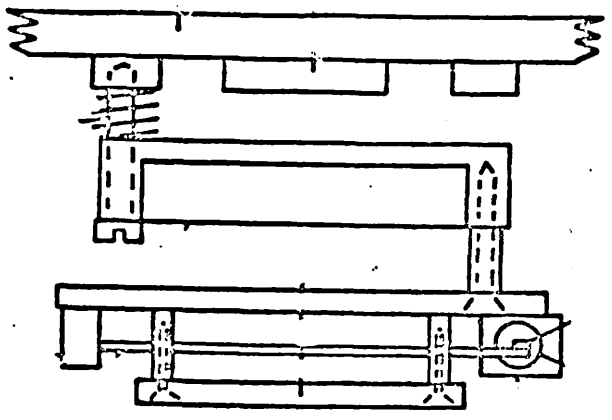

(a) Sample mount

Fig(4.5)

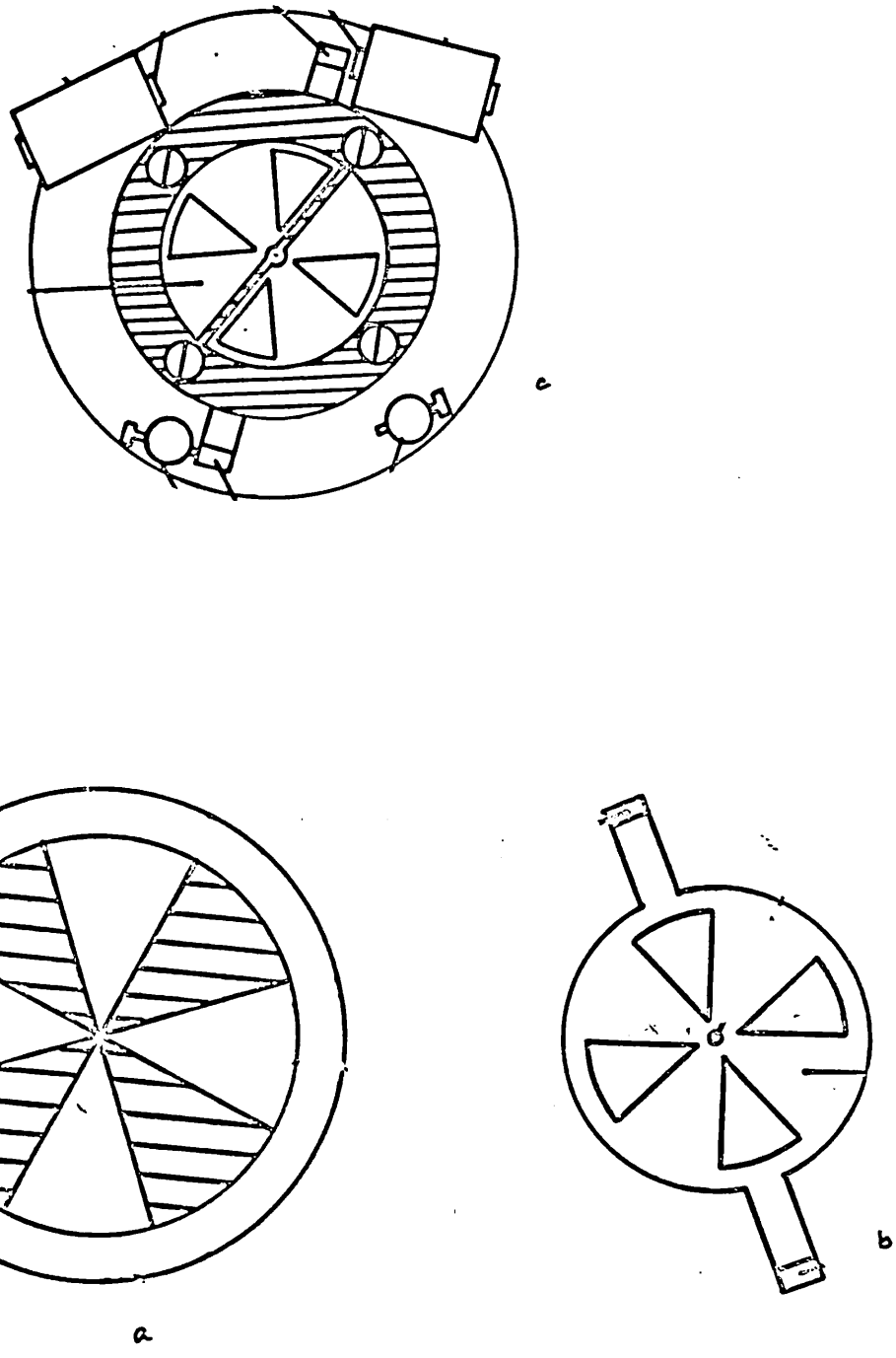

Fig(4.6) Screen and crystal geometry

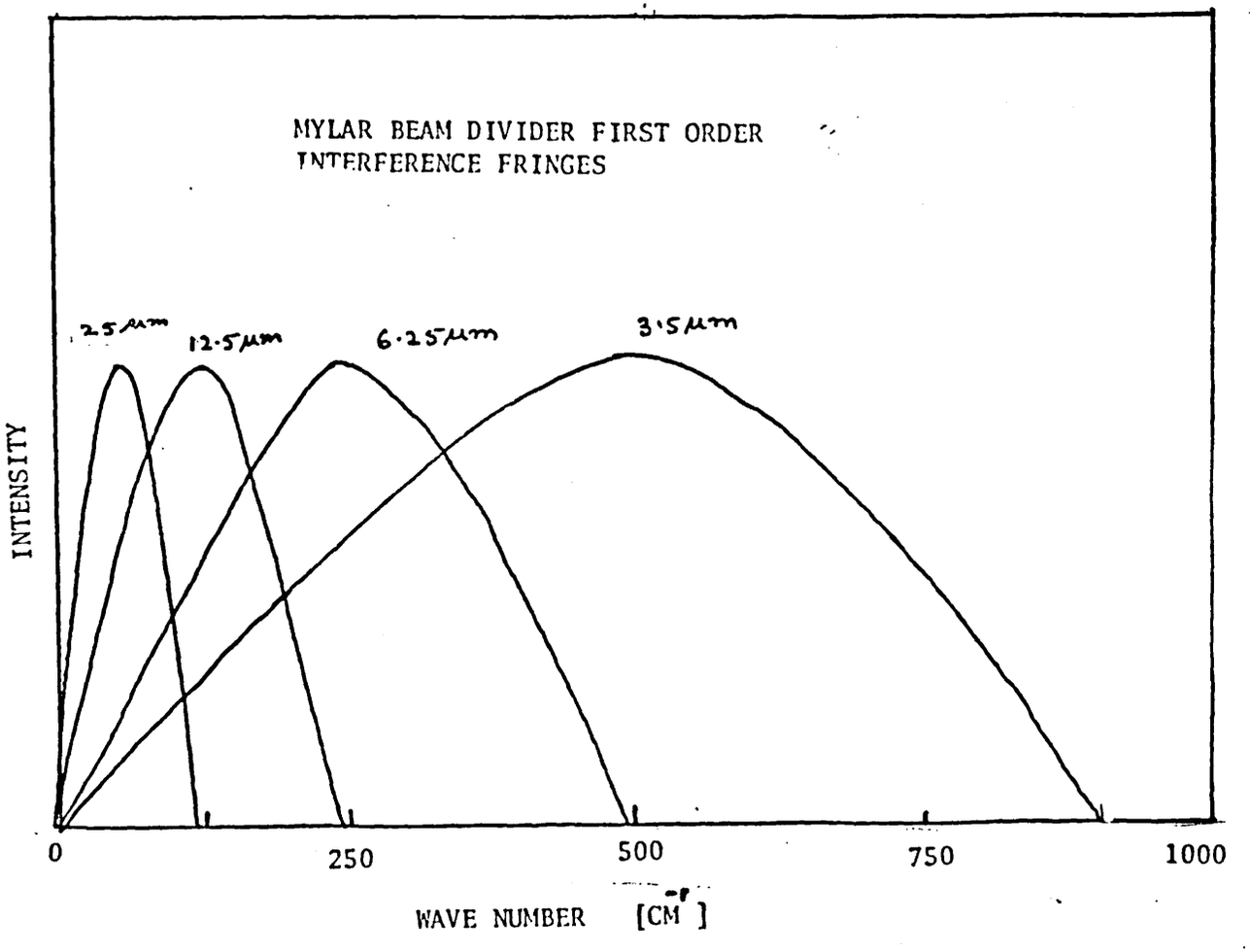
MYLAR BEAM DIVIDER FIRST ORDER
INTERFERENCE FRINGES
25 μm
12.5 μm
6.25 μm
3.5 μm
INTENSITY
0
250
500
750
1000
WAVE NUMBER [CM⁻¹]

Fig(4.7)

94

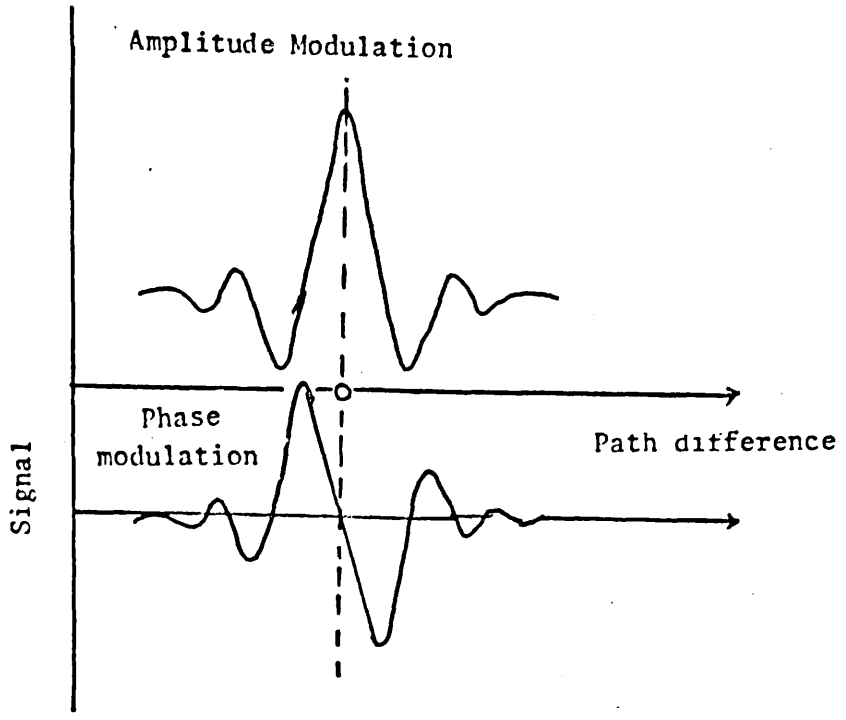

Fig(4.8) Illustrations for amplitude and phase modulation

REFRACTING OPTICS

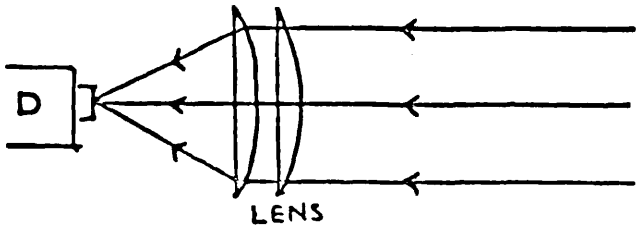

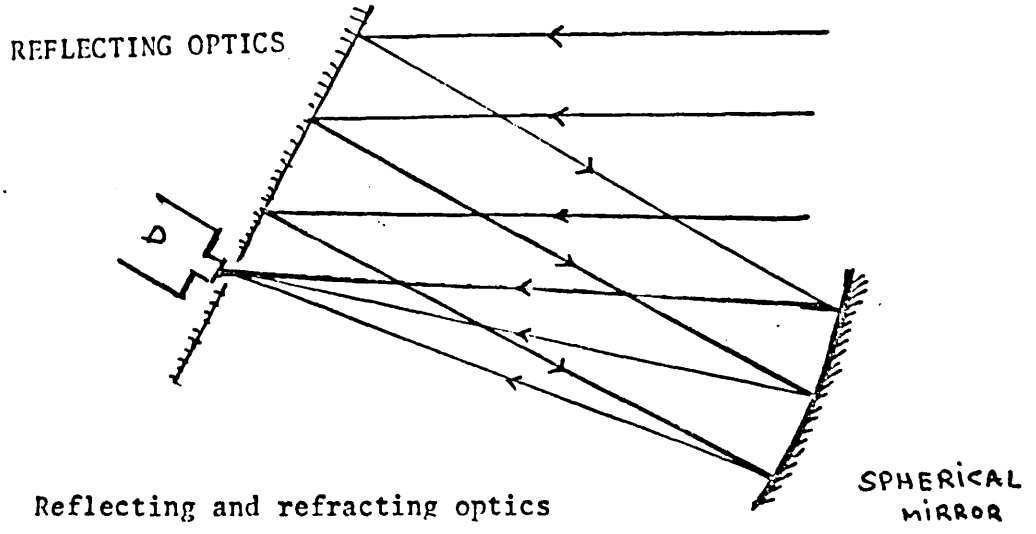

Fig(4.9) Reflecting and refracting optics

A BLOCK DIAGRAM FOR ELECTRONIC ARRANGEMENT.

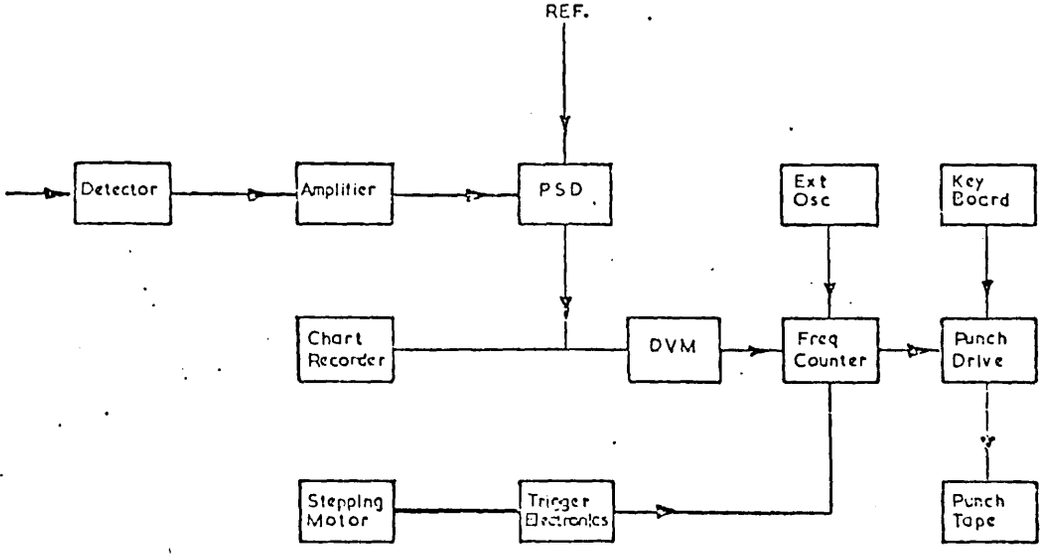

Fig(4.10)

96

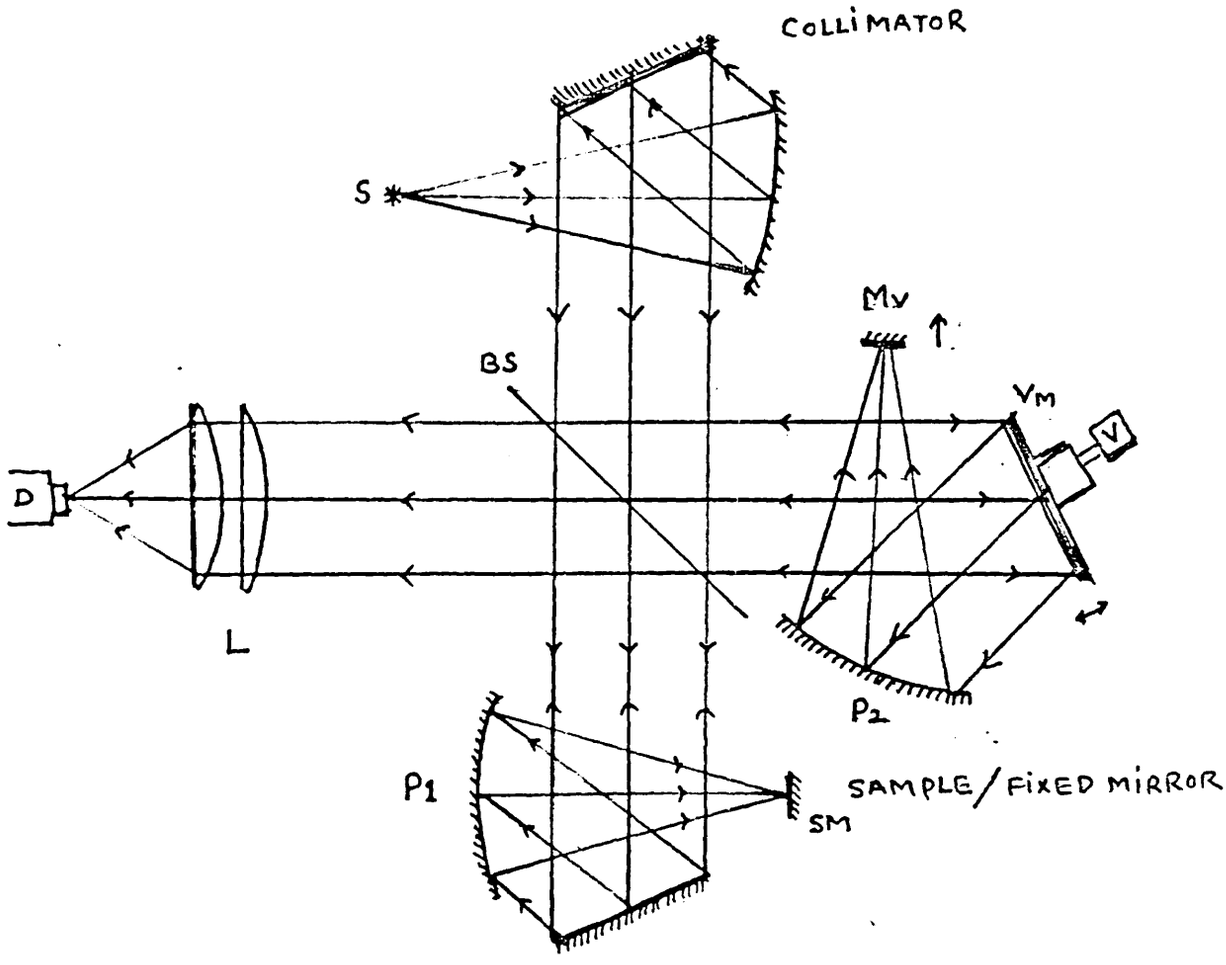

FOCUSED BEAM INTERFEROMETER

Fig(4.11)

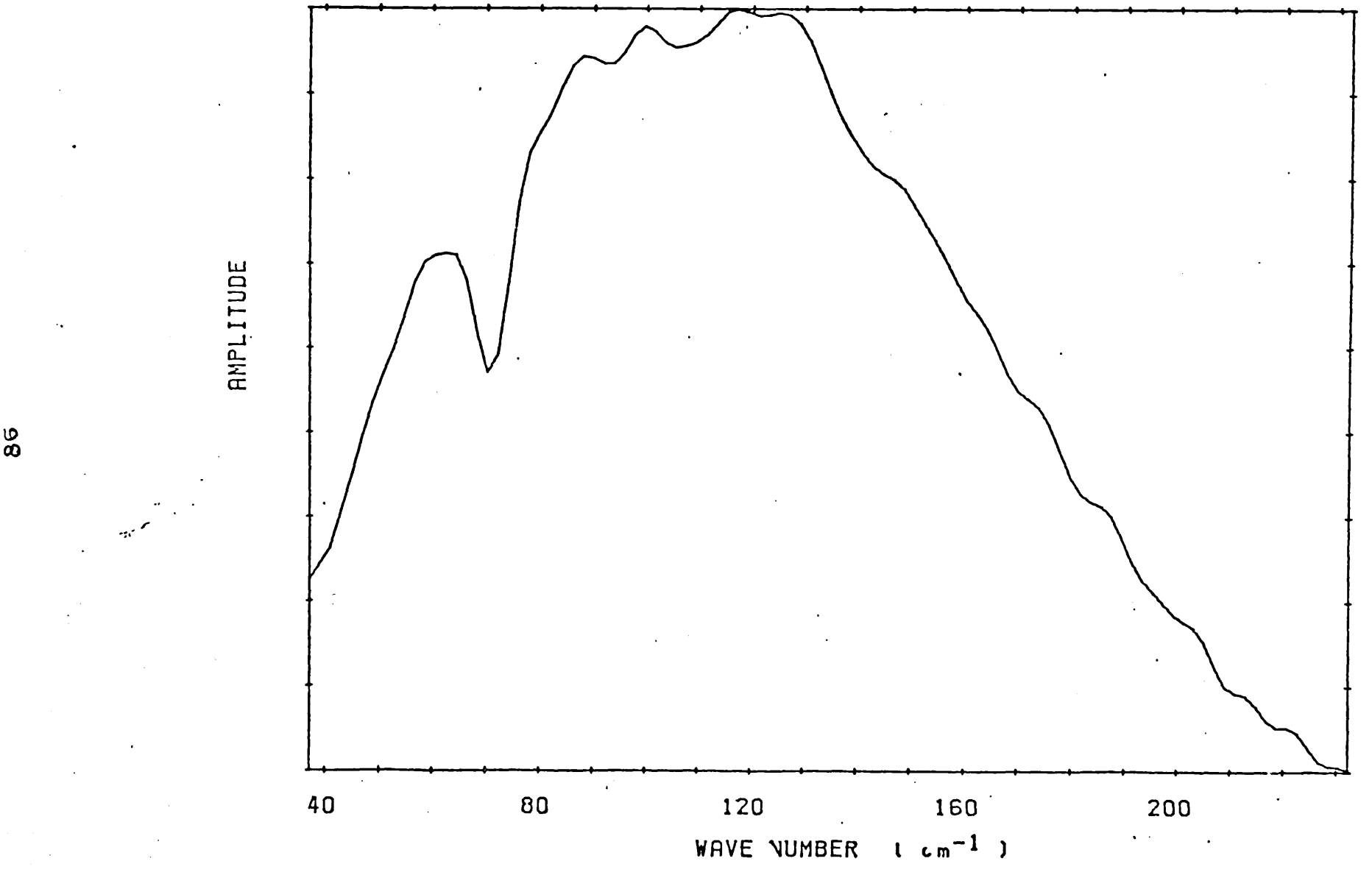

Fig(4.12) Measured background spectrum produced from focussed beam interferometer

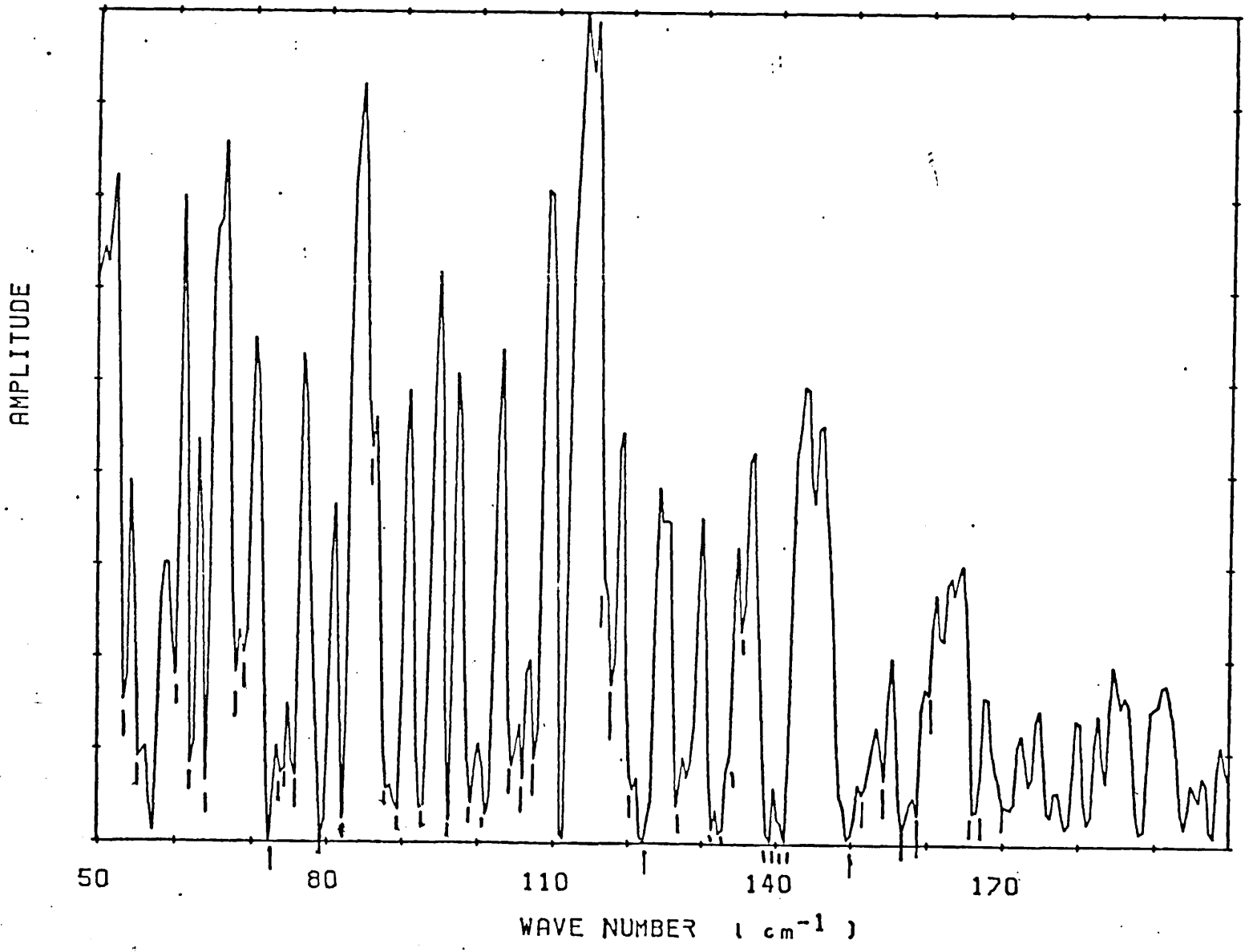

Fig(4.13) Measured far infrared watervapour absorption spectrum

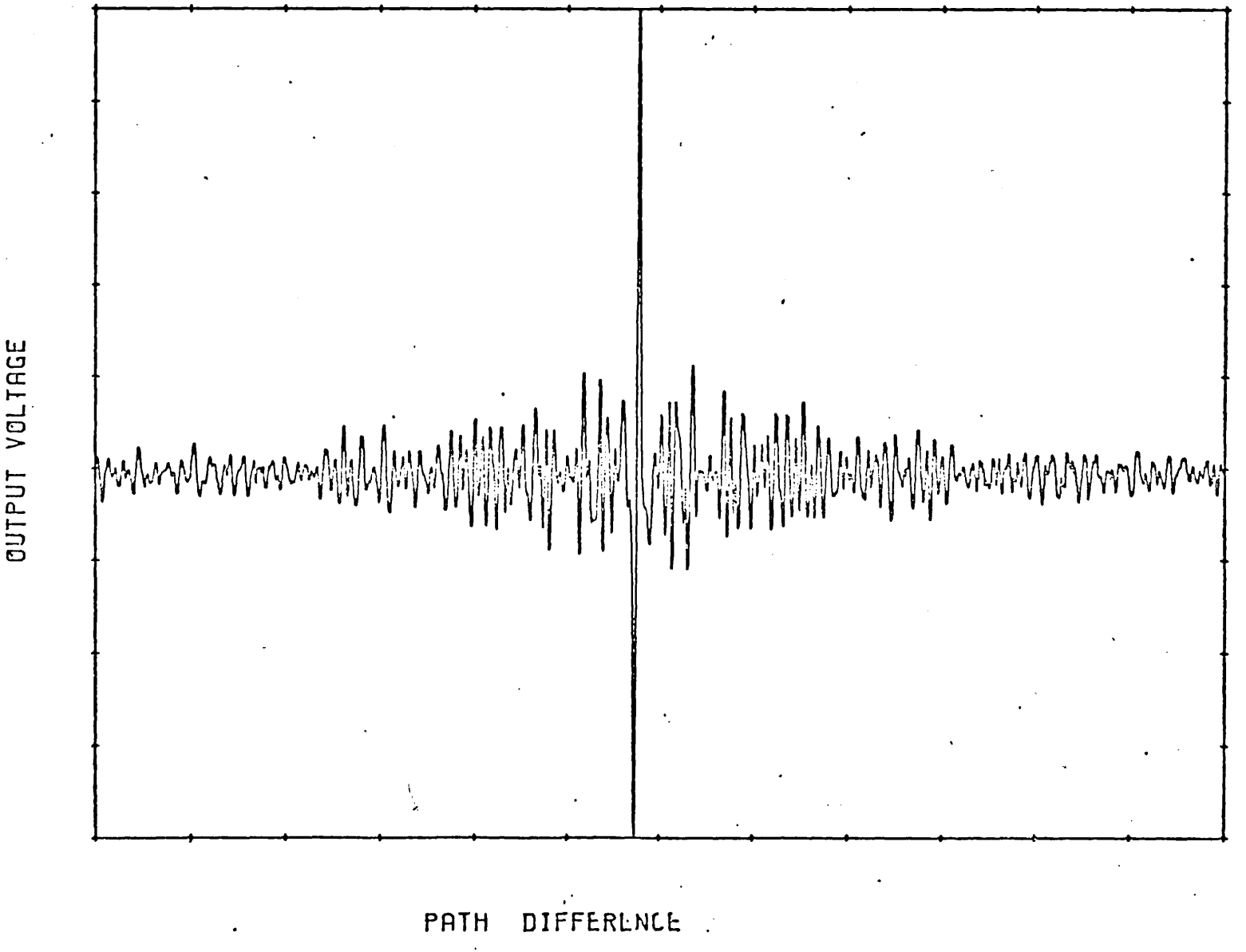

Fig(4.14) Recorded water vapour interferogram

CHAPTER 5

FAR INFRARED OPTICAL PROPERTIES OF SOLIDS

5.1) Introduction

The theory presented in this chapter is concerned primarily with the far infrared optical properties of diatomic cubic crystals associated with atomic vibrations.

To start with we consider the familiar photon-phonon interaction in an ionic lattice within the harmonic approximation, and have derived the LST relation, and dispersion relation for the simple harmonic oscillator. This model is then extended by including a frequency dependent damping function as the simple harmonic oscillator model is insufficient to explain the experimental results. Also a review of the effects of anharmonicity as discussed by Cowley (1963) is given in brief, and a modified form for the dielectric response function is given for interpreting the experimental results.

A brief discussion on infrared selection rules together with tables for infrared active two-phonon transitions for alkali halide and III-V compound semiconductors is given here. The chapter is concluded by describing the Bose-Einstein factor used in evaluating the temperature dependence of phonon combination bands.

5.2) Dispersion relation in diatomic crystals

In diatomic cubic crystals the formal solution for the interaction of electromagnetic radiation with the crystal has been given by many authors like Born and Huang (1954), Zeeman

(1960), Donovan and Angress (1971). We will give here the outline of the derivation of the dispersion relation for far infrared radiation by cubic crystals.

In a crystal with N atoms per unit cell the angular frequency w is a multi-valued function of the wave vector q, and has 3N branches for $w_j(q) \to 0$ as $q \to 0$ which are known as acoustic branches. In an acoustic mode at wave vector $q \sim 0$ the N atoms move in the same direction with the same amplitude. The remaining 3(N - 1) branches have non-zero values of $w_j(q)$ at long wavelength, i.e, the frequencies do not vanish in the low frequency limit and they are called optical modes. Hence for diatomic crystals there are six vibrational branches; three acoustic and three optical ; these optical and acoustic branches are represented by well known w - q plots, i.e, the dispersion curves. In ionic crystals an oscillatory dipole moment is created due to the motion of ions in anti-phase, and this can interact directly with the electric field vector of the incident electromagnetic (EM) radiation. When EM radiation interacts with a crystal lattice the infrared-active branches are modified due to the interaction of the radiation with the ions. The propagation of the EM wave and the lattice waves is not independent, and the modified wave is the combination of EM and mechanical vibrations [Born and Huang (1954)].

The salient features of the phenomenological theory of infra red dispersion in ionic crystals given by Born and Huang are given below. Since our studies are limited to diatomic cubic crystals, henceforth we shall consider only this case. For such

crystals the equation of motion can be described in terms of a macroscopic electric field E and the relative displacement of two ions in a unit cell. The equation of motion and the polarization can be written as (Born and Haung 1954) :

$$\ddot{\underline{W}} = b_{11}\,\underline{W} + b_{12}\,\underline{E} \tag{5.1}$$

$$\underline{P} = b_{21}\,\underline{W} + b_{22}\,\underline{E} \tag{5.2}$$

where in these equations

$$\underline{W} = [\bar{M}/V]^{\frac{1}{2}}(U_+ - U_-) \tag{5.3}$$

and

$$\bar{M} = (M_+ \times M_-)/(M_+ + M_-) \tag{5.4}$$

is the reduced mass of the ions, V is the volume of the unit cell, and $(U_+ - U_-)$ is the relative displacement of the ions in a unit cell. In the above relations $\underline{P}$ and $\underline{E}$ are the dielectric polarization and macroscopic field $\underline{E}$, respectively, and the b's are scalar coefficients. It can be shown that for a cubic diatomic lattice $b_{21} = b_{12}$ as a consequence of the principle of conservation of energy. The above equations of motion are valid only if $\underline{W}$, $\underline{P}$, and $\underline{E}$ vary negligibly as compared to the lattice constant.

Since the interatomic forces in a crystal are usually strongly dependent on the interatomic spacing the lattice potential energy of a crystal can be written as a power series in the displacements of the atoms from their equilibrium positions. If such an expression is terminated at the quadratic term, then this constitutes the so-called harmonic approximation, i.e,

$$V = \xi_0 U_0 + \xi_1 U + \xi_2 U^2 + \qquad (5.4a)$$

In the harmonic approximation the lattice vibrations are true normal modes such that if energy is channeled uniquely into any one lattice mode, then it will remain undissipated in that mode. The harmonic approximation would therefore predict, for example, that the spectral profiles of lattice vibrations would be a set of undamped temperature independent resonances.

We can solve the above sets of relations in the harmonic approximation, by using Maxwell's equations and assuming that $\underline{W}$, $\underline{E}$, and $\underline{P}$ vary with time as

$$(\underline{W}, \underline{E}, \underline{P}) = (W_0, E_0, P_0) \exp i(wt) . \qquad (5.5)$$

Then, using (5.5), equations (5.1) and (5.2) reduce to

$$- w^2 \underline{W} = b_{11} \underline{W} + b_{12} \underline{E} \qquad (5.6)$$

and

$$\underline{P} = b_{21} \underline{W} + b_{22} \underline{E} \qquad (5.7)$$

The dielectric polarization and electric field can be defined by the relation

$$\underline{E} + 4\pi \underline{P} = \underline{D} = \varepsilon \underline{E} \qquad (5.8)$$

Eliminating W from (5.6) and (5.7) then yields

$$\underline{P} = \left[b_{22} + \frac{b_{12} b_{21}}{-b_{11} - w^2} \right] \underline{E} \qquad (5.9)$$

Substituting the value of polarization from (5.8) in (5.9) we can write the dielectric constant as

$$\varepsilon = 1 + 4\pi b_{22} + \frac{4\pi b_{12} b_{21}}{- b_{11} - w^2} \qquad (5.10)$$

Equation (5.10) is in form similar to the infrared dispersion formula

$$n^2(w) = \varepsilon(w) = \varepsilon_\infty + \frac{(\varepsilon_o - \varepsilon_\infty)\, w_o^2}{w_o^2 - w^2} \qquad (5.11)$$

where n(w) is the refractive index for an optical wave of frequency w and $\varepsilon(w)$ is the corresponding dielectric constant, ε_∞ and ε_o are the limiting high frequency and static dielectric constants, respectively, and w_o is the infrared dispersion frequency, i.e, the frequency at which the conductivity $\sigma = \frac{w}{2}\varepsilon''$, reaches its maximum. The scalar coefficients can now be obtained by comparing the dispersion relation (5.11) with (5.10), i.e,

$$b_{11} = -w_o^2 \qquad (5.12)$$

$$b_{12} = b_{21} = [(\varepsilon_o - \varepsilon_\infty)/4\pi]^{\frac{1}{2}} w_o \qquad (5.13)$$

and

$$b_{22} = (\varepsilon_\infty - 1)/4\pi \qquad (5.14)$$

Equations (5.1) and (5.2) can be solved simultaneously using Maxwell's equations. If we assume that W, E, P, and the associated magnetic field H all vary as $\exp[i(k\cdot r - wt)]$, then we have

$$\underline{k}\cdot(\underline{E} + 4\pi\underline{P}) = 0 \qquad (5.15)$$

$$\underline{k}\cdot\underline{H} = 0 \qquad (5.16)$$

$$\underline{k} \times \underline{E} = (w/c)\underline{H} \qquad (5.17)$$

$$\underline{k} \times \underline{H} = -(w/c)[\underline{E} + 4\pi\underline{P}] \qquad (5.18)$$

We notice here that E cannot be zero, for if $\underline{E}$ were to vanish, which implies from (5.17) that H also vanishes, then from (5.18) it is obvious that $\underline{P}$ is also zero and so is $\underline{W}$. Thus $\underline{E}=0$ leads to $\underline{E}=\underline{H}=\underline{P}=\underline{W}=0$. From (5.9) and (5.15) we obtain

$$(\underline{k} \cdot \underline{E}) \left\{ 1 + 4\pi b_{22} + \frac{4\pi b_{12} b_{21}}{(-b_{11} - w^2)} \right\} = 0 \qquad (5.19)$$

This equation allows two alternate possibilities :

(A) Longitudinal waves

$$1 + 4\pi b_{22} + \frac{4\pi b_{12} b_{21}}{-b_{11} - w^2} = 0 \qquad (5.20)$$

On account of (5.9) , (5.20) implies also that

$$\underline{E} + 4\pi \underline{P} = 0 \qquad (5.21)$$

Thus in this case (5.18) reduces to

$$\underline{k} \times \underline{H} = 0 \qquad (5.22)$$

This requires that either H is parallel to k or vanishes, but on the other hand from (5.16) H is either perpendicular to k or vanishes. Thus in this case H=0, and therefore (5.17) reduces to

$$\underline{k} \times \underline{E} = 0 \qquad (5.22a)$$

As E does not vanish it must be parallel to k. Furthermore $\underline{W}$, $\underline{P}$, must also be parallel to $\underline{k}$, as is clear from (5.1), (5.2) and (5.9). Thus, in this case $\underline{W} \| \underline{P} \| \underline{E} \| \underline{k}$, which specifies longitudinal waves. The frequency of the longitudinal mode which we denote by w is then given by the solution of (5.20) as

$$w^2 = -b_{11} + \frac{4\pi b_{12} b_{21}}{1 + 4\pi b_{22}} = w_L^2 \qquad (5.23)$$

Substituting the values of the scalar coefficients from (5.12 - 14) in (5.23) we have

$$w_L^2 = \left[\frac{\epsilon_o}{\epsilon_\infty}\right] w_0^2 \qquad (5.24)$$

which is the well known Lyddane-Sachs-Teller (LST) relation (Lyddane et al 1941). Now we consider the second case i.e,

B) Transverse waves

If $\underline{k}\cdot\underline{E} = 0$ and E is non zero, then E must be perpendicular to k, and it follows from (5.17) that k, E, and H form a right-handed orthogonal system of vectors and their scalar magnitudes are related as follows :

$$\underline{k}\underline{E} = [w/c]\,\underline{H} \qquad (5.25)$$

Hence (5.17) reduces to the scalar relation

$$kH = (w/c)[\,\underline{E} + 4\pi\underline{P}] \qquad (5.26)$$

Eliminating H from (5.25) and (5.26) we have

$$[\,k^2 c^2/w^2]\underline{E} = \underline{E} + 4\pi\underline{P} \qquad (5.27)$$

Now eliminating H and P by using (5.9), (5.27) reduces to

$$(kc/w)^2 = 1 + 4\pi b_{22} + \frac{4\pi b_{12} b_{21}}{-b_{11} - w^2} \qquad (5.28)$$

Since E cannot vanish, once it is specified, W and P are fully determined by (5.6) and (5.9). To summarise, all the solutions in (B) are transverse, namely k, $(\underline{W} \,||\, \underline{P} \,||\, \underline{E})$, $\underline{H}$ are all mutually perpendicular. For a given wave number $\underline{k}$ (5.28) produces two solutions. Since $\underline{k}$ and $-\underline{k}$ are both permitted within the system, there are four independent transverse vibrational modes corresponding to two doubly degenerate frequencies. Thus, putting in the values of the scalar constants, and

as the refractive index is the ratio of the velocity of light to the phase velocity, the wave equation (5.28) reduces to

$$n^2(w) = \varepsilon(w) = \varepsilon_\infty + \frac{(\varepsilon_0 - \varepsilon_\infty)\, w_0^2}{w_0^2 - w^2} \qquad (5.29)$$

From (5.29) we see that $\varepsilon(w)$ rises from its static value ε_0 as w increases, becomes infinite when w reaches the dispersion frequency i.e, $w = w_0$, and then negative for w infinitesimally greater than w_0 and remains negative until becoming zero for the frequency satisfying the relation

$$0 = \varepsilon_\infty + \frac{(\varepsilon_0 - \varepsilon_\infty)\, w_0^2}{(w_0^2 - w^2)} \quad , \qquad (5.29a)$$

the solution of which is $w = (\varepsilon_0/\varepsilon_\infty)^{\frac{1}{2}} w_0$. The dielectric constant is therefore negative between the limits $w_0 < w < w_L$ This implies that the refractive index is imaginary. The crystal is therefore perfectly reflecting i.e, the power reflectivity approaches unity between the transverse optic mode (TO) and longitudinal optic mode (LO) frequencies. This selective reflection of radiation in the neighbourhood of the optical mode frequencies in an ionic crystal is known as reststrahlen reflection.

5.3) Damping in cubic crystals.

The above treatment is of course unrealistic in the sense that no damping term is present in (5.1), since we know from experience that the TO resonance in diatomic cubic crystals is very broad, i.e, the observed reflectivity in this region does

not agree quantitatively with the above case of a harmonic crystal. The effect of damping is to make N real everywhere, but it is nevertheless very small between the TO and LO mode frequencies.

In a real crystal, however, anharmonic effects are present and these lead to energy dissipation within the crystal. These effects cannot be fully accounted for by the phenomenological introduction of a frequency independent term in the equation of motion given by (5.1). Hence the modified equation of motion can be written as

$$\ddot{\underline{W}} = b_{11}\,\underline{W} - \gamma\dot{\underline{W}} + b_{12}\,\underline{E} \qquad (5.30)$$

where γ is positive with the dimension of frequency. If we use the periodic solution

$$(\underline{W}, \underline{E}) = (W_0, F_0)\exp i(wt) \qquad (5.30a)$$

then we can write (5.30) as

$$-w^2\,\underline{W} = (b_{11} + iw\gamma)\,\underline{W} + b_{12}\,\underline{E} \qquad (5.31)$$

Thus by comparing this equation with the undamped Eq(5.1), we reach the conclusion that the addition of a damping term is similar to replacing the scalar coefficient with the term $(b_{11} + iw\gamma)$. Hence the new dispersion formula can be given as

$$\varepsilon(w) = \varepsilon_\infty + \frac{(\varepsilon_0 - \varepsilon_\infty)\,w_0^2}{w_0^2 - w^2 - iw\gamma} \qquad (5.32)$$

In a real crystal the damping may be frequency dependent

and complex and this may give rise to additional structure. Thus under the harmonic approximation this frequency independent model fails to account for detailed structure in the measured infra red spectra (Hisano et al 1972). For most alkali halide materials the variation in Γ_{oj} below the TO mode frequency is small, but Γ_{oj} increases and changes significantly in the LO frequency range. To account for detailed interactions between the normal modes one has to include the higher order terms in the potential function in (5.4a), which are normally known as the anharmonic terms i.e

$$V = \xi_0 U_0 + \xi_1 U + \xi_2 U^2 + \xi_3 U^3 + \cdots \qquad (5.32a)$$

The inclusion of the anharmonic terms in the lattice potential has two consequences. Firstly, the phenomenon of thermal expansion is now allowed, and secondly, the anharmonicity allows interactons between the normal modes. The net effects of these interactions is to open up channels for the decay of phonons which lead to changes in the phonon energies together with the appearance of finite life times for the phonons (Maradudin and Fein 1962, Cowley 1963).

Theoretical and experimental studies of the effects of anharmonicity on various physical properties have been carried out by many authors; in particular Cowley (1963), and Wallis et al (1966). Since the theory of the dielectric response of anharmonic crytals has been given in detail by Cowley, we will only quote the requisite results here. The frequency dependent dielectric susceptibility $\chi_\alpha(w)$ for a crystal possessing cubic

symmetry, and using the first order dipole moment and including the contribution from anharmonicity can be given as

$$\chi_{\alpha}(w) = (1/Nv\hbar)\frac{2\, w\,(oj)\, M_{\alpha}^{2}(oj)}{w^{2}(oj) - w^{2} + 2w(oj)[\Delta(oj,w) - i\Gamma(oj,w)} \qquad (5.33)$$

[Cowley (1963)]

Here v is the volume of a unit cell, N is the number of unit cells in the crystal, w is the angular frequency of the radiation field, w(oj) is the angular frequency of a phonon mode, in the harmonic approximation, belonging to wave vector q=0 and branch index j, and $M_{\alpha}(oj)$ is the α (cartesian) component of the coefficient of the leading term in the expansion of the crystal dipole moment operator in a power series of the phonon field operator. The terms $\Delta(oj,w)$ and $\Gamma(oj,w)$ are the real and imaginary parts of the self - energy of the TO phonon. The real part of the self-energy can be written as the sum of two parts

$$\text{i.e,} \qquad \Delta(oj,w) = \Delta^{E}(oj) + \Delta^{A}(oj,w) \qquad (5.33a)$$

where $\Delta^{E}(oj)$ is a frequency - independent contribution which arises from the thermal expansion of the crystal, and $\Delta^{A}(oj,w)$ is frequency dependent, and arises purely from anharmonic interactions in the crystal.

The lowest order expressions for $\Delta(oj,w)$ and $\Gamma(oj,w)$ which arise from thermal expansion and cubic anharmonicity of the lattice have been derived by Cowley (1963) , and Maradudin and Fein (1962). We reproduce below the dielectric susceptibility and self energy functions which they used in their calculations. Also we will present here the modified expression of these

quantities in terms of experimentally measured quantities.

The expression for the frequency - dependent dielectric susceptibility is given in (5.33), whereas the Hermitian i.e, real part of the frequency dependent self energy can be written as (Cowley 1963).

$$\Delta(oj,w) = -(18/\hbar^2) \sum_{q_1 j_1 j_2} \left| V(oj, q_1 j_1, q_2 j_2) \right|^2 R(w)$$

and $$\Gamma(oj,w) = +(18\pi/\hbar^2) \sum_{q_1 j_1 j_2} \left| V(oj, q_1 j_1, q_2 j_2) \right|^2 S(w)$$

(5.34) and (5.35) respectively.

where $$R(w) = (n_1 + n_2 + 1)\left[(w_1 + w_2 + w)_P^{-1} + (w_1 - w_2 + w)_P^{-1} \right]$$

$$+ (n_2 - n_1)\left[(w_1 - w_2 - w)_P^{-1} + (w_1 - w_2 + w)_P^{-1} \right] \quad (5.36)$$

and $$S(w) = (n_1 + n_2 + 1)\left[\delta(w_1 + w_2 - w) - \delta(w_1 + w_2 + w) \right]$$

$$+ (n_1 - n_2)\left[\delta(w_1 - w_2 + w) - \delta(w_1 - w_2 - w) \right] \quad (5.37)$$

Here S(w) is a function of temperature and wave number resulting from the transition probabilities for phonon creation and destruction, and the conservation of energy between the initial phonon state and final two-phonon state. The first part in (5.37) describes the summation process where two phonons are created and the second part presents the difference process in which one phonon is created and another destroyed.

In (5.36) and (5.37) $w = w(q\,j)$, and $n(q\,j)$ is the occupation number for the mode $(q\,j)$, and is given as

$$n = n(qj) = \exp\left[(\hbar w(qj)/K_B T - 1 \right]^{-1} \quad (5.38)$$

where w(qj) is the frequency of the mode in the harmonic approximation. T is the absolute temperature and K_B is Boltzmann's constant. The summations in (5.34) and (5.35) extend over all phonon modes of the crystal. Also $V(oj, q_1 j_1, q_2 j_2)$ is the cubic coupling coefficient that connects the three modes (oj), $(q_1 j_1)$, and $(q_2 j_2)$, via cubic anharmonicity of the lattice. An explicit expression for the cubic coupling coefficient is given by Johnson and Bell (1969) and Berg and Bell(1971).

The modified relation for the dielectric suceptibility can also be written in terms of experimentally measured quantities as shown below. The frequency dependent dielectric constant can be written in terms of the dielectric susceptibility as function of frequency ν which is here given in wave numbers:

$$\hat{\varepsilon}(\nu) = \varepsilon(\infty) + \hat{\chi}_\alpha(\nu) \qquad (5.39)$$

Therefore, using (5.39),(5.33) can be written as

$$\hat{\varepsilon}(\nu) = \varepsilon(\infty) + \frac{(1/Nvh)[\, 2\nu(oj)\, M_\alpha^2(oj)\,]}{[\,\nu^2(oj) - \nu^2 + 2\nu(oj)\,[\Delta(oj,\nu) - i\Gamma(oi,\nu)]\,]} \qquad (5.40)$$

For zero frequency (5.39) and (5.40) reduce to

$$\chi_\alpha(0) = \varepsilon(o) - \varepsilon(\infty) \qquad (5.41)$$

$$\chi_\alpha(0) = 2\, M_\alpha^2(oj)/\, N\, v\, h\, \nu(oj) \qquad (5.42)$$

Thus using (5.41) and (5.42), Eq(5.40) can be written as

$$\hat{\varepsilon}(\nu) = \varepsilon(\infty) + \frac{[\varepsilon(o) - \varepsilon(\infty)\,]\,\nu^2(oj)}{\nu^2(oj) - \nu^2 + 2\nu(oj)[\Delta(oj,\nu) - i\Gamma(oj,\nu)]} \qquad (5.43)$$

The real and imaginary parts of the anharmonic self-energy of the TO mode can be obtained from (5.33a) and (5.43)as

$$\Delta^{A}(oj,\nu) = (1/2)\,\nu(oj)[(\varepsilon(o) - \varepsilon(\infty))\eta'(\nu) - 1] + [\nu^2/\nu(oj)] - \Delta^{E}(oj) \qquad (5.44)$$

$$\Gamma(oj,\nu) = -(1/2)\,\nu(oj)[\varepsilon(o) - \varepsilon(\infty)]\,\eta''(\nu) \qquad (5.45)$$

where $$\eta'(\nu) = [\varepsilon'(\nu) - \varepsilon(\infty)]/\{[\varepsilon'(\nu) - \varepsilon(\infty)]^2 + \varepsilon''(\nu)^2\} \qquad (5.46)$$

$$\eta''(\nu) = -\varepsilon''(\nu)/\{[\varepsilon'(\nu) - \varepsilon(\infty)]^2 + \varepsilon''(\nu)^2\} \qquad (5.47)$$

The full frequency dependence of the above functions can than be evaluated from the real and imaginary parts of the dielectric constant measured directly by dispersive FTS.

2.4) Selection rules

The mechanism of the interaction of electromagnetic radiation with phonons in a polar crystal which causes additional features besides the fundamental resonance has been discussed by Klienman (1960) and Cowley(1963). These side bands are created due to the anharmonic part of the potential energy associated with the lattice vibrations. This kind of interaction is due to the presence of a dipole moment associated with polar crystals.

On the other hand in the case of homopolar cubic crystals, because of the centre of inversion symmetry (diamond structure) the displacement of two identical atoms for an optic mode at wave vector q=0 produces no coupling because of the zero dipole moment. Thus the anharmonic mechanism will be inoperative in

these cases, Lax and Burstein (1955) have shown that the absorption in such crystals is due to the direct interaction of two or more phonons with the radiation through terms in the electric moment of second or higher order in the atomic displacement. The order of term corresponds to the number of phonons involved. Lax and Burstein also suggested that the second order terms in the electric moment may be observed as the result of one vibrational mode inducing charges on the atoms while the second vibrational mode causes these charges to vibrate, thus producing an electric moment that can couple to the radiation field.

Regardless of the coupling mechanism between the radiation field and the phonons, the selection rules for the interaction of EM radiation with the crystal vibrations are based on the requirements of conservation of energy and momentum and the need for a dipole moment.

If we assume that $\hbar w$ and k are the energy and wave vector of the absorbed photon and q is the wave vector of the created or destroyed phonon of frequency $w(q_i)$ then

$$\hbar w = \sum_i \pm \hbar w(q_i) \qquad (5.48)$$

and

$$k + nb = \sum_i \pm q_i \qquad (5.49)$$

where b is a reciprocal lattice vector and n is a positive or negative integer or zero. Since the wave vector k of a photon in the infrared region is small compared to the phonon wave vector q over most of the Brillouin zone, (5.60) reduces to

$$n\,b = \sum_i \pm q_i \qquad (5.49a)$$

For one and two-phonon processes n=0, and for a three-phonon process n=0, $\pm$ 1. Here we will only consider up to two-phonon processes in the final state. In a one-phonon process a photon from the radiation field is absorbed and a TO phonon is generated at the center of the Brillouin zone ($q \sim 0$). Thus from the above considerations a one- phonon process will have

$$w = \pm w(q) \tag{5.50}$$

$$k = q \tag{5.51}$$

Since $k = 2\pi/\lambda$, where $\lambda \gtrsim 10$ micron, and $|q_{max}|$ i.e, $|q|$ at the zone edge is of the order of π/a where a is the lattice constant, Eq(5.51) becomes equal to $q \approx 0$. Near q=0, w(q) can assume values appropriate to each of the branches. However, only the TO branch possesses an electric moment capable of coupling to the radiation field, and therefore

$$\hbar\, w(q) = \hbar\, w \tag{5.52}$$

A two-phonon process may take place if there are anharmonic terms in the potential function or in the series expansion of the transition moment. For cubic crystals having a center of inversion (like alkali halides and diamond structure crystals), the vectors q_1 and q_2 of the two-phonons belong to different branches. Hence there are no overtones $2w(q_i)$ in such crystals. (Szigeti 1960).

Now we will describe the phenomenon of two-phonon absorption. Here we will consider the effects of electric and potential anharmonicity separately. We have described above the

effects of electric anharmonicity in terms of the coupling of a photon to two phonons which can be presented schematically as in fig(5.1). In two-phonon optical processes due to the non-linearity of the transition moment the photon from the radiation field is absorbed by coupling directly with two phonons of frequency $w(q_1)$ and $w(q_2)$, leading to a summation band

$$\hbar w(k) = \hbar w(q_1) + \hbar w(q_2) \tag{5.53}$$

$$k = q_1 + q_2 \approx 0 \tag{5.54}$$

If the absorption of a photon of energy $\hbar w(k)$ creates one phonon and destroys another the resulting energy is given as

$$\hbar w(k) = \hbar w(q_1) - \hbar w(q_2) \tag{5.55}$$

Both the summation and difference processes are illustrated in fig(5.1).

A two-phonon optical process due to the anharmonicity of the potential function is more complicated. Here at first the photon w(k) from the radiation field first couples to a TO phonon of wave vector $q \sim 0$. This TO phonon serves as an intermediate (virtual) state, which then couples with the two phonons $w(q_1)$ and $w(q_2)$ leading to summation and difference bands as illustrated in fig(5.2). Hence the combination of two phonons should give rise to absorption. However, the absorption maxima are produced due to peaks in the two-phonon density of states. Therefore any structure in the infrared spectrum as a consequence reflects structure in the frequency dependence of the combined density of states of the participating phonons. The regions where the phonon concentration is large in the phonon dispersion curves

are known as critical points. The singularities corresponding to the critical points occur where the dispersion curves for the individual branches are flat. In the case of cubic diamond and zinc blende structure crystals the relevant critical points are Γ, the center of the Brillouin zone, L, the center of a face and X, the center of a face. The coordinates of these points are (0,0,0), (1/2,1/2,1/2) and (1,0,0), respectively, and the other major critical points are W, the peak of coordinates, and K the edge of the zone, having coordinates (1,1/2,0) and (3/4,3/4,0), respectively.

The selection rules for the infra red spectra of crystals due to higher order effects have been calculated by Szigeti (1960) in a lengthy perturbation calculation, the perturbing term being the anharmonic contribution of the electric transition moment and potential function. Burstein at el (1965) have obtained the selection rules for alkali halides using group theoretical arguments. In table (5.1) we represent the infra red active two phonon combinations of alkali halides as calculated by Burstein.

The selection rules for electric dipole moment allowed two-phonon processes for the diamond and zinc blende structure were calculated by Birman (1962, 1963). The two - phonon selection rules for zinc blende structure crystals are given in table (5.2)

5.5) Temperature dependences of two phonon interactions

At any frequency of the incident radiation the temperature dependence of the absorption spectrum is mainly dependent on the number of phonons present to take part in the proposed multipho-

non process at a given temperature. Since the phonons are bosons and obey Bose - Einstein statistics, the temperature dependence of the average excitation (or occupation) number n of phonons of angular frequency w at the absolute temperature T is given by Kittel (1967) as

$$\langle n_i \rangle = [(\exp (\hbar w / k T)) - 1]^{-1} \qquad (5.56)$$

where K is the Boltzmann constant . The quantum mechanical treatment of the interaction of radiation with a system of oscillators gives the expression for the transition probabilities of absorption and emission of one of these phonons. The probabilities of emission and absorption are proportional to the matrix elements of the phonon creation a and destruction a operators respectively. Hence the emission and absorption probabilities are proportional to $(n_i + 1)$, and n_i, respectively (Ziman 1960).

The net number of phonons which are created in a two-phonon summation process is proportional to the difference of probabilities of creation of two-phonons and destruction of two-phonons. Thus if we assume an absorption band is assigned to a two phonon process such that the absorption of a photon is accompanied by the emission of two phonons (i = 1,2) obeying the conservation laws as laid out in (5.48) and (5.49), then the temperature dependence of the net absorption for the summation band is proportional to

$$(1 + n_1) (1 + n_2) - n_1 n_2 = 1 + n_1 + n_2 \qquad (5.57)$$

In order to arrive at the above result we use the fact that the probability of i unrelated events occurring together is given by the product $p_1\ p_2\ p_3 \ldots\ldots p_i$ of the individual probabilities p_i .

In the case of a difference process, if the absorption of a photon results in the creation of one phonon and the destruction of another then the temperature dependence of the absorption is proportional to

$$(1 + n_1)\ n_2 - n_1(1 + n_2) = n_2 - n_1 \qquad (5.58)$$

The temperature dependence of a two-phonon summation band can also be written by using (5.68) and (5.69) as

$$1 + [(\exp(\hbar w(q_1)/KT) - 1)]^{-1} + [(\exp(\hbar w(q_2)/KT) - 1)]^{-1} \qquad (5.59)$$

and the expression for the temperature dependence of the strength of a difference band can similarly be written as

$$[(\exp(\hbar w(q_2)/KT) - 1)]^{-1} - [(\exp(\hbar w(q_1)/KT) - 1]^{-1} \qquad (5.60)$$

From (5.59) and (5.60) we observe that the phonon occupation number of a difference band approaches zero as the absolute temperature tends to zero, whereas the expression for the phonon occupation number for the summation process remains finite.

Table (5.1)

INFRARED ACTIVE TWO-PHONON COMBINATIONS OF ALKALI HALIDES

Symmetry point†	Active combination
Γ	None
X	None
L	TO + LA, TO + TA, LO + LA, LO + TA
Λ, Δ	TO + LA, TO + TA, LO + LA, LO + TA, TO + LO, TA + LA

After E. Burstein, F. A. Johnson, and R. Loudon, *Phys. Rev.* 139, A1239 (1965).

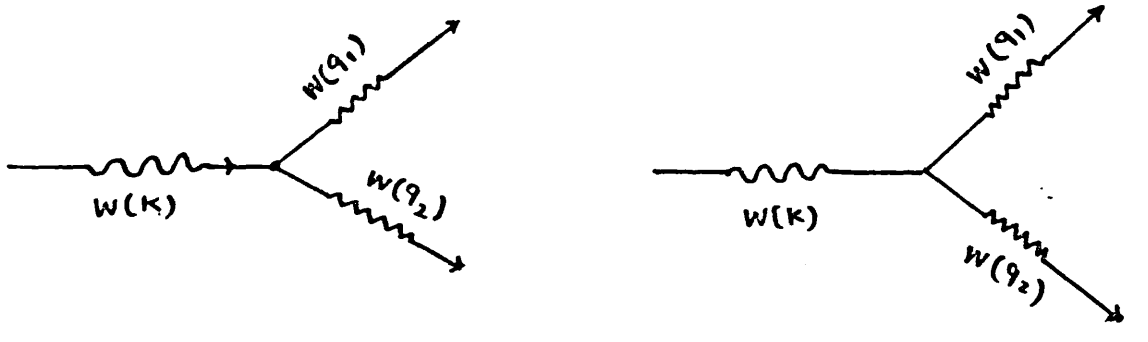

Fig(5.1)

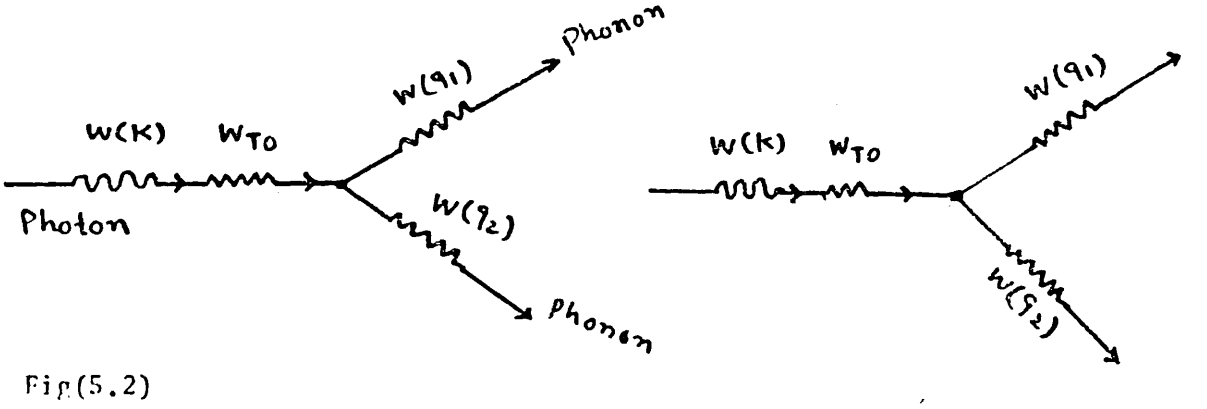

Fig(5.2)

These Figs: represents two-phonon processes

Table (5.2)

DIPOLE-ALLOWED TWO-PHONON PROCESSES IN ZINC BLENDE AT THE CRITICAL POINTS Γ, X, L, AND W

Γ	2LO
	LO+TO
	2TO
X	2TO
	TO+LO
	TO+LA
	TO+TA
	LO+LA
	LO+TA
	LA+TA
	2TA
L	2TO
	TO+LO
	TO+LA
	TO+TA
	2LO
	LO+LA
	LO+TA
	2LA
	LA+TA
	2TA
W	TO_1+LO
	TO_2+LO
	TO_1+LA
	TO_2+LA
	LO+LA
	$LO+TA_1$
	$LO+TA_2$
	$LA+TA_1$
	$LA+TA_2$

CHAPTER 6

EXPERIMENTAL RESULTS AND DISCUSSION

6.1) Alkali halides

Alkali halide crystals and especially CsI and KI were chosen for measurements because their absorption bands fall in the optimum region for the employment of our experimental techniques, and also because theoretical calculations regarding the dispersion curves and selection rules were available in the literature presented by Beairsto and Eldridge (1973), and Eldridge and Kembry (1973). The theoretical calculations for the self-energies of the q=0 TO phonon modes in alkali halide crystals have been given by several authors, especially Cowley (1963) and Wallis (1966), and this provides a good opportunity to test the validity of theoretical calculations with our experimental results.

a) Cesium Iodide, CsI

To determine the optical constants of CsI by dispersive transmission and reflection techniques we used single pass dispersive transmission and dispersive reflection spectrometers. Both the instruments are described in detail in chapter 4.

Pure single crystals of CsI 25mm in diameter and 2mm thick for transmission, measurements were purchased from SPECAC. Since the alkali halides are very strong absorbers in the far infrared region extremely thin samples of the order of 100 micron in thickness were prepared by using the method described in chapter 4. After installing the specimen in the interferometer, the background and sample interferograms were recorded. The ratio of

the Fourier transforms of these two interferograms provides the complex insertion loss $\hat{L}(\nu)$ of the specimen which is related to the amplitude transmission coefficient and phase, as explained in chapter 3. The amplitude transmission coefficient and principle values of the phase spectra so obtained at room temperature and at 77K are given in fig (6.1) and fig(6.2).

Since the specimen used here is very thin, therefore unlike a thick specimen, in order to evaluate the optical constants completely all the transmitted partial waves in the geometric series of Eq(3.52) were included to obtain the single pass complex transmission coefficient. Thus by using the data of fig (6.1) and fig (6.2) the values of complex refractive index were calculated using Eq(3.100). The values of refractive index $n(\nu)$ and absorption index $k(\nu)$ of CsI determined in this way above and below the reststrahlen region at 300K and 77K are given in figs (6.3) and (6.4), respectively.

In the region where the sample was completely opaque i.e, the reststrahlen band, the measurements were done by the dispersive reflection technique. A single crystal of CsI of 40mm diameter and 6mm in thickness was used. One surface of the sample was optically polished to a flatness of about $\pm$0.1micron and partially aluminised in an evaporator using a geometry and screen arrangement as described in chapter 4.

The main problem we came across during the studies of alkali halides, and especially CsI, was the preparation of samples which were very hygroscopic so that prolonged exposure of the crystal to the air had to be avoided. The prepared

specimen was fixed on the base of the cryostat and was aligned parallel to its base. The cryostat was then installed in the fixed mirror arm of the interferometer.

The amplitude and phase reflection spectra were determined by recording the interferogram from the metallized and exposed parts of the crystal surface by moving a screen in front of the specimen, and the detailed procedure is described in chapters(3) and (4).

The amplitude and phase spectra obtained for CsI at 300, 77, and 12K are given in figs (6.5), (6.6), (6.7), respectively. Thus having measured the values of amplitude and phase, the values of refractive index $n(\nu)$ and absorption index $k(\nu)$ were determined using the Fresnel relations for normal incidence. The values of $n(\nu)$ and $k(\nu)$ so obtained at 300 and 77K within the reststrahlen band are given in figs (6.3) and (6.4), respectively, and for demonstration purposes the values of the dielectric constant obtained using Eqs (3.26) and (3.27) for 12K are presented in fig(6.8). Between 60 and 90 cm^{-1} measurements were done by amplitude reflection spectroscopy whereas below 60 and above 90 cm^{-1} measurements were done by dispersive transmission interferometry, all at a resolution of 2 cm^{-1} .

The values of the transverse optic phonon (TO) and longitudinal optic phonon frequencies obtained experimentally at 300, 77, and 12K are indicated in figs (6.3), (6.4), (6.8), and are listed and compared with other results obtained from different techniques in table (6.1). The value of ν_{TO} occurs where $\varepsilon''(\nu) = 2nk$ has its maximum and ν_{LO} occurs where $n(\nu)^2 - k(\nu)^2 = 0$. These values are in good agreement with the results of

Lowndes and Rastogi (1976) and Lowndes (1970), respectively.

The dominant interaction of infrared radiation in cubic ionic diatomic crystals is with the TO lattice vibrational mode of the same wave vector q as the incident electromagnetic wave. This interaction results in the fundamental absorption band characterised by very high absorption and reflection in the neighbourhood of the TO ($q \sim 0$) phonon frequency. Although the main features of the spectra can be reproduced quite well with a model of a classical simple harmonic oscillator as described in chapter 5, this model is not capable of explaining the detailed nature of the spectra. To account for detailed structure in the spectra one must consider the frequency-dependent damping effects of the anharmonic parts of the interatomic forces on the vibrational mode. Theoretical studies of this effect have been carried out by Cowley (1963). We have presented the modified form of that dielectric response function in chapter 5. Now we intend to use it for further analysis of all our results.

The frequency dependent damping function $\Gamma(\omega_j, \nu)$ at 300, 77, and 12K calculated from the optical constant data of figs (6.3), (6.4), and (6.8), respectively, using Eq(5.45), is shown in figs (6.9a), (6.9b), and (6.9c), and the values of $\varepsilon(0)$, $\varepsilon(\infty)$ and $\nu(\omega_j)$ needed for these calculations were taken from the data of Lowndes and Martin (1969). As far as the assignment of the features in the two phonon damping spectra is concerned, in the case of alkali halide crystals the infrared lattice absorption bands due to two phonon emission are relatively few in number as compared to III-V compound semiconductors.

The normal mode frequencies for CsI in the major symmetry directions have been determined using slow neutron inelastic scattering methods by Buhrer and Halg (1971). Also Beairsto and Eldridge (1973) have calculated the dispersion curves together with the selection rules for CsI. The detailed analysis of cubic anharmonicity carried out by Beairsto and Eldridge showed that no two-phonon combinations are allowed at Γ or M, whereas they have shown that the main features in the spectrum of $\Gamma(oj, \nu)$ are expected to arise from two-phonon combinations at the X and R symmetry points.

The measurements performed by us on CsI agree quite well both qualitatively and quantitatively with the calculations of Beairsto and Eldridge. The minor discrepancy in the measured frequencies in some of the features observed here in the two-phonon spectra with their calculated spectra are due to inaccuracies in their input data as they have indicated in their publication. We therefore have used the frequencies measured by Buhrer and Halg rather than those calculated by Beairsto and Eldridge at the X and R symmetry points. The observed features of two-phonon summation and difference processes are indicated in figs (6.3) and (6.9) at 300K. Two summation bands occur above the TO frequency at 84 and 112 cm^{-1} whereas a broad difference band is observed at 30cm^{-1}. The correlation between the positions of the measured features in $\Gamma(oj, \nu)$, and the spectral distribution of these combinations is in good agreement with the results of Beairsto and Eldridge.

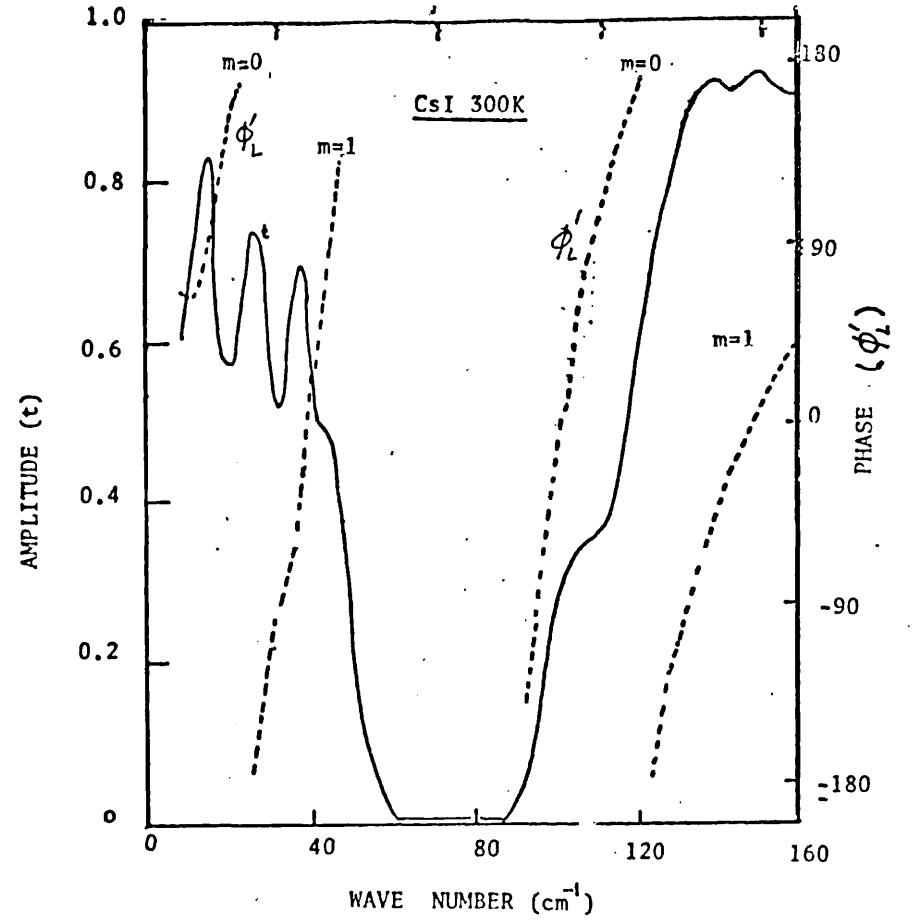

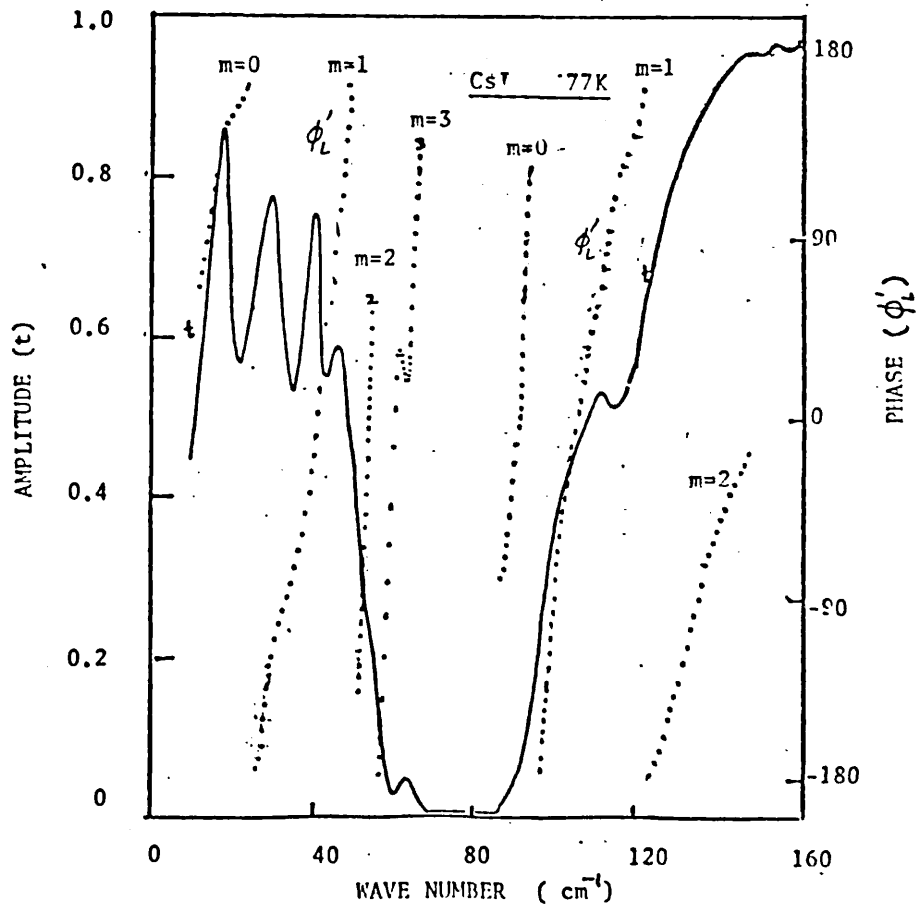

Figs(6.1-6.2) Measured transmission amplitude and phase spectra for CsI at temperatures of 300 and 77K

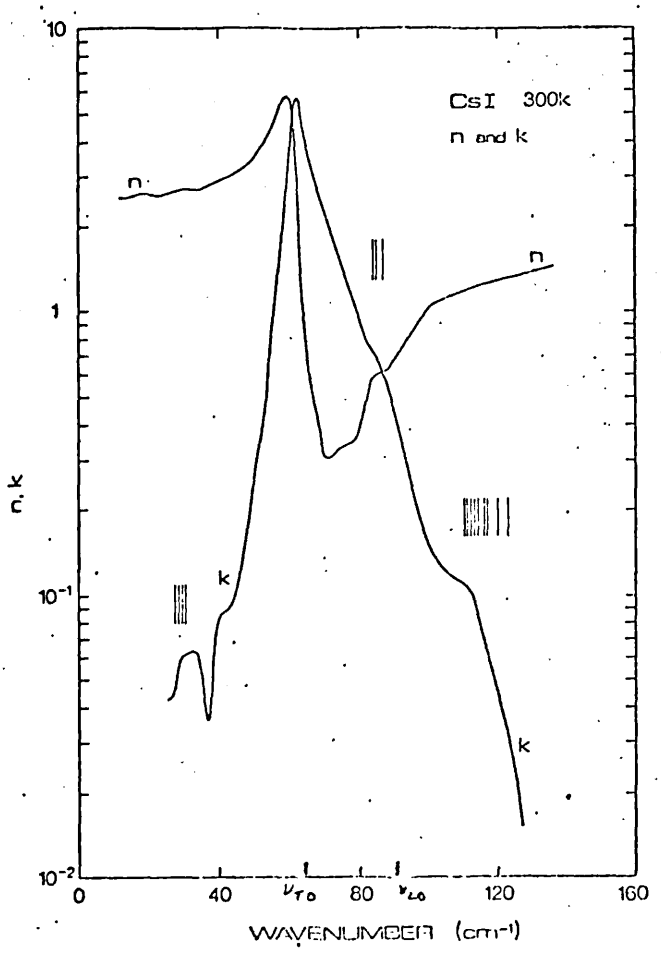

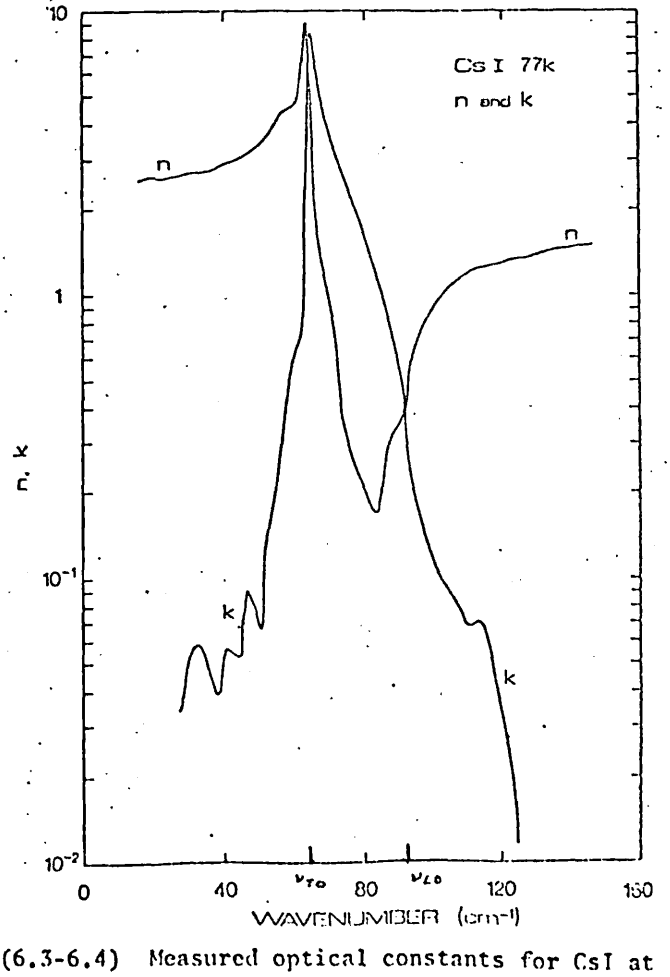

Figs(6.3-6.4) Measured optical constants for CsI at 300 and 77k

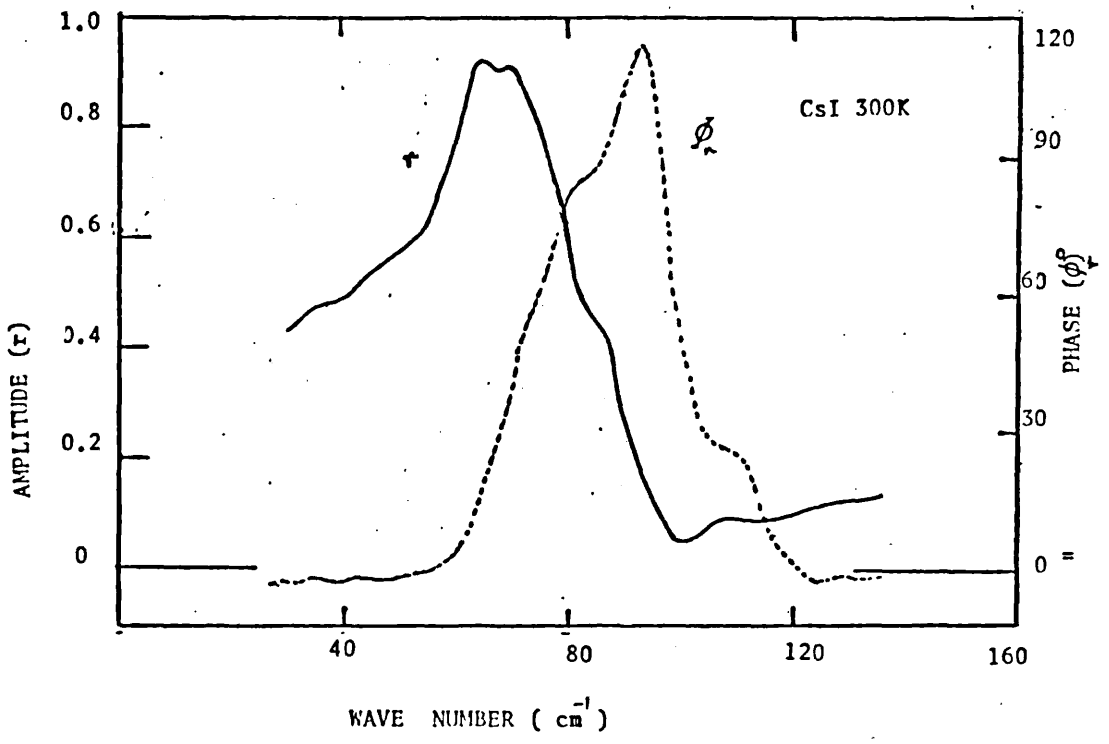

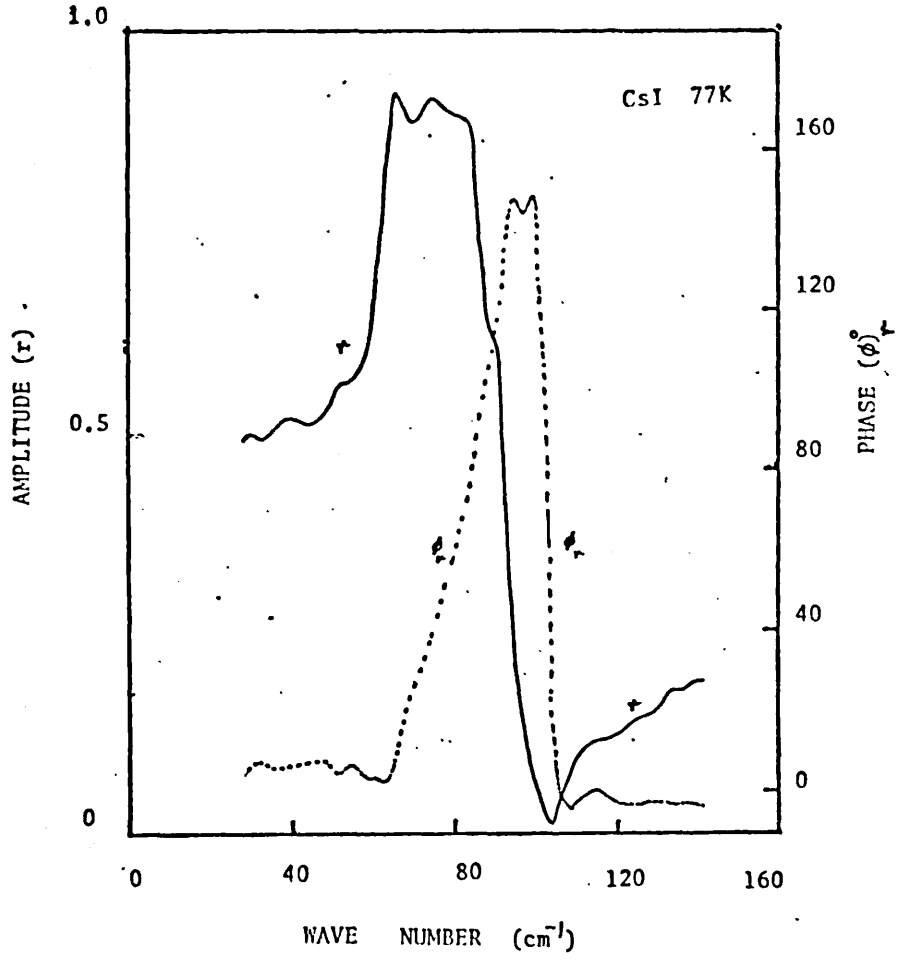

Figs(6.5-6.6) Measured reflection amplitude and phase spectra for CsI at 300 and 77k

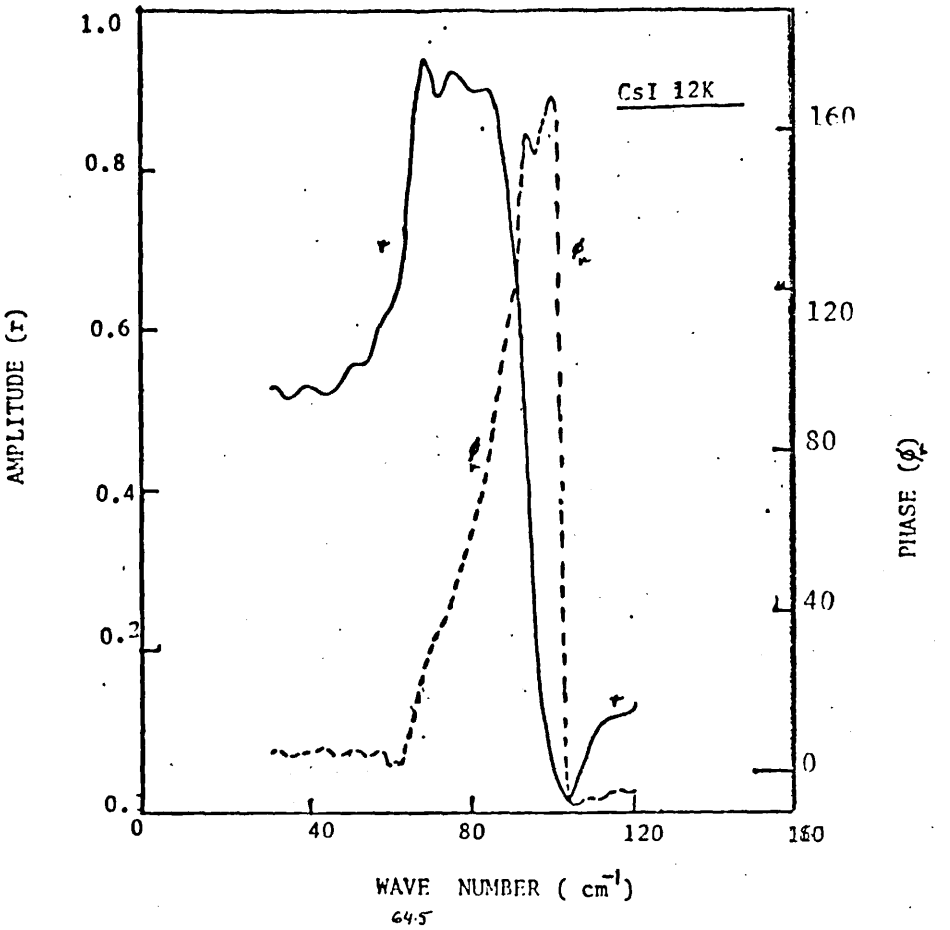

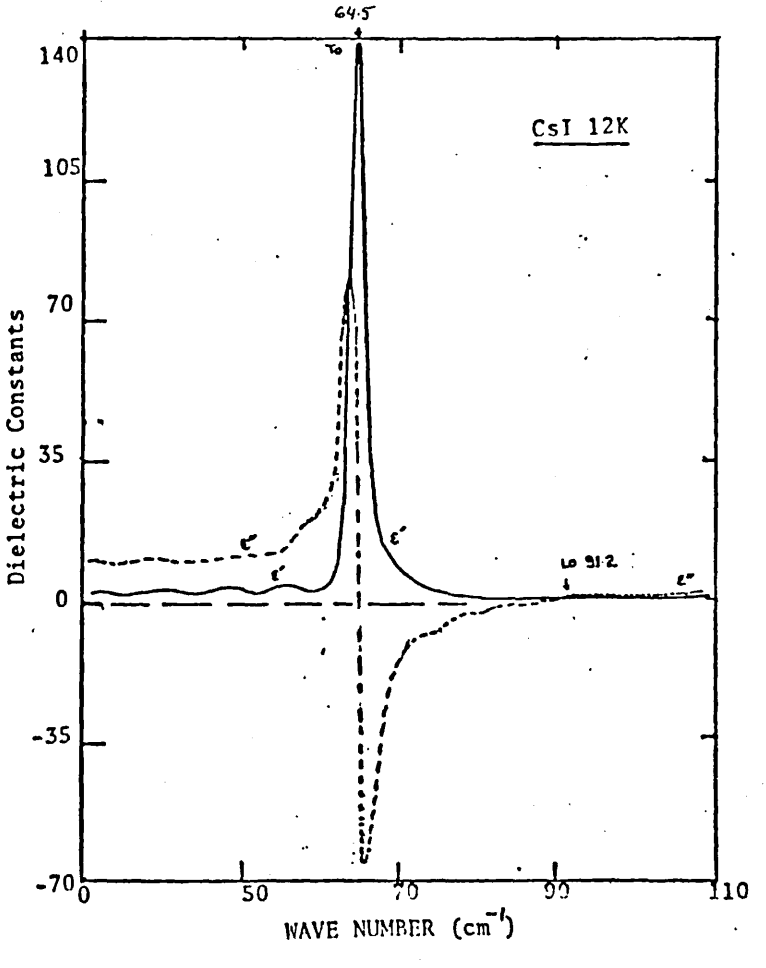

Fig(6.7) Measured reflection amplitude and phase spectra for CsI at 12K

Fig(6.8) Measured dielectric constants for CsI at 12K

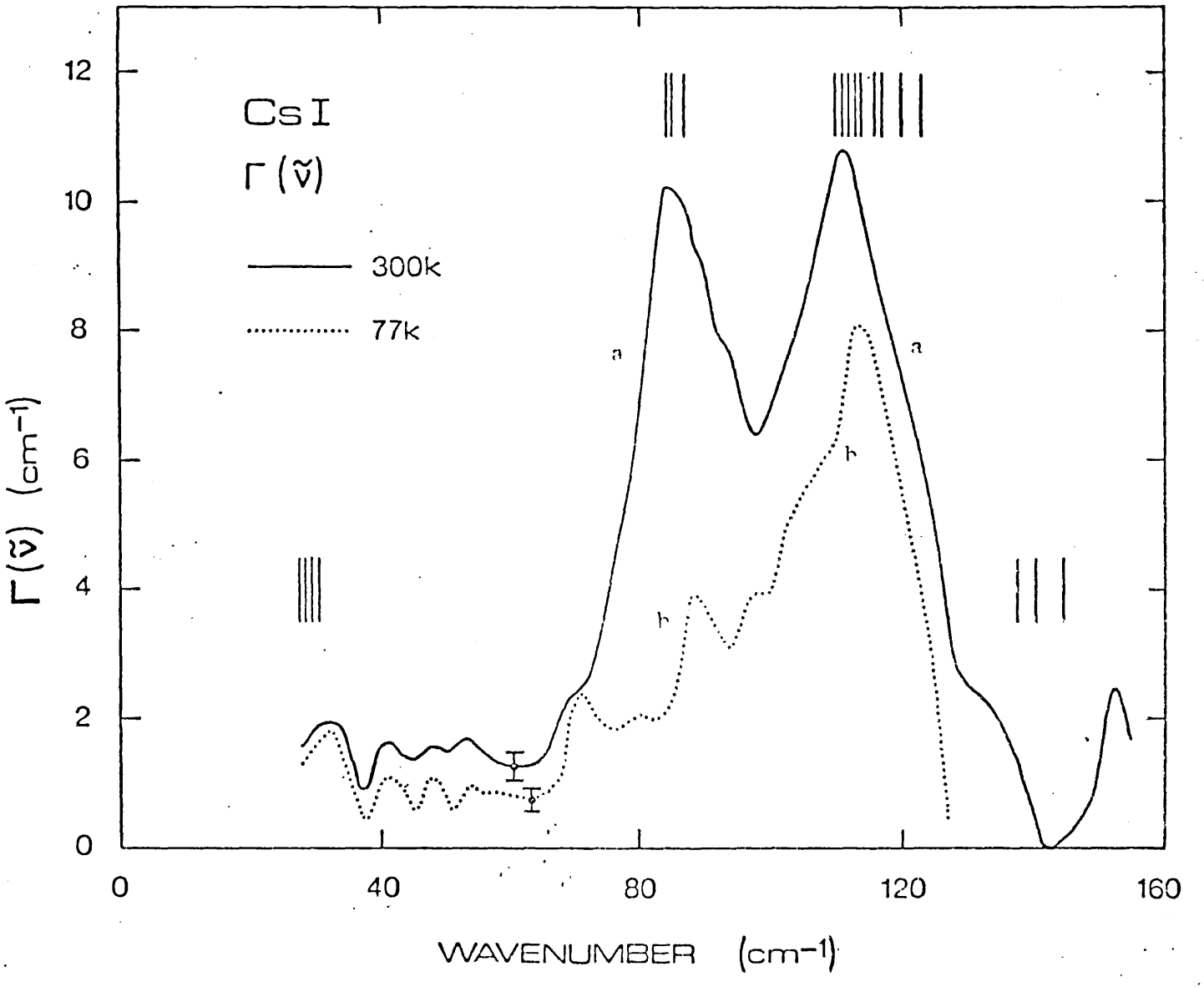

Fig(6.9) Measured frequency dependent imaginary part of anharmonic self-energy for CsI at 300 and 200K

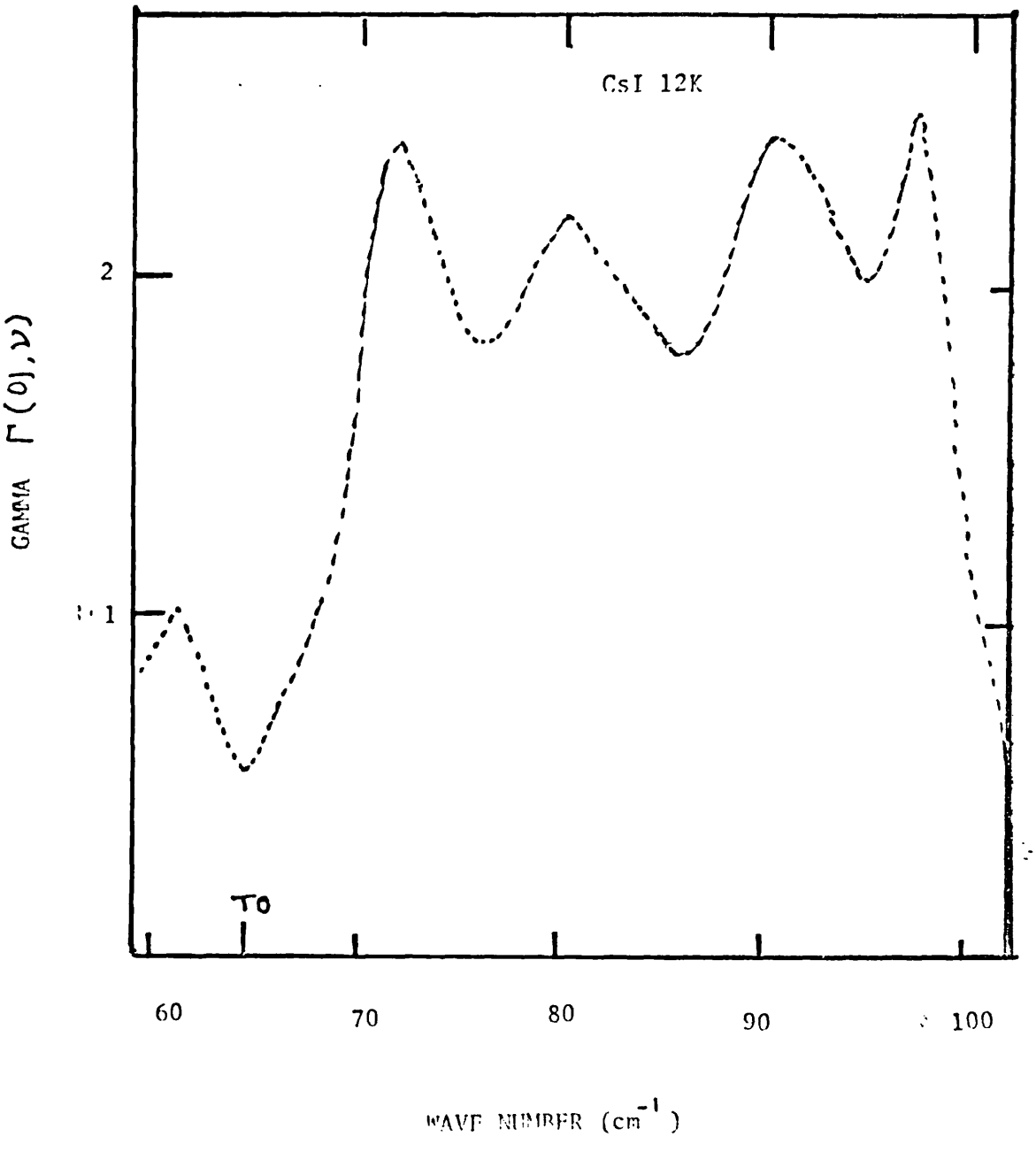

Fig(6.9c) Measured frequency dependent imaginary part of anharmonic self-energy at 12K

Table (6.1) Summary of CsI Results

Parameters in cm^{-1}	Present measurement	Lowndes and Rastogi 1976	Lowndes 1970
ν_{TO} 300K	61.5	62.1 ± .3	-
ν_{TO} 77K	64.5	65.5 ± .3	-
ν_{TO} 12K	64.5	65.8 ± .3	-
ν_{LO} 300K	90.2	-	90.5
ν_{LO} 77K	91.0	-	91.0
ν_{LO} 12K	91.2	-	91.5
$\Gamma(oj,\nu)$ 300K	1.2 ± .2	1.3 ± .3	-
$\Gamma(oj,\nu)$ 77K	0.8 ± .3	0.6 ± .3	-
$\Gamma(oj,\nu)$ 12K	0.51± .3	0.5 ± .2	-

b) Potassium Iodide, KI

The optical constants $n(\nu)$ and $k(\nu)$ of pure single crystals of KI have been determined as a function of frequency using two Michelson interferometers in the asymmetric mode. The measurements in the reststrahlen region were made on a single crystal of KI 40mm in diameter and 6mm thick polished to a flatness of 0.1 micron on the reflecting surface by using a reflection interferometer as described earlier. The values of the extinction coefficient $k(\nu)$ away from the reststrahlen band are not as accurate as those determined between the TO and LO frequencies. This is because away from the fundamental the phase becomes very small and is difficult to measure accurately by the dispersive reflection technique. Therefore the complementary measurements, i.e, the single pass transmission measurements, were performed on a sample of KI of about 200 micron thickness.

Thus using reflection techniques the measurements were performed in the reststrahlen range of 80 to 150 cm^{-1}, and in the rest of the frequency range the measurements were done by the single pass transmission method. In both cases the measurements were made at 300 and 200K, and figs (6.10), (6.10a), (6.11) and (6.11a) show the experimentally measured amplitude reflectance r and phase ϕ_r and amplitude transmittance t and phase ϕ_t at 300 and 200K, respectively. The data for amplitude reflectance and transmittance and phase represent in each case an average of at least four separate experimental runs with a resolution of $2cm^{-1}$.

The measured values of refractive index and absorption index at 300 and 200K obtained from the phase and amplitude are

shown in figs (6.12) and (6.13). The room temperature results agree very well with those of Berg and Bell (1971). The TO and LO mode frequencies at wave vector q=0 are also indicated in figs (6.12) and (6.13). The values of the TO frequency measured here (102 ± 0.5 at 300K and 105.5 ± 0.5 cm^{-1} at 200K) are in good agreement with the values determined by Lowndes and Rastogi (1976) from transmission measurements on thin films. Also the values of the LO frequency at these two temperatures determined in the present work are compared in table (6.2) with the experimental values obtained by Lowndes (1970) and Berg and Bell (1971), and with the calculated values of Eldridge and Kembry(1973) obtained using the Lyddane-Sachs-Teller relation in the harmonic approximation. The agreement between the various experimental results and the theoretical calculations with the present measurements is excellent as can be seen in table (6.2).

The full frequency-dependence of the imaginary part of the self-energy at 300 and 200K is then calculated by using Eq(5.45) and the data shown in figs (6.12) and (6.13) respectively, and the values of the static and high frequency dielectric constants were taken from Lowndes and Martin (1969). The results obtained for $\Gamma(oj,\nu)$ at 300 and 200K are shown in figs (6.14) and (6.15), respectively, and the error bars show the uncertainty propagated into $\Gamma(oj,\nu)$ at a few selected frequencies from standard deviations in the measured amplitude and phase spectra.

The assignments proposed here for the frequencies of two phonon processes, i.e, the summation and difference bands in KI at room temperature are numbered in fig (6.14) and are listed in

table(6.3). These assignments correspond to the most prominent features listed by Eldridge and Kembry (1973) in their table 3. The important factor to note here is that Eldridge and Kembry derived their phonon frequencies from dispersion curves measured by Dolling et al (1966) at 90K by inelastic neutron scattering. All the frequencies in the Brillouin zone were reduced by Eldridge and Kembry by 5% in order to approximate the room temperature dispersion curves. Thus, as the original neutron data has an experimental uncertainty of the order of $2cm^{-1}$ in each phonon frequency the uncertainty in the phonon frequencies calculated by Eldridge and Kembry is probably at least $4cm^{-1}$.

The agreement between the expected and observed frequencies of two-phonon processes in KI at 300K listed in table(6.3) is quite reasonable. From fig (6.14) we also observe that the overall spectrum of $\Gamma(oj,\nu)$ agrees quite well with the calculations of Berg and Bell, rather than with those of Fischer (1974). It appears that Fischer's self consistent theory over estimates the life time of the decaying phonons and as a result all the critical points appearing in the damping function are washed out by the line broadening effect. Thus it fails to reproduce the structure in the spectrum of $\Gamma(oj,\nu)$ revealed by this measurement.

The discrepancy between the measured and calculated values of $\Gamma(oj,\nu)$ in the vicinity of the TO frequency can be accounted for by including three-phonon damping [Eldridge and Staal (1977)]. The temperature dependence of $\Gamma(oj,\nu)$ is determined by the occupation number of the phonons created and destroyed in the

various decay processes as described in section (5.6). We have listed the temperature dependence in table (6.4) for those frequencies which are used in assignments of the summation and difference bands as calculated by Eldridge and Kembry. As we see, the intensities of the numbered features in fig (6.14) should decrease by a factor of between 0.64 and 0.68 between 300 and 200K. The overall temperature dependence of $\Gamma(\omega_j,\nu)$ observed from fig (6.14) is in quite reasonable agreement with the expected behaviour.

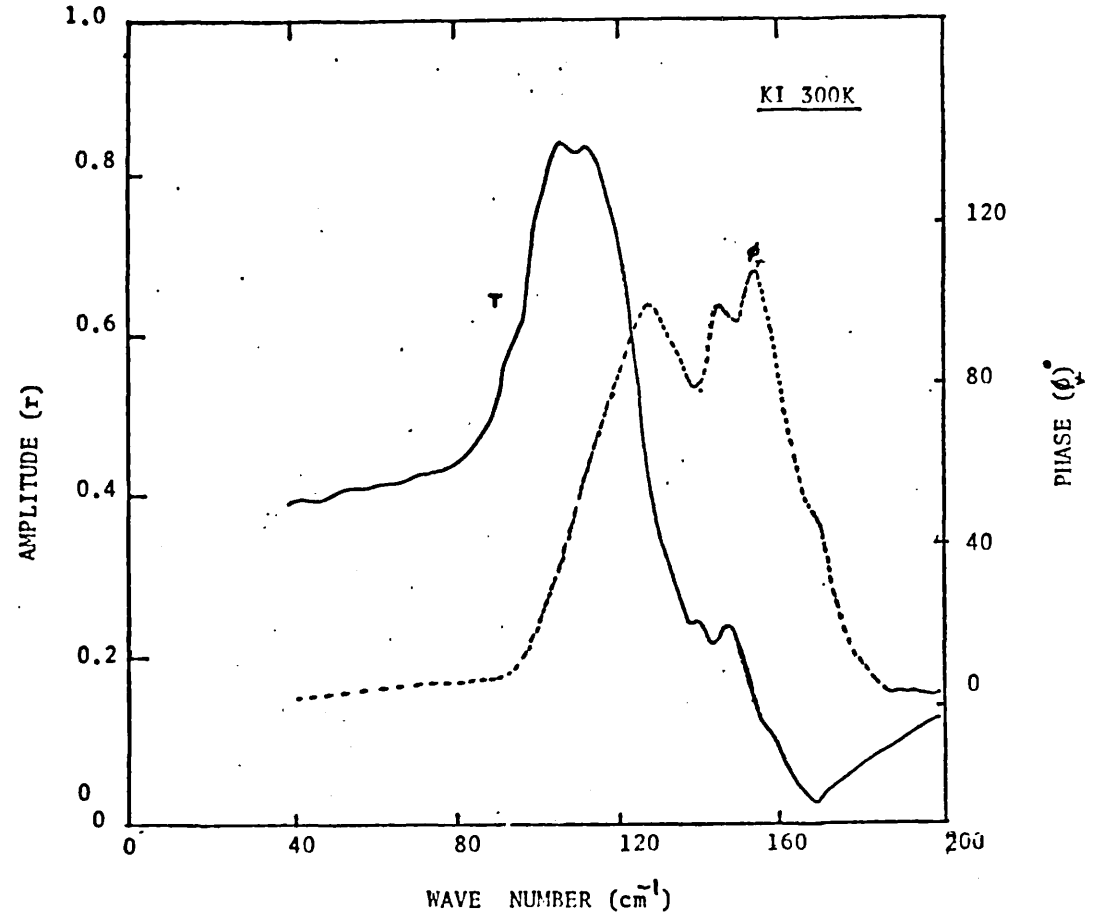

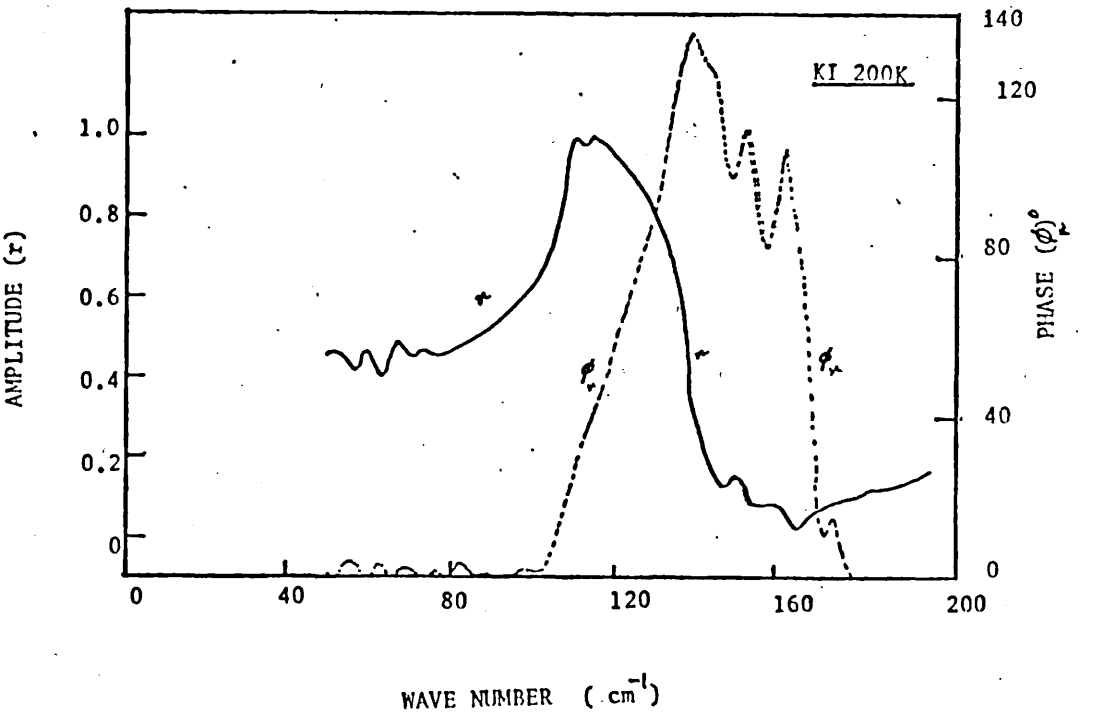

Figs(6.10-11) Measured reflection amplitude and phase spectra for KI at 300 and 200K

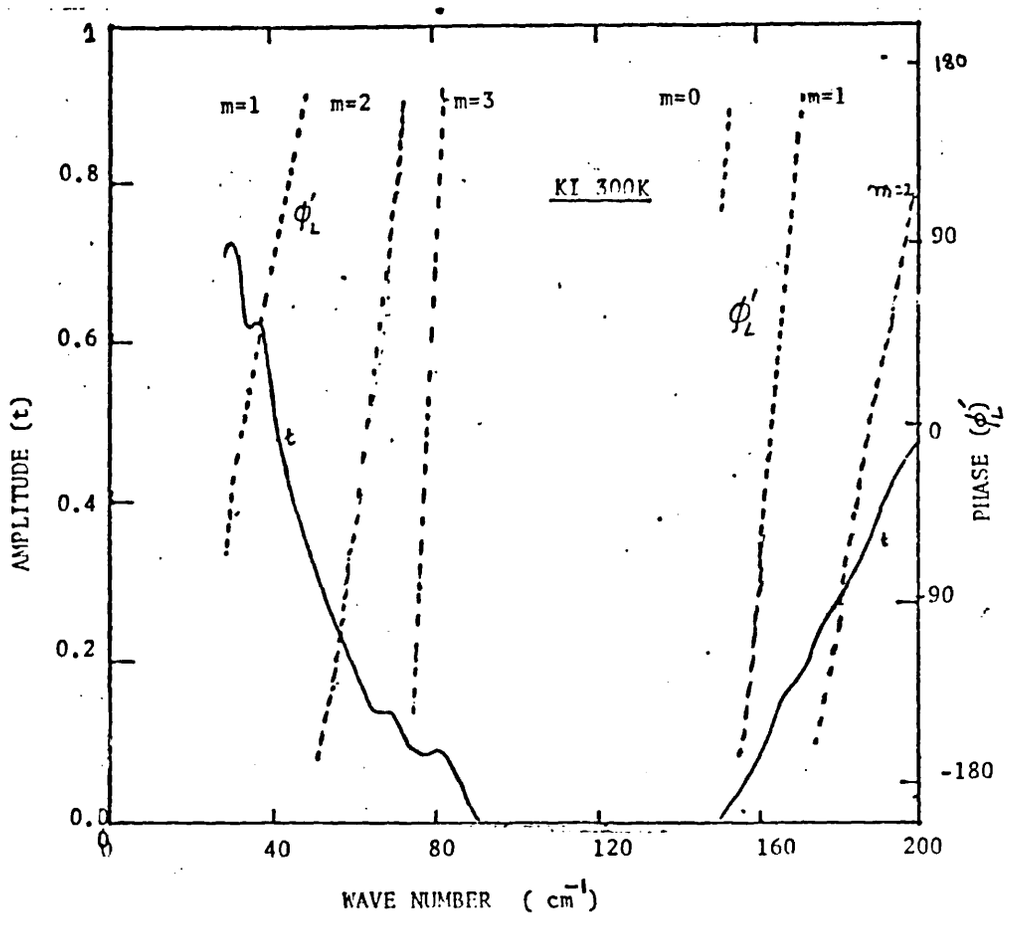

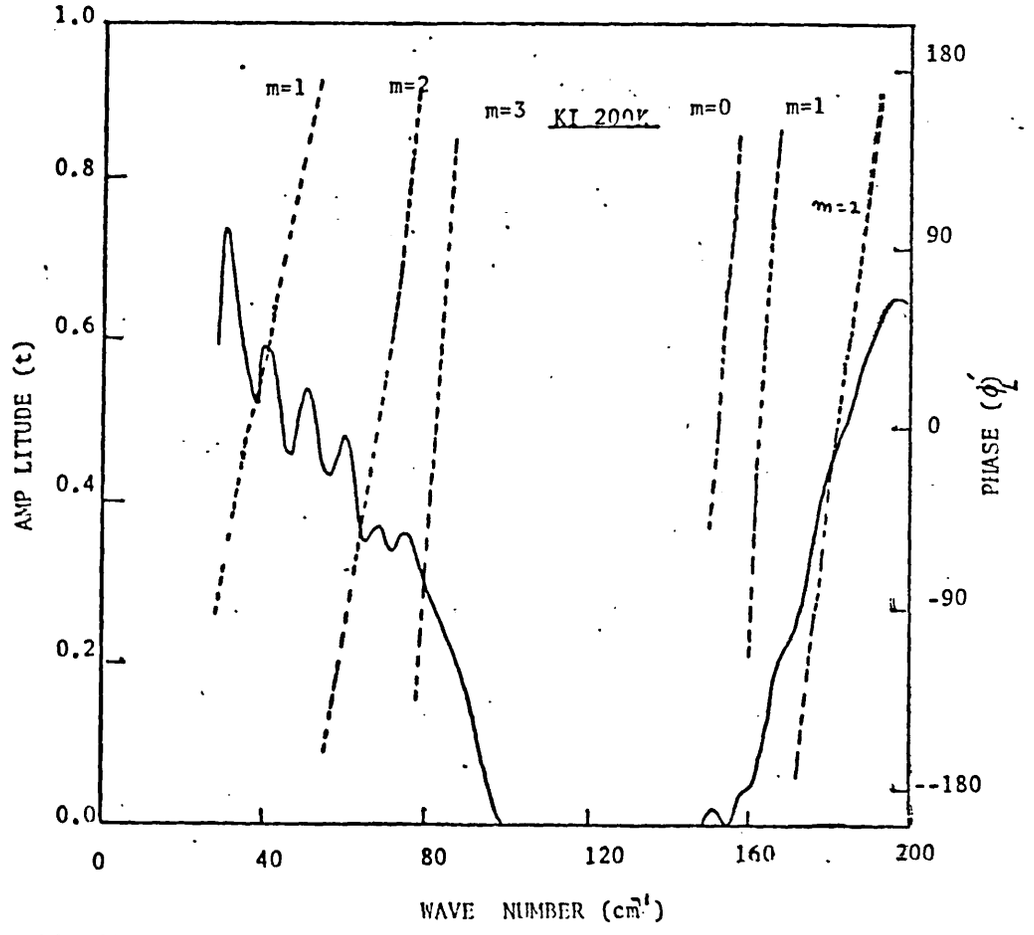

Figs(6.10a-11a) Measured transmission amplitude and phase spectra for KI at 300 and 200K

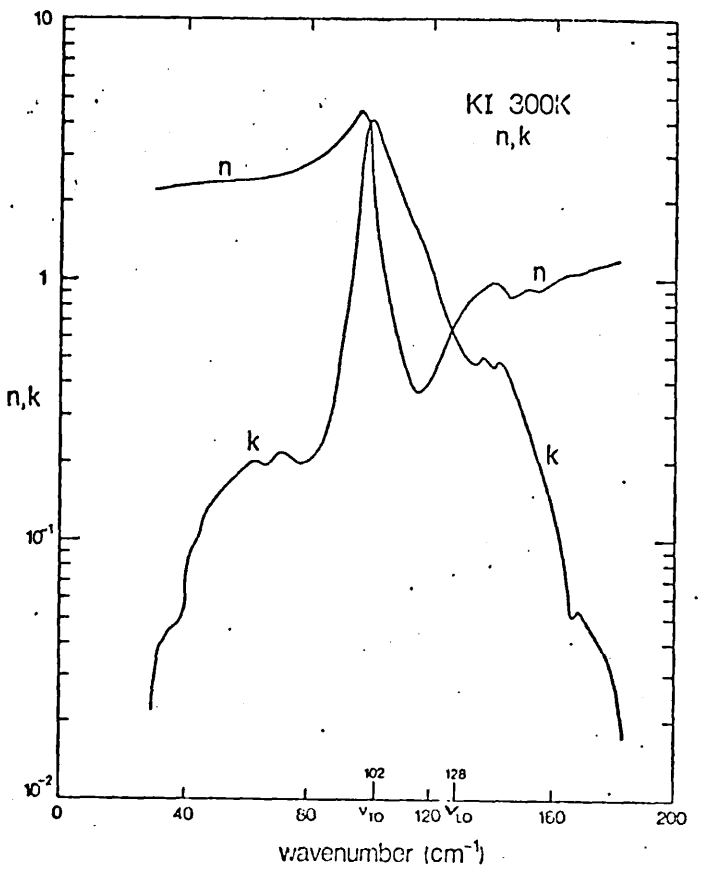

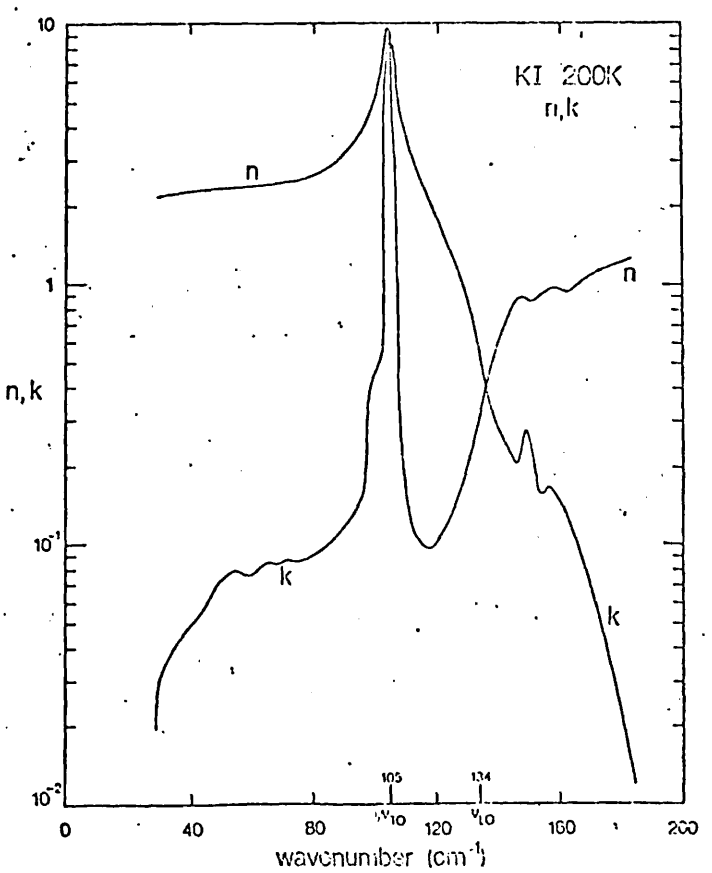

Figs(6.12-13) Measured optical constants for KI at 300 and 200K

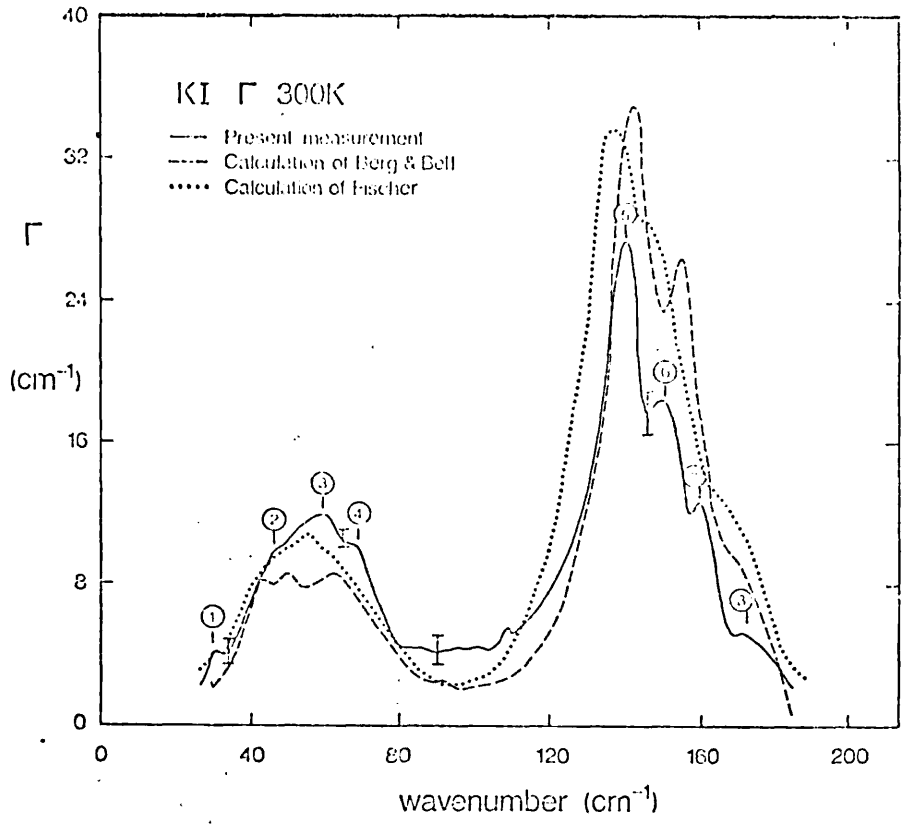

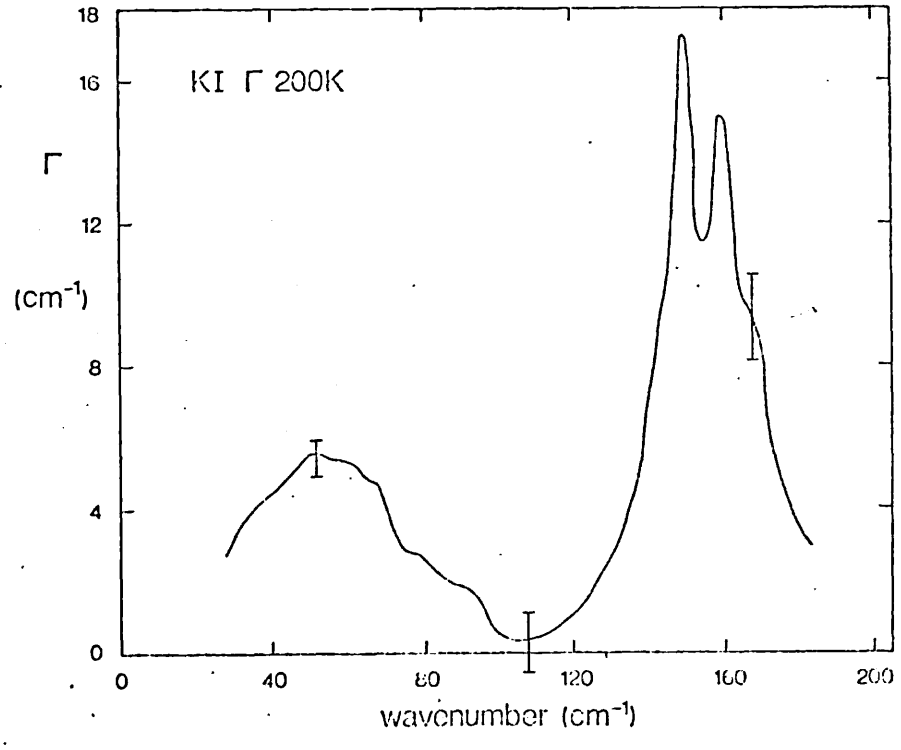

Figs(6.14-15)
Measured frequency dependent imaginary part of anharmonic self-energy for KI at 300 and 200K. The measurements at 300K are compared with calculations by Berg and Bell(1971) and Fischer (1974). Assignments for the numbered features are listed in table(6.3)

Table(6.2)

Comparison of values of $\tilde{\nu}_{LO}$ obtained in the present work with previous values obtained by (a) Kramers-Kronig analysis of the reflection spectrum of a single crystal (b) grazing-angle thin film reflectance data (c) DFTS (d) calculation including cubic anharmonicity and (e) the Lyddane-Sachs-Teller relationship used in the harmonic approximation

Source	200K	300K
This work	134	128
Lowndes 1970 KK[a]	134.5	129
Film[b]	134	127
Berg and Bell 1971[c]		129
Eldridge and Kembry 1973		
Anharmonic calculation[d]		128
LST[e]		140

Table(6.3)

Two-phonon combination bands in KI at 300K

Feature	Phonon assignments	Combination	Expected frequency (cm^{-1})	Observed frequenc (cm^{-1})
1	$\Sigma_1(LA)\Sigma_4(TO)$	Difference	28.5	30
2	$\Sigma_4\ \Sigma_4$	Difference	40	46
	$L_3'\ L_3$		40	
	$W_1\ W_2'$		43.7	
3	$\Sigma_1(LO)\Sigma_4(TA)$	Difference	60	59
	$\Gamma \rightarrow W$		62.3	
4	$L_1'\ L_3$	Difference	70.3	72.5
5	$\Sigma_4\ \Sigma_4$	Summation	142.5	140
	$L_3'\ L_3$		142.5	
6	$\Sigma_1(LA)\Sigma_4(TO)$	Summation	153.9	150
	$W_1\ W_2'$		153.9	
	$(L_3'\rightarrow W_2')+(L_1\rightarrow W_1)$		153.9	
7	$\Sigma_1(LO)\Sigma_4(TA)$	Summation	163.4	161.5
8	$\Delta_1\ \Delta_1$	Summation	171	172
	$\Sigma_1\ \Sigma_1$		174.8	
	$L_1'\ L_3$		172.9	

Table (6.4)

Temperature Dependence of the intensities of two-phonon bands in KI

Temp K°	Difference Band = $(1 + n_1)n_2 - n_1(1 + n_2) = n_2 - n_1$				Summation band= $(1 + n_1)(1 + n_2) - n_1 n_2 = 1 + n_1 + n_2$			
Theory	$\Sigma_1(LA)\Sigma_4(TO)$	W_2' W_1	$\Sigma_1(LO)$ $\Sigma_4(TA)$	L_1' L_3	L_3' L_3	W_1 W_2'	$\Sigma_1(LO)\Sigma_4(TA)$	L_1' L_3
200/300	0.65	0.65	0.65	0.66	0.67	0.67	0.67	0.68
ExPT.								
200/300	0.75	0.56	0.47	0.48	0.64	0.79	0.73	0.74

6.2) III-V Compound Semiconductors.

The far infrared optical properties of several undoped III-V compound semiconductors of the zinc blend structure were studied in the reststrahlen region and below the TO frequency by dispersive reflection spectroscopy.

a) Indium Arsenide, InAs

The amplitude and phase spectra of an undoped InAs crystal 3mm thick and 20 mm in diameter were measured at room temperature by dispersive reflection spectrometry. These measurements were done at a resolution of 3 cm^{-1}, and the random noise level was of the order of 1% in the whole region of the scan.

In fig (6.16) we represent the experimentally measured amplitude reflection coefficient and phase reflection spectra of InAs within the frequency range 140 to 290cm^{-1}, which includes both the fundamental lattice resonance at about 219cm^{-1} and the onset of free carrier absorption which is apparent at lower frequencies from these spectra. The data for the amplitude reflection and phase spectra represents an average of several experimental runs. The complex refractive index obtained using the above set of data is shown in fig(6.17).

The results of the present measurements on InAs are in good agreement with those by Gast and Genzel(1973), but in this measurement some side bands which have not previously been observed are resolved. In order to investigate this further we calculated the dielectric response from the complex refractive index, and this is given in fig (6.18). From the real $\varepsilon'(\nu)$ and imaginary

$\varepsilon''(\nu)$ parts of the dielectric constants we obtained values of the transverse optic mode frequency ν_{TO}, and longitudinal optic mode frequency ν_{LO}, from the position of the maximum value of $\varepsilon''(\nu)$ and the position where $\varepsilon'(\nu)$ is zero, respectively, in the spectra given in fig (6.17). The values of ν_{TO} and ν_{LO} so obtained are in good agreement with the published values given by Kunc et al (1975), and these values are listed in table (6.6).

To calculate the full frequency dependence of the imaginary part of the anharmonic self-energy function of InAs at 300K, we used in Eq(5.45) the values of $\varepsilon'(\nu)$ and $\varepsilon''(\nu)$ from the data of fig(6.18) and also the experimentally determined values of ν_{TO} together with the values of $\varepsilon(0)$ and $\varepsilon(\infty)$, taken from Kunc et al (1975). The frequency dependent imaginary part of the anharmonic self-energy function $\Gamma(oj,\nu)$ is shown in fig (6.19). If we compare the spectrum of $\Gamma(oj,\nu)$ with other more conventional spectra like the absorption coefficient it is apparent from fig (6.19) that the absorption peak appearing in the conventional spectrum is completely suppressed here, and therefore all the weak phonon combination side bands are more prominent.

The analysis of two-phonon spectra is performed by considering the features which correspond to singularities in the two-phonon density of states which occurs when two dispersion curves are parallel, or one is horizontal, particularly at the Γ, X and L symmetry points. As shown by Birman (1963) all possible two phonon processes at the points Γ, X, and L are infrared active except for the two over-tones 2LO(X), and 2LA(X), for zinc blend structure materials, resulting in some 34 two-phonon

features. In addition to this there will be more critical points in the two-phonon density of states elsewhere in the Brillouin zone.

The structure in the spectrum of $\Gamma(oj,\nu)$ reported here agrees well with that in the infrared transmission and emittance spectra within the frequency range 250-290cm^{-1} reported previously by Stierwalt and Potter (1967) and Lorimer and Spitzer (1965), and besides these features there are a number of weak features at frequencies below 200cm^{-1} which have not been reported before. These weak features carry insufficient information to allow us to decide with absolute certainty which combination of phonons gives rise to a particular peak in the observed spectrum, especially when the experimental phonon dispersion curves determined by neutron spectrometry are not available because of the high neutron absorption coefficient of In. Nevertheless the features observed here in the spectrum of $\Gamma(oj,\nu)$ agree well with the calculations of Talwar and Agrawal (1974). Assigned features are marked in fig (6.19) and are listed in table (6.5), together with the calculated frequencies of Talwar and Agrawal. All the features below 190cm^{-1} are due to two- phonon difference processes, whereas above 190cm^{-1} all the observed peaks in the spectrum of $\Gamma(oj,\nu)$ are due to two-phonon summation processes. We suggest here that measurements be performed over a wider frequency range and at higher resolution to include as many two-phonon combination bands as possible, and also that measurements be made at low temperatures.

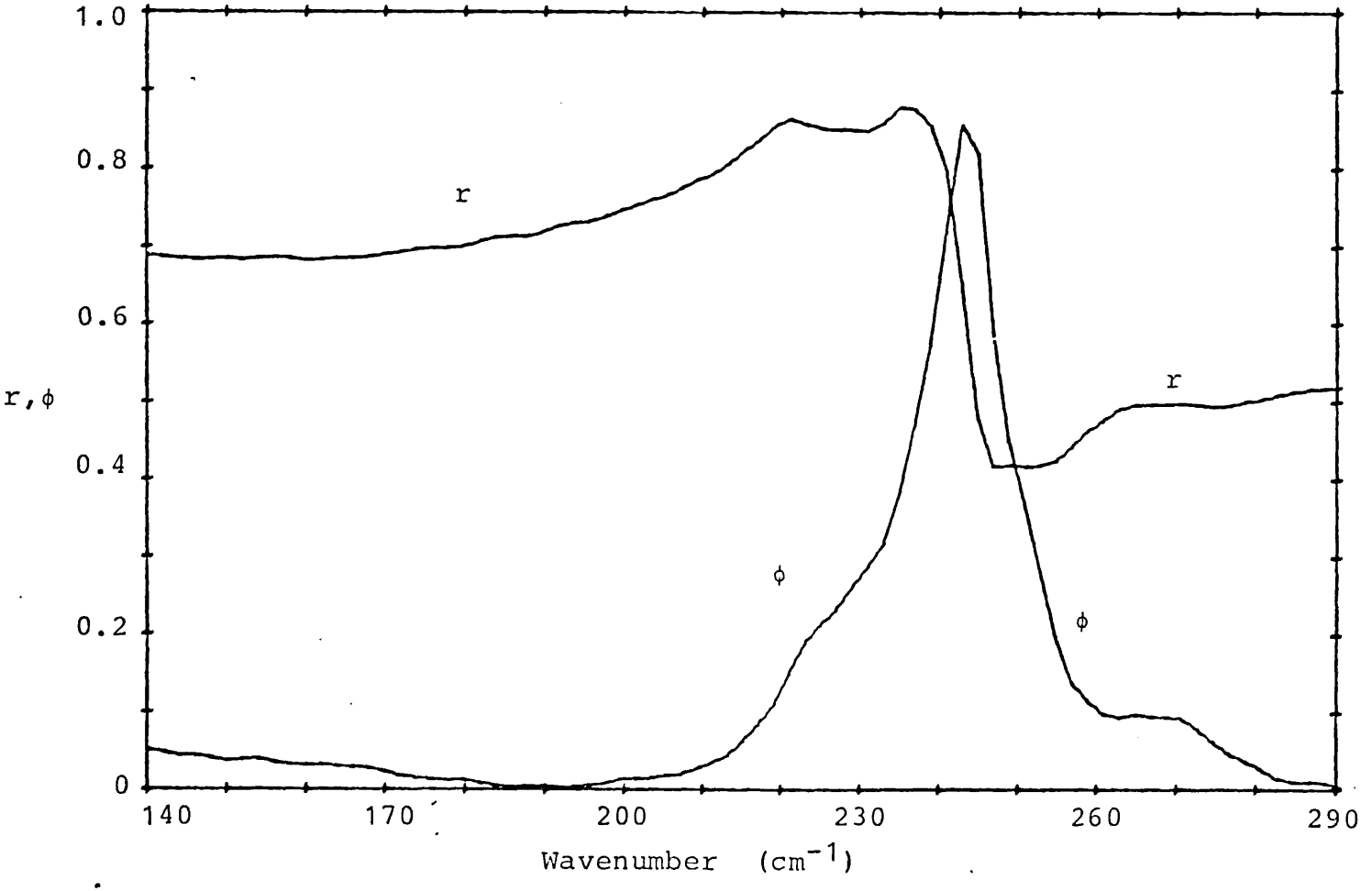

Figure (6.16)The amplitude and phase reflection spectra, r and ϕ, respectively, of InAs measured at 300 K. The phase is in radians.

149

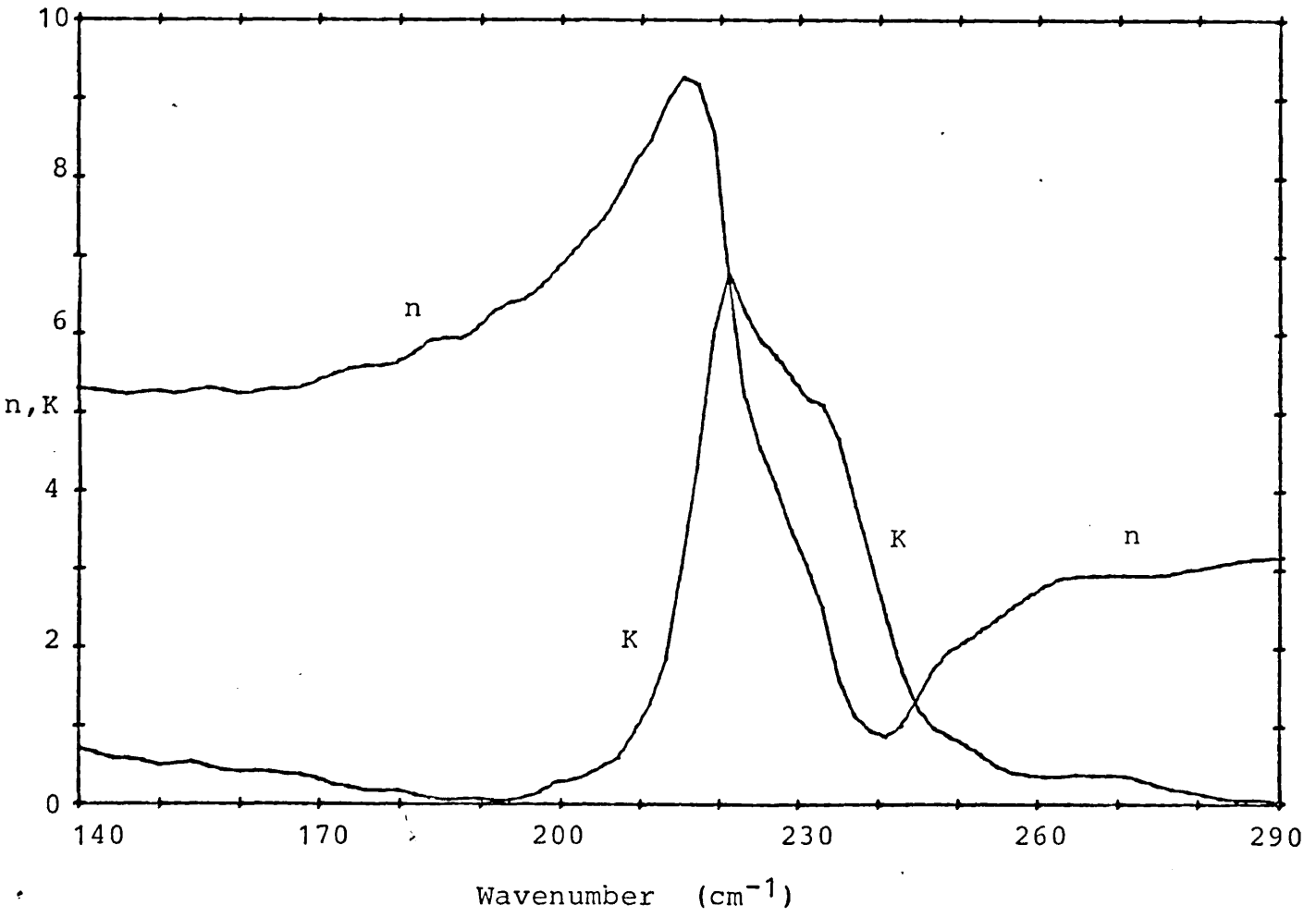

Figure 6.17 The refractive index, n, and extinction coefficient, K, of InAs at 300 K.

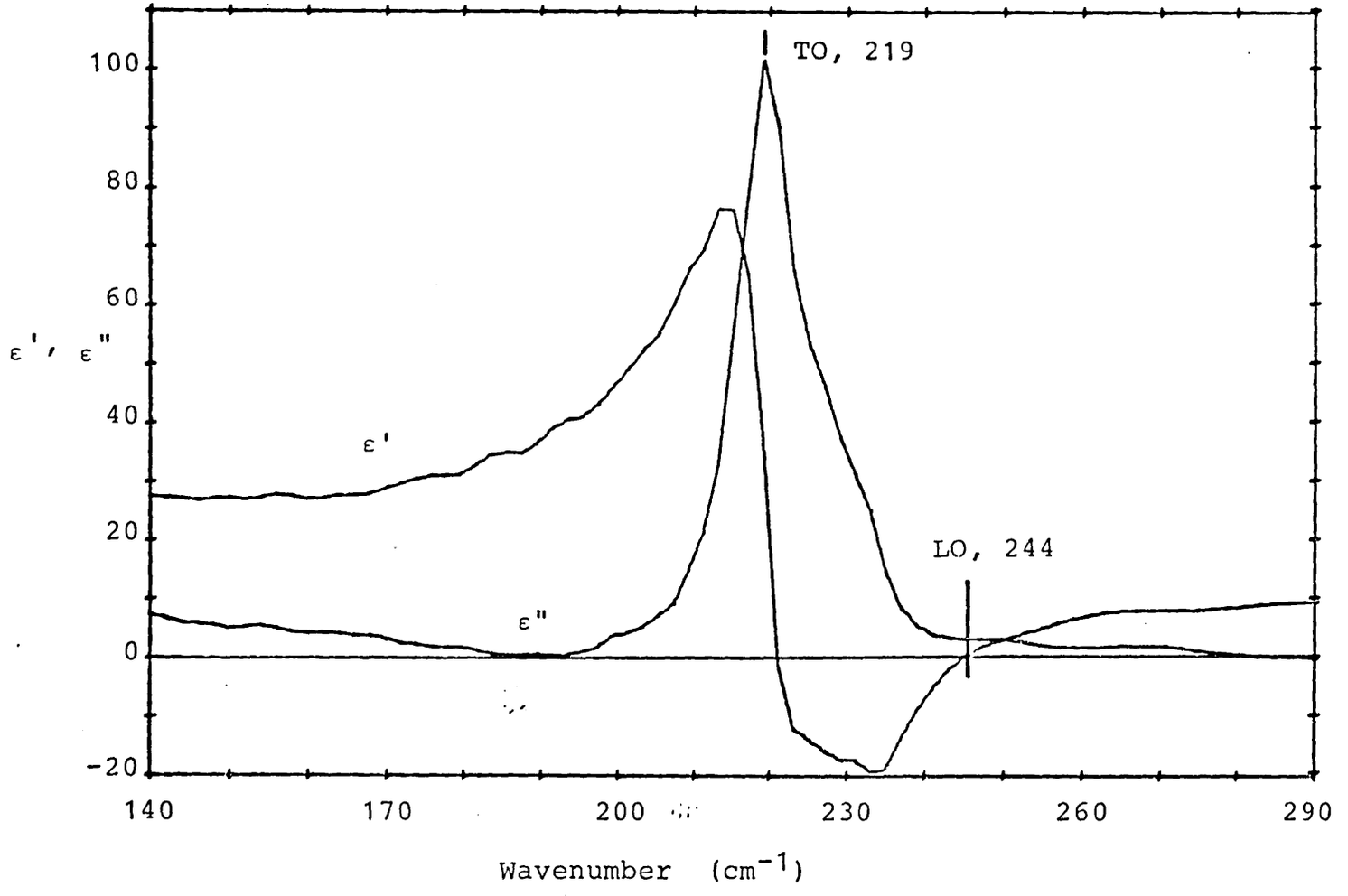

Figure 6.18 The dielectric functions, ε' and ε", of InAs at 300 K.

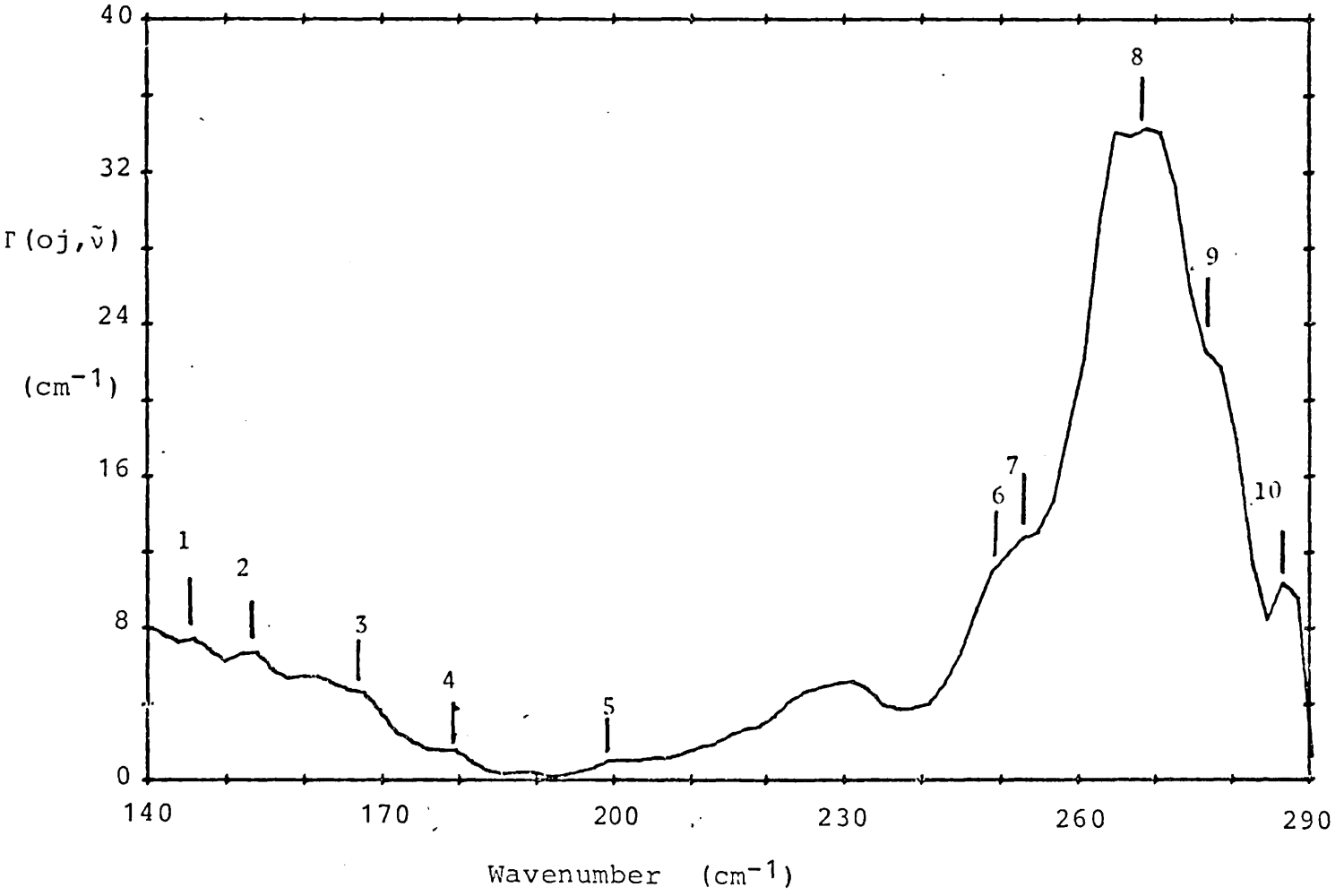

Figure 6.19 The experimentally determined anharmonic damping function, $\Gamma(\omega,\tilde{\nu})$, of InAs at 300 K. The marked features are discussed in the text.

Table(6.5)

Assignment of two-phonon combinations for InAs at 300K

Feature No:	Observed cm^{-1}	Calculated cm^{-1}	Assignments (Talwar 1974)
1	146	145	LO - TA (X)
2	153	157	TO - TA (X)
3	167	168	LO - TA (L)
4	179	180	TO - TA (L)
5	199	198	LA + TA (X)
6	248	248	TO + TA (L)
7	253	251	LO + TA (X)
8	264	263	TO + TA (X)
9	277	276	2LA (L)
10	287	286	$W_2 + W_6$

b) Indium phosphide, InP

To study the far infrared optical properties of InP at 300K measurements have been made in the spectral range of 200 to 420cm^{-1} on an undoped single crystal 3mm thick and 20mm in diameter by using dispersive reflection spectroscopy. These measurements were performed at a resolution of 3cm^{-1}, and the amplitude and phase spectra obtained are given in fig (6.20). These spectra are the average of at least three separate experimental runs. The reproducibility and reliability of all the spectra presented in this section can be easily assessed from the amplitude and phase spectra of the three individual runs overlaid in the same plot as shown in figs (6.21) and (6.22), respectively.

Using the data of fig (6.20) the optical constants of InP determined at 300K are given in fig (6.23), and it appears that no such measurements on InP using the dispersive technique have been reported before.

Fig (6.24) shows the dielectric constants obtained by using the data of fig (6.23), and the values of ν_{TO} and ν_{LO} are indicated in the figure. These values agree well with those of Ulrici and Jahne (1976), and are listed in table (6.6).

In order to calculate the frequency dependent imaginary part of the anharmonic self-energy $\Gamma(\omega j, \nu)$, we made use of Eq (5.45) and the data of the fig (6.24). The results so obtained are given in fig (6.25), the values of ν_{TO}, $\varepsilon(0)$, and $\varepsilon(\omega)$ used in the above calculations were taken from Kunc et al (1975). In table (6.7) we list the frequencies of features observed due to two-phonon summation and difference processes in the spectrum of

$\Gamma(oj,\nu)$. The mode frequencies used in this critical point analysis were taken from Ulrici and Jahne. Besides phonon pairs located at major symmetry points like X and L, certain features which could not be attributed to phonons at X and L critical points are assigned to pairs of phonons near the W point, which indicates that in III-V compound semiconductors the phonons on the hexagonal face of the Brillouin zone play an important role in producing the singularities in the two-phonon spectra. [Koteles and Datars (1976)]

The frequencies of all the features marked in fig (6.25) and listed in table (6.7) agree well with the calculated frequencies of Ulrici and Jahne, and also the features numbered 3,5,8,9,10,and 11 have been previously observed by Koteles and Datars (1976) using conventional techniques, whereas the rest of the observed features in the spectrum of $\Gamma(oj,\nu)$ in fig(6.25), have not been reported before. In this two-phonon assignment process we have been able to minimize the uncertainty in a few of the zone boundary frequencies given by Ulrici. Thus if we choose the frequency at LO(X) as 333cm^{-1}, TA(X) as 67cm^{-1}, and LO(L) as 340cm^{-1}, then the observed features reported here are very close to the calculated frequencies of Ulrici, and also these corrections bring the critical point frequencies given by Ulrici close to those of Borcherds et al (1975) measured by neutron scattering. Thus the measured two-phonon spectra also help in removing the uncertainty in the calculated zone boundary frequencies.

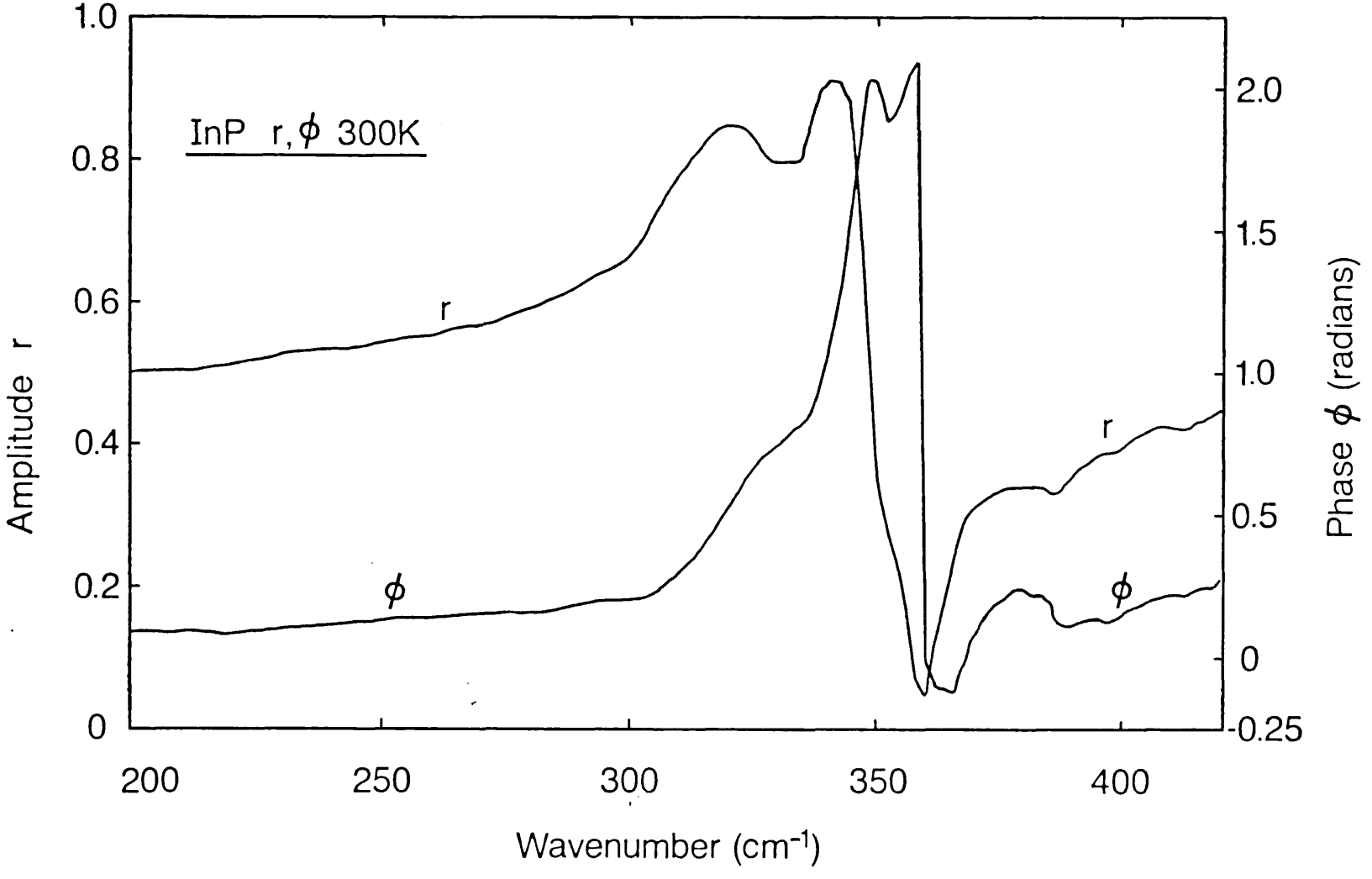

Fig(6.20) Measured reflection amplitude and phase spectra for InP at 300K

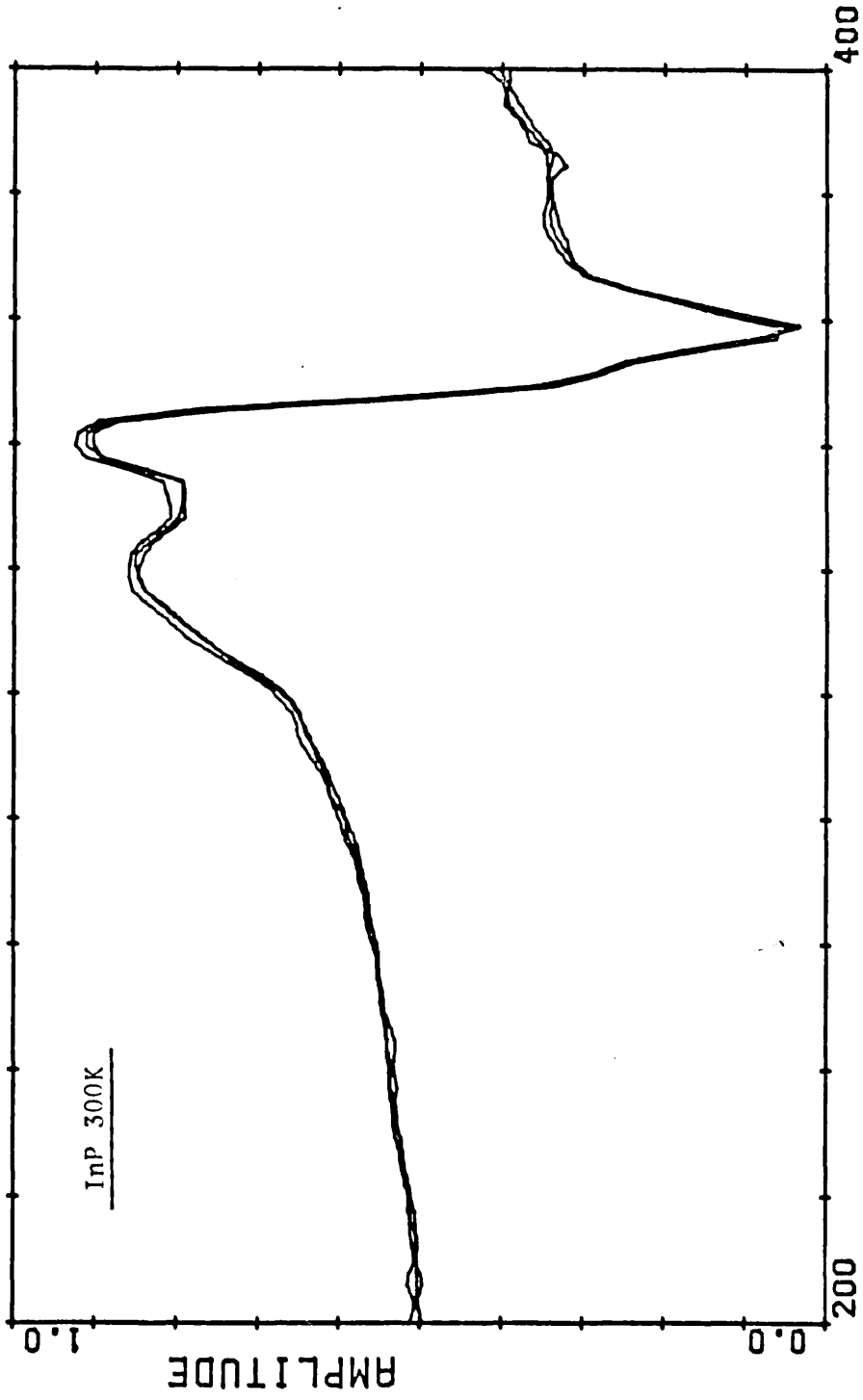

Fig(6.21) Amplitude spectra for InP of three individual runs overlaid

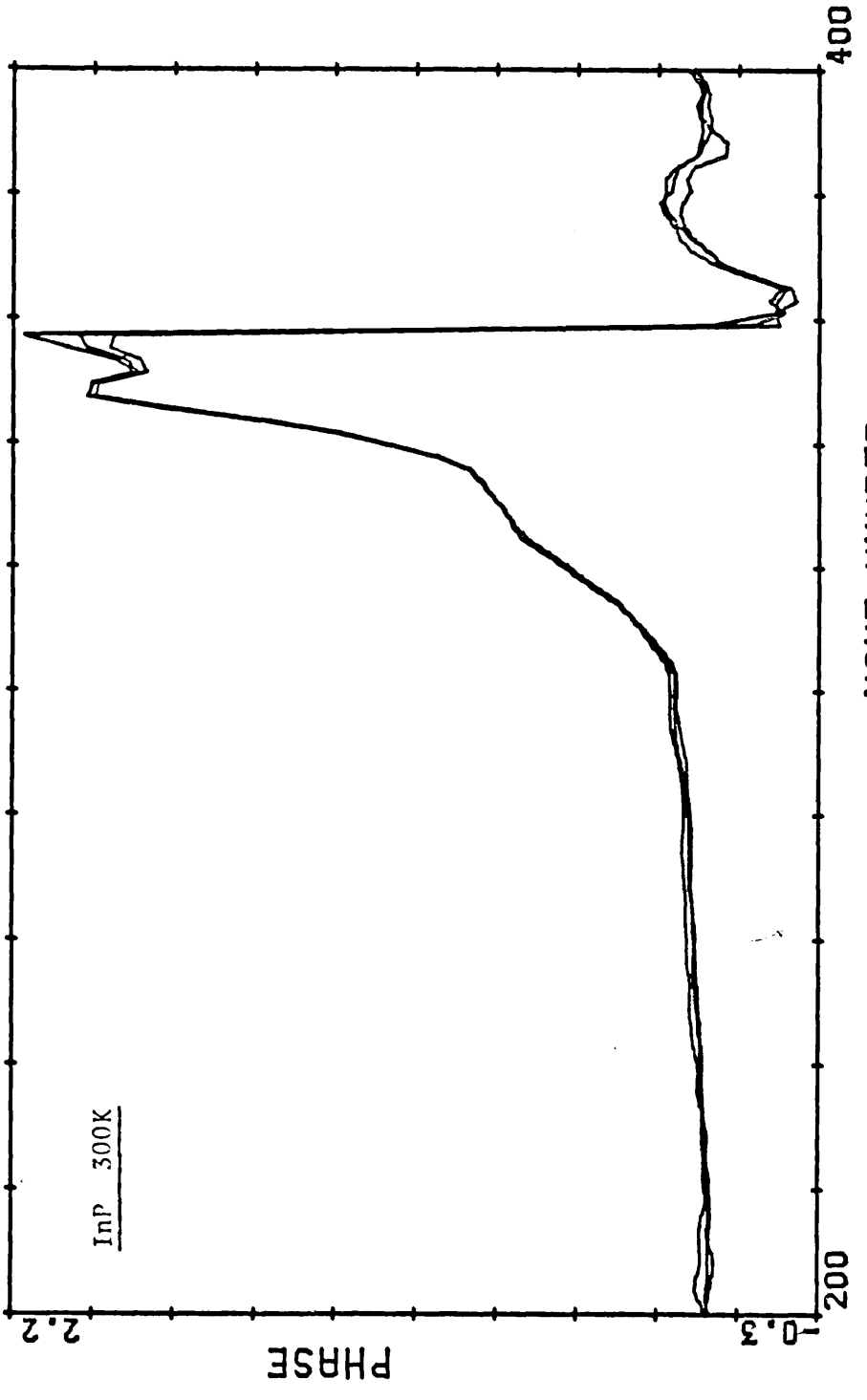

Fig(6.22) Measured phase spectra for InP of three individual runs overlaid

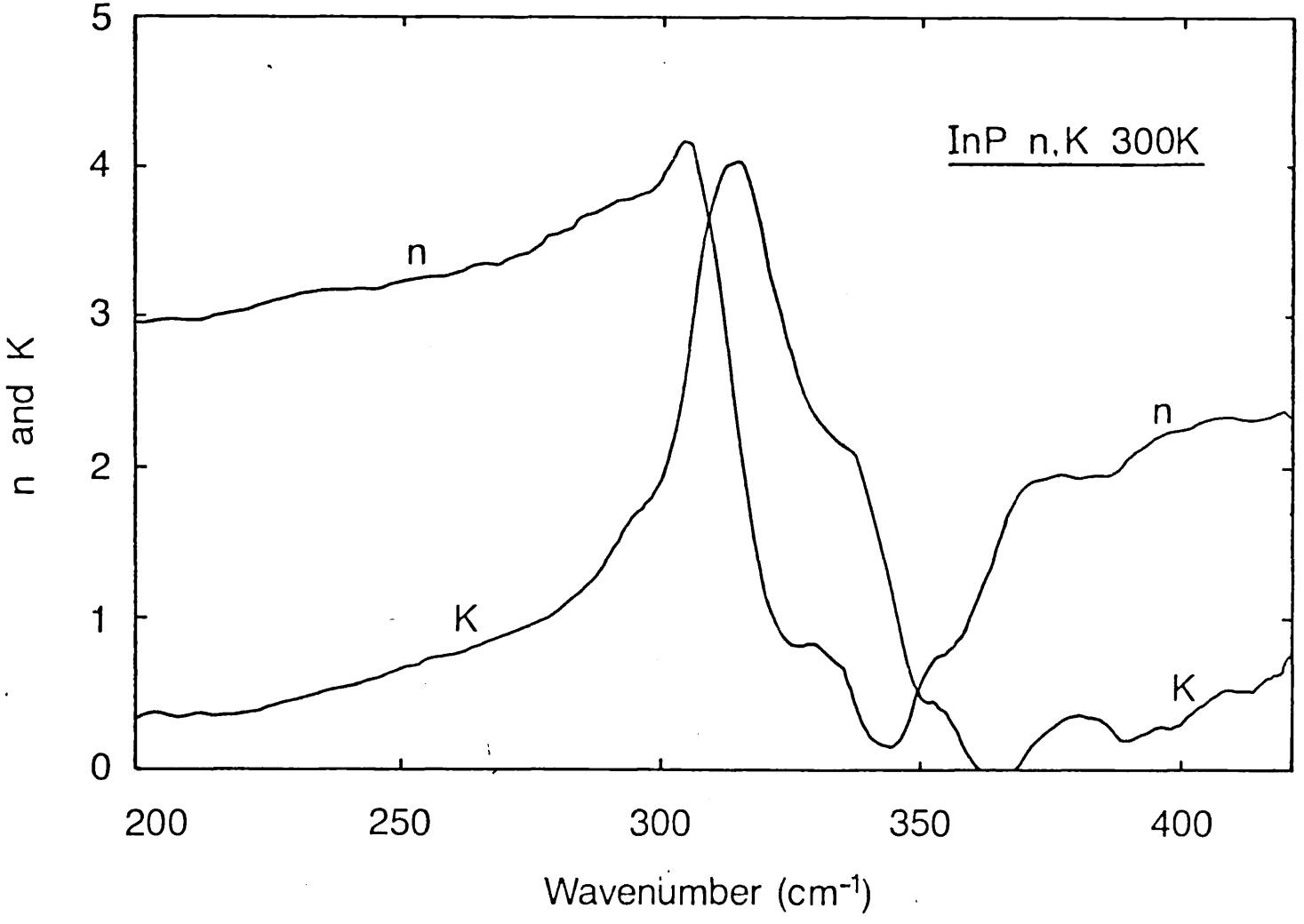

Fig(6.23) Measured optical constants for InP at 300K

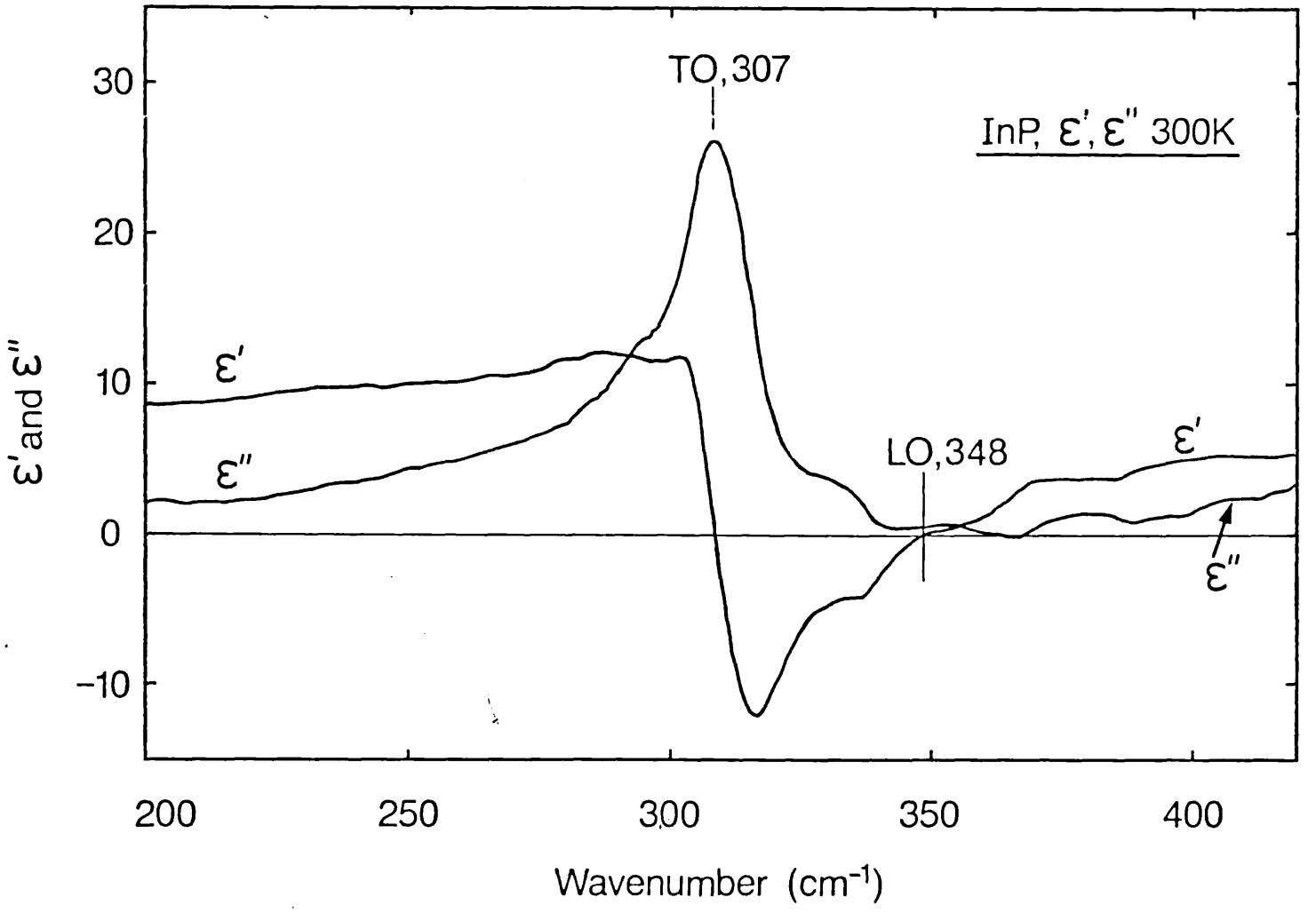

Fig(6.24) Measured dielectric constants for InP at 300K

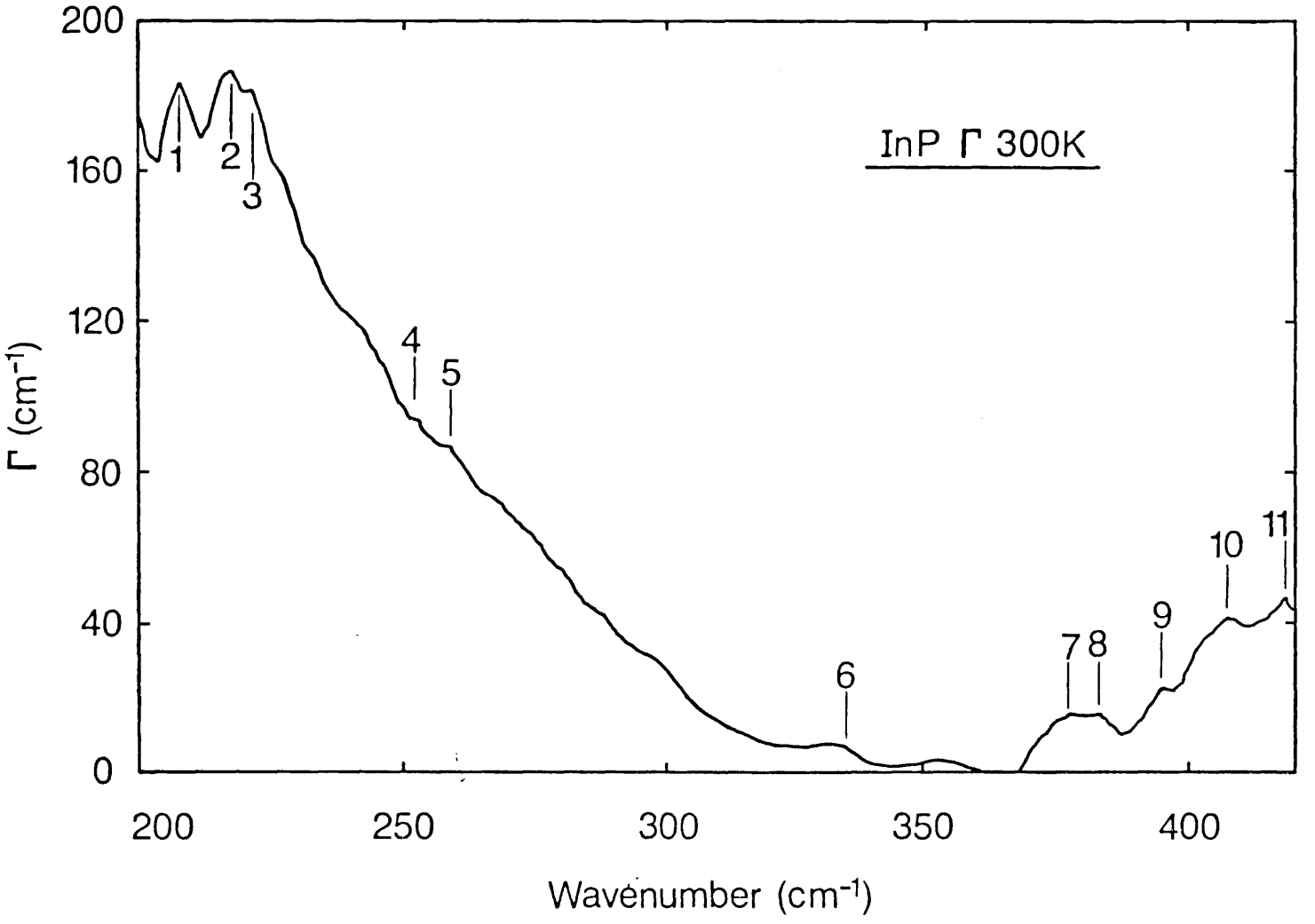

Fig(6.25) Measured frequency dependent imaginary part of anharmonic self-energy for InP at 300K. Assignments for the numbered are listed in table(6.7)

Table(6.6)
Summary of results for InAs and InP at 300K

Frequency in cm^{-1}	InAs		InP	
	ν_{TO}	ν_{LO}	ν_{TO}	ν_{LO}
This Expt:	219	244	307	348
Kunc	219	243	304	345
Ulrici	-	-	305 ± 3	345 ± 1

Table(6.7)

Two-phonon combination bands observed in the spectum of $\Gamma(oj, \nu)$ for InP.

Feature no:	Observed cm^{-1}	calculated cm^{-1}	Assignments Ulrici 1976
1	207	205	$W_4 + W_5$
2	216.5	215	$W_1 - W_5$
3	222	223	LA + TA (L)
4	252.1	250	TO - TA (X)
5	259	258	LA + TA(X) TO - TA(L)
6	335	336	2LA(L)
7	377	373	$W_3 + W_6$
8	383	384	TO + TA(X)
9	395.2	396	LO + TA(L)
10	407.5	405	$W_2 + W_5$
11	419	420	$W_1 + W_5$

CHAPTER 7

CONCLUDING REMARKS

Following recent developments the technique of dispersive Fourier transform spectroscopy has now been improved to the point that measurements can be made on solids with an accuracy which surpasses that attainable by alternate methods. This technique provides direct experimental measurements of the optical constants and the dielectric response of solids in the far infrared, and gives access to valuable information on the lattice dynamics of crystals.

Measurements of the far infrared optical properties of alkali halides like CsI and KI have been performed at room temperature and at low temperatures using this technique to illustrate the advantages over conventional spectroscopic techniques. To exploit the full advantage of amplitude spectroscopy when investigating detailed structure close to strong absorption bands, such as the reststrahlen band in alkali halide crystals [Johnson and Bell (1969) and Parker et al (1976)], a single pass dispersive transmission technique was used to complement the technique of dispersive reflection spectroscopy.

Thus the combination of these two techniques provides a powerful tool comparable in sensitivity with the technique of Raman scattering, and as a consequence we are able to obtain the first experimental determination of the frequency dependent anharmonic damping functions of the transverse optic phonon for CsI and KI at ambient and low temperatures. The various lattice

dynamical results obtained here are very encouraging and a good correlaton between experimental and published theoretical calculations is obtained. In both cases the structure associated with anharmonicity was revealed which had not previously been observed by conventional power spectroscopy. In the case of compound semiconductors like InAs and InP, the exploitation of the dispersive reflection technique in the far infrared region at ambient temperature has made possible the investigation of detailed structure associated with phonon combination bands in the spectrum of $\Gamma(oj,\nu)$, and also provides an access for the first time to many combination bands within the reststrahlen region. A number of these features in the spectrum of $\Gamma(oj,\nu)$ have been observed for the first time, and their assignment was carried out by using published values of critical point frequencies. As a consequence the dispersive technique should help in establishing precise phonon frequencies at the symmetry points in these materials. Further confidence can be obtained in these frequencies by performing the measurements at low temperatures. The experimental results obtained on these compound semiconductors agree quite well with the preveously published data where it is available.

Since the performance of the dispersive reflection interferometer was limited due to specimen size, the construction and design of a prototype focused beam interferometer which over comes the problems associated with the reflection interferometer is given in detail together with the demonstration of its feasibility in chapter 4. A possible future development would be to incorporate low temperture facilities and

to develop a new technique for replacing the smaller specimens (5mm in diameter) with the reference mirror to achieve phase accuracies similar to those obtained by Parker et al (1974-75-76) for specimens of large diameter.

REFERENCES

Beairsto J A B, and Eldridge J E, Can. J. Phys. 51, 2550 (1973)

Bell E E, Infrared Phys. 6, 57 (1966)

Bell R J, "Introductory Fourier transform spectroscopy". Academic Press New York (1972)

Berg J I, and Bell E E, Phys. Rev. 4B 3572 (1971)

Birch J R, and Parker T J, Chapter 3 in Vol II "Infrared and millimeter waves" Ed. Button K J, Academic Press, New York (1979)

Birman J L, Phys. Rev. 127, 1093 (1962)

Birman J L, Phys. Rev. 131, 1489 (1963)

Borcherds P H, Alfrey G F, Saunderson D H, and Woods A D B, J. Phys. C, 8, 2022 (1975)

Born M, and Wolf E, "Principles of optics" Pergamon press Oxford (1970)

Born M, and Huang K, "Dynamical theory of crystal lattices" Clarendon press Oxford (1954)

Buhrer W, and Halg W, Phys. status. Solidi. b(46), 679 (1971)

Beunen J A, Costley A E, Mok C L, Neill G F, Parker T J, and Tait G, JOSA 71 (1981)

Burstein E, Johnson F A, and Loudon R, Phys. Rev.139A, 1239 (1965)

Chamberlain J E, Gibbs J E, and Gebbie H A, Nature London. 198, 874 (1963)

Chamberlain J E, Gibbs J E, and Gebbie H A, Infrared Phys 12 145 (1969)

Chamberlain J E, "The principles of interferometric spectroscopy" Wiley Publications New York (1979)

Chamberlain J E, Chantry G W, Findlay F D, Gebbie H A, Gibbs J E,

Stone N W B, and Wright A J, Infrared Phys. 6 195 (1966)

Chantry G W, "Submillimeter spectroscopy" Academic press" New York (1971)

Connes J, J. Physics Rad 19, 197 (1958)

Conte S D, and de Boor C, "Elementary numerical analysis" Mc Graw -Hill New York (1972)

Cooley J W, and Tukey J W, Math. Comput. 19, 297 (1965)

Costley A E, Hursey K H, and Ward J M, JOSA 67, 979 (1977)

Cowley R A, Advances in Physics 12, 421 (1963)

Dolling G, Cowley R A, Schittenhelm C, and Thorson I M, Phys Rev. 147, 577 (1966)

Donovan B, and Angress J F, "Lattice vibrations" Chapman and Hall, London (1971)

Eldridge J E, and Staal P R, Phys. Rev. B16, 384 (1977)

Eldridge J E, and Kembry K A, Phys. Rev. B8, 746 (1973)

Fellgett P, J. Phys. Radium. 19, 187 (1958)

Fischer K, Phys. Stat Sol. (b) 66, 449 (1974)

Fleming J W, and Chamberlain J E, Infrared Phys Vol 14, 277 (1974)

Gast J, and Genzel L, Opt Commun 8, 26 (1973)

Gebbie H A, and Vanasse G A, Nature, London 178, 432 (1956)

Hardy J R, and Karo A M, "The lattice dynamics and statics of alkali halide crystals". Plenum Press. New York (1979)

Hisano K, Placido F, Bruce A D, and Holah G D, J. Phys. C5, 2511 (1972)

Jacquinot P; JOSA. 44, 761 (1954)

Johnson K W, and Bell E E, Phys. Rev. 187, 1044 (1969)

Kittel C, "Introduction to solid state physics", Wiley New York (1967)

Kleinman D A, Phys. Rev. 118, 118 (1960)

Koteles E S, and Datars W R, Solid stat commun. 19, 221 (1976)

Kunc K, Balkanski M, and Nusimovici M A, Phys. Stat. Sol (b)72 229 (1975)

Lax M, and Burstein E, Phys. Rev. 97, 39 (1955)

Lorimor O G, and Spitzer W G, J. Applied Phys. 36, 1841 (1965)

Lowndes R P, Phys. Rev. B1 2754 (1970)

Lowndes R P, and Martin D H, Proc Roy Soc. A308, 473 (1969)

Lowndes R P, and Rastogi A, Phys. Rev. B14 3598 (1976)

Maradudin A A, and Fein A E, Phys. Rev. 128, 2589 (1962)

Martin A E, "Infrared interferometric spectrometers" ESPC. Oxford New York (1980)

Martin D H "spectroscopic Techniques" North Holland Publishing Corp. Amsterdam (1967)

Martin D H, and Puplett E, Infrared Phys. 10, 105 (1970)

Michelson A A, " Light waves and their uses" University of Chicago press. (1902)

Narahari Rao K, Humphreys C J, and Rank D H, " Wave length standards in the infrared " Academic Press New York (1966)

Pai K F, Parker T J, and Lowndes R P, JOSA 68, 1322 (1978)

Parker T J, Chambers W G, and Angress J F, Infrared Phys. 14, 207 (1974)

Parker T J, and Chambers W G, IEE Conf Publ. No 129 P169 (1975)

Parker T J, Ledsham D A, and Chambers W G, Infrared Phys. 16, 293 (1976)

Parker T J, Chambers W G, Ford J E, and Mok C L, Infrared Phys. 18, 571 (1978)

Parker T J, and Lowndes R P, J. Phys. E. 12, 495 (1979)

Robinson T S, and Price W C, Proc. Phys. Soc. London. B66 969 (1953)

Russell E E, and Bell E E, Infrared Phys. 6, 75 (1953)

Sears F W, and Salinger G L, "Thermodynamics, Kinetic theory and statistical thermodynamics " Addison- Wesley Publication company New York (1975)

Staal P R, and Eldridge J E, Infrared Phys. 17, 299 (1977)

Stierwalt D L, and Potter R F, " Emittance studies", Semiconductors and semimetals, Vol3 Eds. R K Willardson and A C Beer, Academic press New York (1967)

Strong J, J. Opt. Soc. Am. 43, 336 (1957)

Szigeti B, Proc. Roy. Soc. (London) A 258, 377 (1960)

Talwar D N, and Agrawal Bal K, Phys. Stat. Solidi (b) 63, 441 (1974)

Ulrici B, and Jahne E, Phys. Stat. Sol (b) 74, 601 (1976)

Wallis R F, Ipatova I P, and Maradudin A A, Sov. Phys. Solid. State. 8, 850 (1966)

Ziman J M, "Electrons and Phonons" Oxford, Clarendon Press (1960)

Zwick U, Irslinger C, and Genzel L, Infrared Phys. 16, 263 (1976)

PUBLICATIONS BASED ON THE WORK DESCRIBED IN THIS THESIS

1. A. Memon, T. J. Parker, C. L. Mok, and W. G. Chambers
Study of the anharmonic self-energy of the transverse optic mode in CsI at 77 and 300K by dispersive Fourier transform spectrometry. Recent developments in Condensed Matter Physics. Vol 5, 1981. In press

2. A. Memon, and T. J. Parker
Study of the far infrared optical properties of KI by dispersive Fourier transform spectrometry. Int. J. Infrared and Millimeter waves Vol 2. To be published in July issue, 1981

3. A. Memon, T. J. Parker and J. R. Birch
A study of the far infrared dielectric response of InAs at room temp by dispersive Fourier transform spectrometry. Proc. 1981 Int. Conf. on Fourier transform spectroscopy, Columbia, South Carolina. In press